Universidad Carlos III de Madrid
Universitat Politècnica de Valencia

University Degree in Biomedical Engineering
2016-2020

Bachelor Thesis

CHARACTERISATION OF ATRIAL FLUTTER VARIANTS BASED ON THE ANALYSIS OF SPATIAL VECTORCARDIOGRAPHIC TRAJECTORY FROM STANDARD ECG

Samuel Ruipérez Campillo

Prof. Dr. José Millet Roig
Prof. Dr. Francisco Sales Castells Ramón
Prof. Dr. Manuel Desco Menéndez

Madrid, July 2020

Evaluation Board

Prof. Dr. Sara Guerrero Aspizua
Dr. David Pérez Benito
Dr. Raquel Giménez Pérez

Final Mark:
10.0 - Honours (Matrícula de Honor)

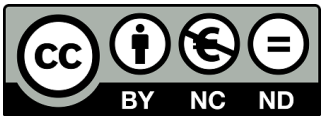

ABSTRACT

After atrial fibrillation, atrial flutter* is the most common atrial tachyarrhythmia. Its diagnosis relies on the twelve lead electrocadriogram* analysis of the distinctive waves in several leads. Nonetheless, the accurate identification of the type of atrial flutter still requires an invasive procedure. The maneuver for healing atrial flutter consists on ablating* a section of the anatomy of the atria, to stop the macroreentrant circuit* to keep happening, allowing the signal to travel to the ventricles in stead of staying at the atria.

The region to ablate directly depends on the place at which the macroreentrant circuit is located, which at the same time depends on the type of atrial flutter. Being able to non-invasively detect the atrial flutter variant would produce a great advantage when healing this illness. The hypothesis stated at this dissertation is based on the slow conduction regions as the key factor to distinguish the atrial flutter class. This and unveiling further relations between cardiac illnesses and their signal's alter ego are the purpose of this research project.

With such aim, different methods are developed based on the vectorcardiographic* representation of electrocardiograms from patients suffering from different atrial flutter types. These methods consist on the characterisation of vectorcardiographic signals from different standpoints. Besides, a mathematical model is implemented to create a large database with synthetic vectorcardiographic signals allowing to test the validity of the utilised methods.

The results prove the importance of slow regions in the vectorcardiographic representation of the patient's signals to characterise the atrial flutter type non-invasively. Furthermore, the analysis of the outcome of the different methods reveal a wide variety of features relating characteristics of the vectorcardiographic signal to the anatomy and physiology of this cardiac disease. Hence, not only results supporting the hypothesis were successful (taking into account some limitations), but also a variegated assortment of results unmasked remarkable relations among the vectorcardiographic signal and the characteristics of the atrial flutter disease.

*Key Concepts for Fast Readers:

Macroreentrant Circuit: Path that an electrical signal takes surrounding an obstacle in the cardiac tissue. It prevents the electrical signal from being transmitted to the ventricles in the case of atrial flutter, as the electrical signal gets stuck in this path or macroreentrant circuit.

Atrial Flutter: Atrial tachyarrhythmia characterised by the existence of a macroreentrant circuit around an obstacle in the atria. It is characterised by several beats of the atria per ventricular beat.

Cardiac Ablation: Maneuver to scar a part of the tissue of the heart that entails the persistence of an abnormal heart rhythm. In the case of atrial flutter, ablation is performed in a region of the macroreentrant circuit, avoiding the electrical signal to remain in that path.

Electrocardiogram: Graphic representation of the electrical activity of the heart as a function of time. The standard surface electrocardiogram shows 12 leads. Each lead measures the voltage difference between two surface electrodes placed over the skin of the patient.

Vectorcardiogram: 3D representation of the projection of the main vector defining the electrical activity of the heart. In layman's terms, it records the magnitude and direction of the electrical forces or potential differences of the heart during the cardiac cycle.

AGRADECIMIENTOS

En primer lugar, me gustaría mostrar mi agradecimiento a los que habéis confiado en mí para llevar a cabo este proyecto desde el primer momento. Dr. José Millet y Dr. Francisco Castells, gracias por vuestro apoyo, ejemplo, exigencia e instrucción. He aprendido muchísimo de vosotros y la infinidad de vuestro conocimiento en este campo. Pero esto no supone el final de hacer ciencia juntos, sino un punto y seguido para seguir descubriendo los misterios de las enfermedades cardiacas y desvelando secretos hacia una medicina menos invasiva. Valencia, Burdeos, Toledo e Italia han sido el principio de este bonito sincretismo. Gracias también a la Dra. Raquel Cervigón y a los cardióglogos Dres. Jose Luis Merino y Sergio Castrejón, de cuya experiencia he podido aprender y formarme, al Dr. Manuel Desco por mentorizarme y ayudarme a mejorar desde la UC3M, al Dr. Javier Rodríguez, cuyo apoyo ha sido fundamental este año y que me ha aportado una visión fascinante de la ciencia, y a todos los profesores que habéis constituído los pilares de mi formación.

De lo que sí supone un final este proyecto es de una etapa soberbia en todos sus sentidos. Estos años en la Universidad Carlos III de Madrid me han permitido crecer como persona y como profesional en el campo de la ingeniería biomédica y de la cienca. Por tanto, os agradezco inmensamente vuestro apoyo, a aquellos que me habéis acompañado durante esta etapa. Especialmente, a los que habéis estado conmigo en todo momento, aquí, en Madrid (y en Estados Unidos), y que habéis llegado para quedaros. Entre ellos, gracias a Diego por escuchar el desarrollo de este proyecto desde sus inicios hasta su final durante estos curiosos meses.

Finalmente, no puedo olvidar a aquellos que me acompañáis desde antes de esta historia. Gracias a aquellos amigos con los que comparto mis raíces, y a mi familia. Especialmente, gracias a ti, Irene, por estar siempre ahí y enseñarme tanto sobre la vida.

CONTENTS

1. INTRODUCTION 1
1.1. Statement of the Problem, Contextualisation and Motivation 1
1.2. Study Design and Aspirations 2
1.3. Outlined Objectives and Contribution of the Author 3
1.4. Structure of This Bachelor Dissertation 4
2. STATE OF THE ART 6
2.1. The Heart in the Circulatory System 6
2.2. Anatomy of the Heart 7
2.2.1. Grounds on the anatomy of the heart: A Generic Approach 7
2.2.2. Left Atrium Anatomy 8
2.3. Activation and Electrical Activity of the Heart 10
2.3.1. Fundamentals of Heart Physiology 10
2.3.2. Cardiac Action Potential 10
2.3.3. Heartbeat and Propagation of the Electric Signal 11
2.4. Electrocardiography: Measuring the Electric Activity of the Heart 14
2.4.1. Historical Context and Fundamentals of the Surface ECG 14
2.4.2. Measuring the Electric Activity of the Heart: ECG Features 15
2.5. Vectorial Analysis of the Electric Signal 18
2.5.1. A Vector that represent an Electric Potential 18
2.5.2. Vectorial Analysis of the Cardiac Cycle and Relation to the ECG Signal . 19
2.5.2.1. Vectorial Analysis of the QRS Complex 19
2.5.2.2. Vectorial Analysis of the T Wave 20
2.5.2.3. Vectorial Analysis of the P Wave and Atrial T Wave 20
2.6. The Vectorcardiogram 22
2.6.1. Fundamentals 22
2.6.2. The derivation of the VCG: Frank's Leads System and The Inverse Dower Transform 23
2.7. Atrial Tachyarrhythmias and their Electrophysiological Foundations 24
2.7.1. Atrial Tachycardia 24
2.7.2. Atrial Fibrillation 24

2.7.3. Atrial Flutter . . . 25
2.7.3.1. Electrocardiographic Signal of AFL . . . 26
2.7.3.2. AFL Treatment: Catheter Ablation . . . 28
3. MATERIALS . . . 29
4. METHODS I. VCG ANALYSIS . . . 30
4.1. Acquiring and Processing the ECG Signal . . . 30
4.2. Computation of the Patient's Representative Vectocardiogram . . . 30
4.3. Analysis of the VCG features . . . 34
4.3.1. Slow Conduction Velocity Regions . . . 34
4.3.2. Quantisation of Slow Velocity Regions: SVPOT, SVPOD and their Rate. 35
4.3.2.1. Slow Velocity Percentage Over Time (SVPOT) . . . 35
4.3.2.2. Slow Velocity Percentage Over Distance (SVPOD) . . . 37
4.3.2.3. Rate SVPOT/SVPOD . . . 37
4.3.3. Angular Velocity Profile . . . 37
4.3.4. Variability or Consistence of the VCG . . . 39
4.3.5. Arc or Circumference Parameter . . . 40
4.4. VCG Archetypes of AFL Variants . . . 41
4.5. Similarity among VCGs and Characterisation . . . 42
4.6. Statistical Analysis . . . 42
5. METHODS II. VCG GENERATOR: A MATHEMATICAL MODEL . . . 44
5.1. Introduction to the Mathematical Model . . . 44
5.2. Grounds of the Synthetic VCG Generator . . . 45
5.2.1. Definition of an Ellipse . . . 45
5.2.2. Perimeter of an Ellipse . . . 46
5.2.3. Polar Coordinates . . . 46
5.3. The Semi-axes of the Projections . . . 47
5.3.1. Relations among a and b . . . 47
5.3.2. Definition of c in Terms of a Normalised Random Variable in Matlab . . . 49
5.4. Angular and Radial Variables . . . 50
5.4.1. Angle Variation: Irregular Discretisation . . . 50
5.4.2. Variation of the Radius: Creating Random Geometries . . . 55
5.5. Definition of the Cartesian Coordinates of the Ellipsoidal Loop . . . 57

5.6. Smoothing the Synthetic VCG and Velocity Profile . . . 58
5.7. Modalities: Subgroups of Ellipsoidal figures . . . 59
6. RESULTS AND DISCUSSION . . . 60
6.1. Introduction and Organisation of Results and Discussions . . . 60
6.2. Analysis of the Synthetic VCGs Results . . . 60
6.3. Analysis, Interpretation and Discussion of the Patient's Results . . . 64
6.3.1. General VCG Features: Number of cycles, Loop Time Length Consistence Intra-Patient . . . 65
6.3.2. Slow Conduction Region Distribution Analysis: SVPOT, SVPOD and Rate . . . 68
6.3.3. Arc or Circumference Parameter . . . 70
6.3.4. Archetype Correlation: Fundamental Results Supporting the Hypothesis . 72
7. FINAL CONCLUSIONS . . . 81
8. CONTRIBUTION, LIMITATIONS AND FUTURE APPROACHES . . . 82
8.1. Scientific Contribution . . . 82
8.2. Current Limitations of this Research Project . . . 82
8.3. Guides for Future Work . . . 83
9. REGULATORY FRAMEWORK AND SOCIO-ECONOMICAL IMPACT . . . 85
9.1. Regulatory Frames: Bioethics, Licensing and Law . . . 85
9.2. Socio-Economical Impact . . . 86
9.2.1. Socio-Economical Environment . . . 86
9.2.2. Project Resources and Costs . . . 86
9.2.2.1. Human Resources . . . 86
9.2.2.2. Material Resources and Equipment . . . 87
9.2.2.3. Resources to Cover Congresses . . . 87
9.2.2.4. Total Costs . . . 88
BIBLIOGRAPHY . . . 89

LIST OF FIGURES

2.1 Simplified scheme of the pulmonary and systemic circulation. 6
2.2 Three primary planes of the body and heart 7
2.3 Anatomical features over a section of the heart 8
2.4 Anatomical structures of left atrium and surrounding structures 9
2.5 Autonomic innervation of the heart. 10
2.6 Membrane potential and ion permeabilities of cardiac contractile and autorhythmic cells. 12
2.7 Scheme of the pathway that the action potential follows in the process of activation of the heart. 13
2.8 Representation of Eithoven's Triangle. 15
2.9 ECG Signal from a healthy patient. 16
2.10 Illustration of the relation between the events in the cardiac cycle in terms of the electrical activity, and the principal features of the ECG signal. . . 17
2.11 Mean vector representing the potential difference and current flow at the an instant of depolarisation and standard directions of mean potential vectors in relation to leads I, II, III, aVR, aVL and aVF 18
2.12 Evolution of the Vectorial representation and its corresponding voltage variation for lead I, II and III over the cardiac cycle 21
2.13 Illustration of the representation of the electrical potential variation of the heart through the vectorcardiogram over a drawing of the heart and chest of a human individual 22
2.14 VCG signal extracted from a healthy patient over several heart beats, highlighting the P and T waves representation and QRS complex VCG loop . 23
2.15 Representation of lead II and V1 from a patient suffering from multifocal atrial tachycardia 25
2.16 Representation of the 12-lead ECG from a patient suffering from AF, highlighting the representative lead II 26
2.17 Leads I, II, III, aVR, aVL and aVF from an ECG signal recorded from a patient suffering from typical or common AFL 27
2.18 Leads I, II, III, aVR, aVL, aVF and Vq from an ECG signal recorded from a patient suffering from reverse or CCW AFL 27
2.19 Schematic drawing illustrating catheter ablation of AF or AFL by radio frequency energy or cryoballoon ablation 28

4.1 Representation of the ECG signal of a patient suffering from common CW AFL under the influence of adenosine. 31

4.2 Correlation coefficient of a ECG signal over itself when displacing it over time. 32

4.3 Reconstruction of a VCG from 10 loops under the adenosine effect blocking the ventricle contribution to the signal and average of the VCG loop in 2 and in 3 dimensions 33

4.4 Velocity profile of the transmission of electrical impulse in the trajectory in a macrorreentrant atrial loop from a patient suffering from perimitral CCW AFL. 35

4.5 VCG reconstruction from a ECG atrial signal, highlighting slow velocity regions in both the VCG and ECG representation from which the atrial VCG loop is averaged. 36

4.6 Velocity profile of the transmission of electrical impulse in the trajectory in a macrorreentrant atrial loop from two patients suffering from perimitral CW AFL. 38

4.7 Conduction velocity and angular velocity profile from a patient suffering from perimetral CW AFL. 39

5.1 Definition of an ellipse for a major axis a greater than the minor axis b. . 45

5.2 Representation of a circle and an ellipse over a constant time discretisation illustrating a 2D signal increasing through angle. 50

5.3 Representation of the angular discretisation design in the VCG generator in relation to synthetic VCGs 52

5.4 Representation of the angular discretisation design in the VCG generator in relation to synthetic VCGs, slow regions, and their velocity profile. . . 56

5.5 Representation of two chirp signals with normalised radius variation and two examples of target frequencies 57

5.6 Synthetic VCG created by the mathematical model , represented after sampling, and velocity profiles before and after having applied an adapted low pass Savitzky–Golay filter over the 3-dimensional VCG loop. 58

6.1 Box plot of the correlation coefficient of types I to IV with their representative archetypes. 61

6.2 ROC curves for all patients corresponding to each of the groups 62

6.3 Variation of correlation coefficient under the modification of parameters having the rest fixed in the synthetic VCG Generator. 64

6.4 Box plot of the correlation coefficient of all synthetic VCG types with two archetypes. 65

6.5 Representation of the average consistence intra-patient and the average number of cycles for all the patients belonging to the different AFL groups. 66

6.6 Representation a box and whiskers plot for the parameter of Average Time per VCG loop. 67

6.7 Representation a box and whiskers plot for the parameter of SVPOT, SVPOD and SVPOT/SVPOD. Rate 69

6.8 Representation a box and whiskers plot for the arc or circumference parameter in radians and in a normalised unitless version. 71

6.9 Representation in a box plot for correlation coefficient from the archetype of each AFL type with the patients from its group (using the LOO algorithm) and the rest of patients. 74

6.10 Depiction of the common CCW AFL VCGs and their archetype in 3D (frontal, transversal and sagittal planes) and their x,y,z components. . . . 77

6.11 Depiction of the common CW AFL VCGs and their archetype in 3D (frontal, transversal and sagittal planes) and their x,y,z components. 78

6.12 Depiction of the perimitral CCW AFL VCGs and their archetype in 3D (frontal, transversal and sagittal planes) and their x,y,z components. . . . 79

6.13 Depiction of the perimitral CW AFL VCGs and their archetype in 3D (frontal, transversal and sagittal planes) and their x,y,z components. . . . 80

LIST OF TABLES

5.1 Main characteristics defining each synthetic VCG type according to their sense, plane and rotation and initial angle. 59

6.1 Average Correlation Coefficient of the Patients from Each Group with All the Archetypes 61

6.2 AUC for All Patients in Two Modalities 63

6.3 Number of VCGs vs Number of Cycles From Which They Were Averaged 65

6.4 Average Cycle Number and Consistence Intra-Patient 66

6.5 Number of VCGs vs Average Time Length 67

6.6 Results Of svpod And svpot Parameters For AFL Groups 68

6.7 Results Of Arc Parameter For All Afl Groups 71

6.8 Results Of Correlation Of Archetypes With Patients From AFL Groups 73

6.9 Correlation Among Archetypes 73

9.1 Human Resources 87

9.2 Material Resources 88

9.3 Resources for Congresses 88

9.4 Total Costs 88

ACRONYMS

AF Atrial Fibrillation. 24–26, 28, 69, 84, 86
AFL Atrial Flutter. viii, xiii, 1–5, 7, 9, 25–35, 37–41, 44, 63, 65–68, 70, 72–81, 83, 84, 86
AN Atrioventricular Node. 13, 17, 19, 20, 25
ANOVA Analysis of Variance. 43, 62
AP Action Potential. 10–13, 20
AT Atrial Tachycardia. 24, 25
AUC Area Under the Curve. 43, 63
AV Atrioventricular Valve. 8, 9

BSS Blind Source Separation. 30

CCW Counterclockwise. xiii, 1, 27–29, 32, 33, 35, 42, 59, 65, 66, 68, 71–77, 79
CP Correlation Parameter. 35, 39, 40, 42, 44, 61, 63, 66, 67, 73, 76
CTI Cavotricuspid Isthmus. 1, 2, 26, 28
CW Clockwise. xiii, 1, 28–31, 38, 39, 42, 59, 65–76, 78, 80, 83

ECG Electrocardiogram. 1–5, 13–17, 19–21, 23–36, 38, 39, 41, 44, 65, 81

ICA Independent Component Analysis. 30
IDT Inverse Dower Transform. 3, 23, 30, 36, 39, 81

LA Left Atrium. 5, 8, 9, 27, 28
LAA Left Atrial Appendage. 9
LOO Leave One Out. xiii, 42, 44, 72–74
LV Left Ventricle. 6, 8, 9

MC Macroreentral Circuit. 1, 2, 24–26, 34, 35, 39, 40, 42, 44, 66, 68–72

PCA Principal Component Analysis. 30

RA Right Atrium. 1, 6, 8–10, 13, 26, 28
ROC Receiver Operating Characteristics. xii, 43, 62–64
RV Right Ventricle. 6, 8

SN Sinoatrial Node. 9, 13, 17, 20, 24
SVPOD Slow Velocity Percentage Over Distance. viii, ix, xiii, 35, 37–39, 68–70
SVPOT Slow Velocity Percentage Over Time. viii, ix, xiii, 35, 37–39, 68–70

VCG Vectorcardiogram. vii–ix, xii, xiii, 2–5, 13, 19, 22–24, 29–45, 47–52, 55, 56, 58–60, 62–65, 67, 71–74, 76–80, 83, 84

1. INTRODUCTION

1.1. Statement of the Problem, Contextualisation and Motivation

Atrial flutter (AFL) is the second most common atrial tachyarrhythmia with an increasing prevalence nowadays [1, 2], even since surgical ablation was established in the last decades, being the most common approach to the treatment today [3]. Furthermore, its importance also relies on its linkage to other diseases [4–6], and it is expected to find an increase in its prevalence of more than one hundred percent in the United States by 2050 [4], and in the European Union by 2060 [7]

AFL is defined as a supraventricular arrhythmia which is physiologically caused by a macroreentrant electrochemical circuit at the atria [8]. This macroreentrant circuit (MC) follows a path of activation around an obstacle with size on terms of a few centimetres of radius [9]. The most frequent type of AFL is defined by a common pattern in the right atrium (RA) due to its anatomical features [10, 11]. This pattern follows a MC around the tricuspid valve which could be in both senses, clockwise (CW) and counterclockwise (CCW) [12]. On this path there is an isthmus of slow conduction, necessary for the perpetuation of the circuit, allowing the refractory period of myocytes to take place for been again activated [8, 13, 14].

Though first described more than a century ago [15], the mechanisms and techniques used for AFL diagnosis have seen little more than minor changes to their executions. Throughout the diagnosis's history, the process has heavily relied on the twelve lead electrocardiogram (ECG) analysis and the distinctive waves in leads II, III, aVF, aVL, V1,V2. The electrocardiographic pattern is similar to the one of an atrial tachycardia (heartbeat $\geq$ 240pulses/min) with a continuous and regular wave [8]. In 2001, more than three decades after the first classification of AFL, the European Society of Cardiology and the North American Society of Pacing and Electrophysiology developed the current classification for the disorder [16]. These societies based this new categorisation on both the ECG and the electrophysiological mechanisms. Nonetheless, accurate identification of the type of AFL still requires invasive procedures such as the guided by a reference multipolar catheter on the anterior and septal RA to record the activation sequence while another catheter is used for mapping [17, 18].

Not only does the presence of MCs determines the diagnosis, but the fact that no microreentrant circuits are usually found is also a key point that suggests surgical ablation as the most effective treatment for AFL [19]. In order to treat the common AFL, a surgery is needed with the final objective of blocking bidirectionally the cavotricuspid isthmus (CTI) [20, 21] through radiofrequency or cryoablation, so the definition of the target and the path of the MC is necessary. For other types,

different anatomical regions would be ablated to interrupt the macroreentry. A steerable catheter is used for ablation of this region [17, 21, 22], which is normally the narrowest part of the circuit path and, in the common AFL case, it can be accessed from the atrioventricular node [23]. Some other options have been proposed during the latter history [24, 25], but nowadays the maneuver is well defined [26].

In order to establish a simple classification of the types of AFL which will then lead to the type of surgical intervention [27], we can focus on the MC. In the most common case (near 90%), its path goes around the right atrium surrounding the tricuspid valve [8]. For this case, the target ablation site is the CTI [24]. The rest of cases (approx. 10%) are denoted as atypical, and from those the MC around the mitral valve is the most frequent - referred as perimitral AFL. In these situations the MC cannot be identified until the intra-atrial electrical mapping is performed [28]. Therefore, a method to distinguish among different atypical AFL types and identify the most probable MC from the ECG would be valuable in order to obtain key information prior to the electrophysiologic study.

A vectorcardiographic approach [29], defined from the dipolar nature of the heart [30], is employed for the representation of 3 dimensional surface loops .Thus, the vectors representing the changes of magnitude and direction of electrical activity of the atria are represented and can be helpful to identify different patterns generated by the evolution of the wavefront propagation [31].

Flutter vectocardiograms (VCGs) have been previously described [32], but no clear correlation has been demonstrated to proven mechanisms. Although the analysis of ECG is used to detect flutter cases [33], some variations that have been proved to exist, are no easily distinguished from atypical AFL [34, 35]. Nonetheless, the vectorcadiographic approach shows the activation sequence [36], and this can help to determine specific features depending on the AFL type.

I hypothesise that there is a correlation between the VCG attributes and the type of AFL that the patient suffers. This correlation is thought to be directly related to the distribution of slow conduction areas at the atria. Thus, differences in the VCG loop pattern will be studied to characterise from them the VCG archetype defined as characteristic for each group.

1.2. Study Design and Aspirations

The objective of the bachelor's dissertation is to demonstrate the correlation between the VCG signal of a patient suffering from AFL and the type of AFL that this patient suffers from. Several parameters need to be evaluated, based on the motley assortment of peculiarities of each temporally discretised VCG signal. The cornerstone of this analysis is related to the distribution of slow conducting regions in the atria, represented in its VCG projection. Hence, the allocation of this

characteristic areas in the representation of the three-dimensional anatomy of the atria is to be proved as the fundamental feature to distinguish among AFL types.

In order to analyse the signal of the patient, an algorithm needs to be created to pre-process the ECG signal of the patient and to transform it into a VCG signal based on the Inverse Dower Transform (IDT) approach. This signal is then processed, analysed and discretised in time. Features are extracted and analysed to discriminate among different AFL groups. Archetypes will be created from a group of VCG coming from patients suffering from the same AFL types, previously studied clinically from cardiologist from 'La Paz' Hospital. New cases will be contrasted through the algorithm with the different archetypes showing a weighted correlation parameter which will allow the program to define which AFL this new unidentified patient is diagnosed.

To test the algorithm and give robustness to the feature analysis and weighted correlation parameter that shows for identifying the AFL, a large VCG database is required, so it will be created. With such purpose a mathematical model needs to be implemented, recreating the characteristics of VCG signals, with a wide variety of random parameters, leading to millions of possible shapes so that there are not equal synthetic VCG models generated. Those will be classified in groups whose common characteristic will happen to be the slow velocity region. Thence, based on that database, the algorithm will be tested illustrating its success in identifying the class of the VCG model from the variegated shapes, orientation and velocity profiles.

Finally, proved the robustness of the algorithm and its analytic capacity, a statistical analysis will be performed over the results provided by the algorithm applied to a list of patients with different AFL diseases. Those are already diagnosed by well-known cardiologists providing our golden standard, so the quality of the results can be corroborated, and the statistical analysis is robustly contrasted.

1.3. Outlined Objectives and Contribution of the Author

This research project in carried in a laboratory with a group of researchers. The present one is carried out by the student and the following objectives are the contribution of the author of this dissertation to the project and laboratory team.

- To write an organised dissertation with a broad state of the art from general to specific issues helping people from different more or less related fields to completely understand the problematic, methodology, results, discussions and conclusion.
- To create representative VCGs from ECG signals of patients suffering from different AFLs.

- To write an algorithm that computes representative VCGs for each AFL type from the different VCGs of the patients of each group.
- Design a methodology of quantifiable variables that characterise VCG signals from a wide variety of standpoints such as slow velocity conduction regions, shape features or correlation among loops.
- To create a mathematical model that works as a synthetic VCG generator to study properties of the designed variables and the characterisation of VCG loops. A large database of synthetic VCGs is created from this model.
- Develop a methodology to evaluate the synthetic VCG generator and the synthetic database.
- To interpret the statistical analysis.
- To accomplish a detailed discussion about the results of both the synthetic and real VCGs as well as the physiological grounds of the outcome and critically evaluate the success of the project.
- To demonstrate the relation between the VCG loop of the patients and the AFL that this patient is suffering from based in several features but giving special emphasis to the distribution of slow conduction regions.
- To place the project in the appropriate regulatory framework and socio-economical environment and describe its costs and impact.

Note that the statistical algorithms and their election have not been performed by the author of this dissertation. On this topic, illustrative figures, interpretation and discussion of their outcome have been, as mentioned in the objectives. Some complex electronic-based algorithms in the pre-processing of the ECG signal have not been performed either by the student. The organisation and settlement of the protocol that the cardiologists employed to acquire the ECG signals from patients that were undergoing cardiac surgery was neither performed by the author of this dissertation -nor was the surgery.

All figures from the 'State of the Art' section have been retrieved or modified from the indicated sources (except of one, created by the author). The other 26 figures have been created by the author of this dissertation.

1.4. Structure of This Bachelor Dissertation

This bachelor's dissertation is structured with the aim of describing a complex project in a clear, ordered, concise and approachable manner, faithful to the materials, methods and results obtained during the process.

At first, a brief abstract summarising the thesis is described, followed by the current section of introduction, where the problem is stated and contextualised based on a broad selection of significant scientific sources. The latter are specifically chosen from scientific literature of the last five years or from world-wide repeatedly cited references of the addressed subject.

Having the topic introduced and exposed, the state of the art is painstakingly written acquainting all the necessary concepts to fully comprehend the importance of the presented matter and its variants and fundamentals. The essential notions to latter understand the materials and methods are also carefully described. The structure of this part is as follows: general concepts are firstly introduced to understand the context of the topic and, in each subsection, the focus on the specific topic of interest appears gradually. For instance, the circulatory system is firstly introduced to lead to the study of the anatomy of the LA (as interesting to understand the variety of possibilities of atypical and the importance of the problem) or the electrochemical principles of conduction in the heart. Similarly, this electrical activity is related to the electrocardiographic recording that will later be bound to the ECG features distinguishing atrial tachyarrhythmias, AFL among them. Thus, concepts are interconnected and presented from different perspectives from the general, to the specific. This section is of great significance to understand the proposal and contextualisation of the problem in the introduction, and the latter interpretation of the results and discussion.

The foremost section of this work is the materials, methods I and methods II. The source of the ECG signals for the project is described first. Then, in the first methodology section, the algorithm to analyse the features of VCGs and the definition of the designed parameters for this purpose, as well as the statistical analysis tools, are described. In methods II, the mathematical model to generate three dimensional VCG shapes is explained in detail. The overarching conclusions are then elaborated.

Reaching the end, the socio-economical and the regulatory frames are described, following current regulations, the socio-economical impact and other interesting matters that contextualises the research project and its contribution.

Finally, the scientific contribution, limitations and future approaches to clinical studies and further strategies are described, followed only by the bibliography, which indeed concludes this bachelor's thesis.

2. STATE OF THE ART

2.1. The Heart in the Circulatory System

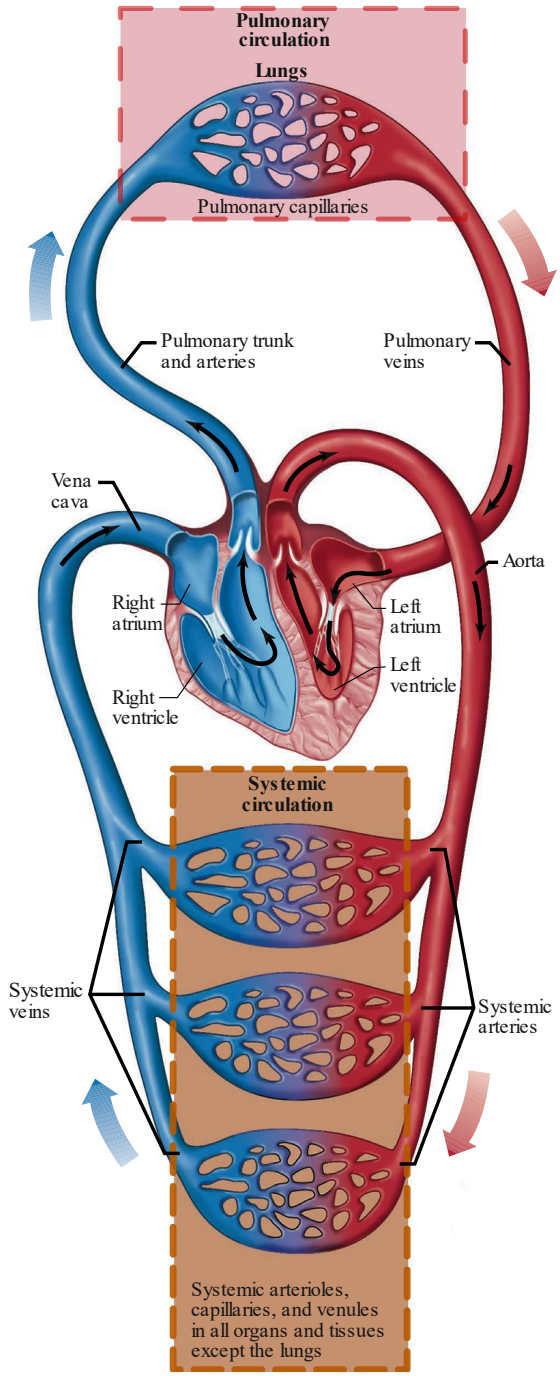

Figure 2.1. Simplified scheme of the pulmonary and systemic circulation. Colours illustrate this process depicted with the colour change from blue to red but are not related to the actual colour of blood in these vessels. (retrieved from [37]).

The circulatory system fulfils the necessity of our multicellular bodies of having transported substances in an efficient manner over long distances among cells, tissues and organs. Random movement or diffusion from higher concentrated regions to those with a lower concentration of solutes would not be enough to meet the metabolic requirements of the of every cell in the human body [37]. Thus, the cardiovascular system provides other anatomical structures with these necessities to accomplish their metabolic activity. It is composed by the heart which acts as a pump, the blood vessels acting as interconnected tubes and blood, a fluid containing solutes, water and cells.

The heart oversees pumping blood in the closed loop that forms the circulatory system. The path that blood follows is divided in pulmonary circulation - including the pathway from the right ventricle (RV) of the heart through the lungs to the la - and systemic circulation -from left ventricle (LV) to all tissues and organs except for lungs, to the RA of the heart [38]. Thus, arteries carry blood from the heart to the different tissues and to the veins, which will take blood back to the heart. A simplified scheme of the circulatory system and the position of the heart as its pump is observed in figure 2.1, where blood is oxygenated (red vessels) as it flows through the lungs and then loses some oxygen (blue vessels) which is delivered to tissues and organs.

2.2. Anatomy of the Heart

The anatomy of the heart has been studied for a long time, being the first noticeable approaches those of the sixteenth-century anatomist A. Vesalius [39]. L. da Vinci, a great figure of the European Renaissance and comparative anatomist also developed studies and drawings of the cardiac anatomy [40]. There are dozens of leading figures in medicine that have developed an extensive knowledge about the anatomy and physiology of this organ. In the first subsection, the grounds are introduced to better understand some terms used when describing diseases in later sections. In the second, details about the left atrium are described, since these concepts will be essential in the understanding of complexity of some atypical AFLs.

2.2.1. Grounds on the anatomy of the heart: A Generic Approach

The orientation of the heart within the thorax needs to be described to understand the figures of the 2-dimensional planes of this organ. Although the body is usually studied in coronal, axial and sagittal views, three orthogonal anatomic planes, the heart's primary planes are by convention the long-axis, four chamber and short-axis – in the same order of frontal, horizontal and sagittal views [41, 42]. Nonetheless, these two systems of reference are not aligned (see figure 2.2), something to take into account to understand the representations presented in this dissertation.

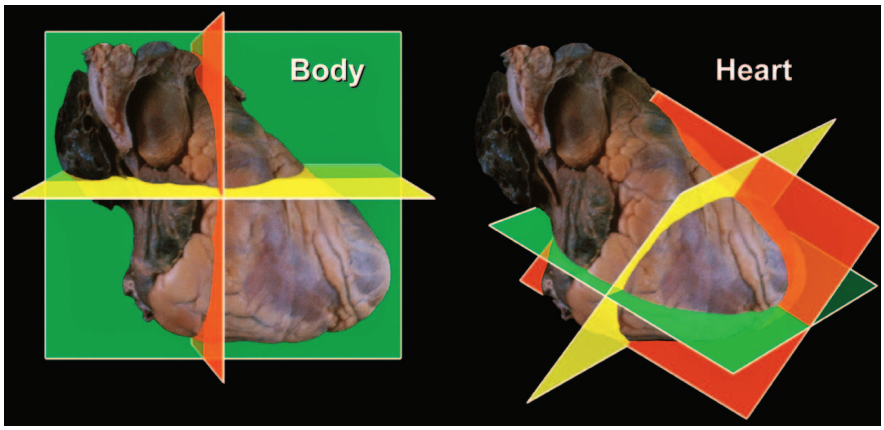

Figure 2.2. Three primary planes of the body (left) **and heart** (right). **Left:** The major axes are aligned with midline structures (i.e. oesophagus). **Right:** The planes are aligned diagonally to the ones in A. The axis in A do not define the planes in B, but their oblique position and vice versa (Modified over a figure retrieved from [41])

The heart is located in the chest, covered by the epicardium and the pericardium, a fibrous sac serving for protection. Both are separated by a watery fluid acting as lubricant. Its wall is denominated as myocardium, mainly formed by cardiac muscle cells, and its inner surface area is the endothelium [37].

There are four main cavities in the human heart, two in each half of this muscle. Each of the halves is constituted by an atrium and a ventricle separated by the

atrioventricular valves (AVs) that allow flow from the atrium to the ventricle. The ventricles are separated by a muscular wall, the interventricular septum. The left AV is the bicuspid or mitral valve, and the right AV is the tricuspid valve. AVs are passive because they allow the flow of blood according to a pressure gradient so that when it decreases from the ventricle to the atrium they are opened, while they remain closed in the opposite case because of their one-way nature. To maintain such nature, valves are fastened to the papillary muscles by the chordae tendineae [43, 44].

Finally, to allow blood to go into the arteries when ventricular contraction occurs and eschew blood from entering ventricles during relaxation, two valves known as semilunar valves are found in the pulmonary trunk and in the aorta [37, 44]. The first is denominated pulmonary valve and the second aortic valve, and their mechanism of opening and closing depends also on the pressure gradient among the ventricle and these arteriae. An overall scheme of with the fundamental terms of the heart in a plane given by the long axis [44] is presented in figure 2.3.

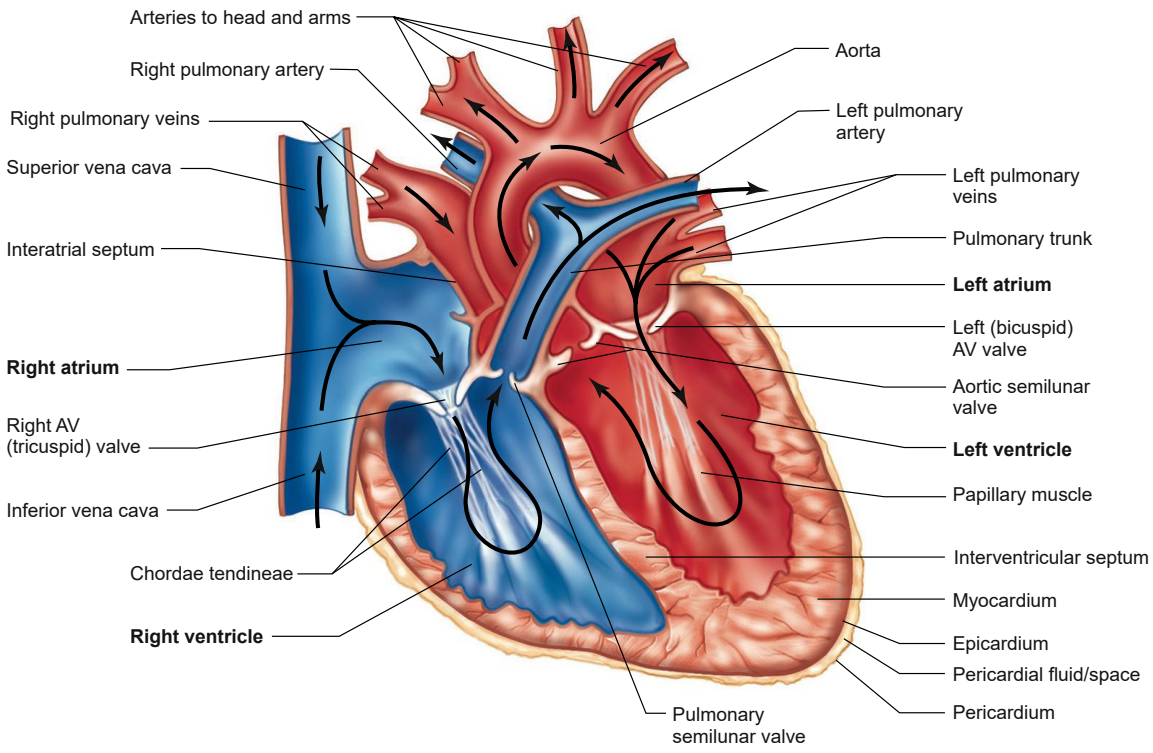

Figure 2.3. Scheme of a section of the heart. Following the colour code of figure 2.1, blue vessels and chambers (RA and RV) represent the pulmonary circulation and red ones (LA and LV) the systemic circulation. Arrows represent the direction of the blood flow (retrieved from [37]).

2.2.2. Left Atrium Anatomy

The LA is the most superior and posterior chamber of the heart [45]. It receives oxygenated blood that will enter the systemic circulation path after being pumped to the LV. The anatomy of the LA is of noticeable importance because of the wide variety of surgical procedures such as ablations or valve repairs that require access

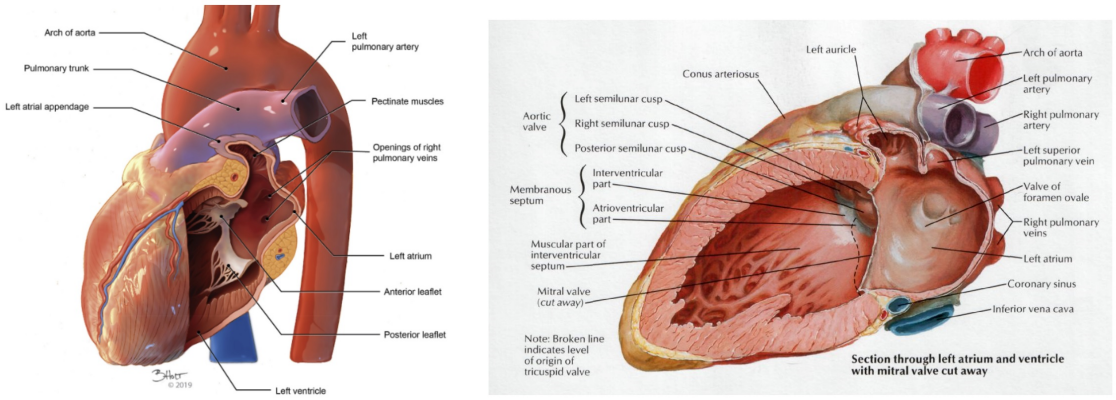

Figure 2.4. Anatomical structures of LA and surrounding structures. On the left, general attributes of the left atrium (Illustration by Brandon Holt ©2019, provided under CC-BY–NC–ND, retrieved from [49]). On the right, section with the detailed description of anatomical structures of LA and general structures of the junction between LV and LA, as well as structures delimiting LA (retrieved from [52]).

to this chamber and its different structures [46].

The RA and LA are separated by the obliquely positioned inter-atrial septum [47]. This left chamber is characterised by its cuboidal shape enclosed by anterior, left lateral, medial, posterior and superior walls. Posterior to the pericardial sinus, which is behind the aortic root, obliquely due to the terminal ends of the pulmonary veins at the posterior wall, the anterior wall is found [46, 47]. Behind the aorta, the atrial wall is notably fragile, something to consider when ablating with a catheter [48], something important in the treatment of some atrial tachyarrhythmias – particularly in AFL. On the other side, the LA and LV are separated by the mitral AV [43].

In comparison to the RA, the LA is smaller, thicker and its walls hold three different opening: distally, the mitral valve; laterally, the left atrial appendage (LAA) and proximally, the pulmonary veins [46, 47]. Nevertheless, as the wall comes near to the mitral annulus, it narrows down [49].

Summarising the structure of LA chamber, its origin comes from the pulmonary veno-atrial junctions, delimited by a fibro-fatty tissue section, thresholding the atrioventricular junction at the mitral orifice [48, 49]. From the body of LA, there is an aperture to the LAA, which is smaller, slenderer and more curved than the one in the RA [47, 49]. Inferior and superior pulmonary veins pour blood into the LA which contains the aforementioned LAA on the lateral side, a septal portion and an inferior vestibule [46]. Besides, the left lateral ridge is plausible for ectopic foci to occur [50], treated by an ablation procedure. Note that ectopic foci are abnormal pacemaker sites that displace automaticity in the heart [51] – outside the sinoatrial node (SN).

An overall view of the anatomical structures that have been revised in this section can be observed in figure 2.4.

2.3. Activation and Electrical Activity of the Heart

2.3.1. Fundamentals of Heart Physiology

The heart cells are muscle cells organised in firmly bound slim layers composing the myocardium. When contraction occurs in the atria or ventricles, which is approximately once per second and three billion times in a standard lifespan, all these cells are activated [37, 53].

Innervation takes an essential place when addressing the activation of the heart cells. Sympathetic postganglionic fibres coming from thoracic and spinal nerves innervate both the atria and the ventricles releasing norepinephrine to the beta-adrenergic receptors on cardiac muscle [54]. In the case of the atria, muscarinic receptors for acetylcholine, which is innervated by parasympathetic fibres coming from vagus nerves, come across [55, 56]. A simple representation of this autonomic innervation process is described in figure 2.4.

The heart also needs supply for myocardial cells to perform the exchange of substances to carry out their metabolism. The coronary arteries, which exit from the first branch of the aorta (see figure 2.3), oversee supplying blood to myocardial cells, and the coronary sinus drain these venules and veins to the RA.

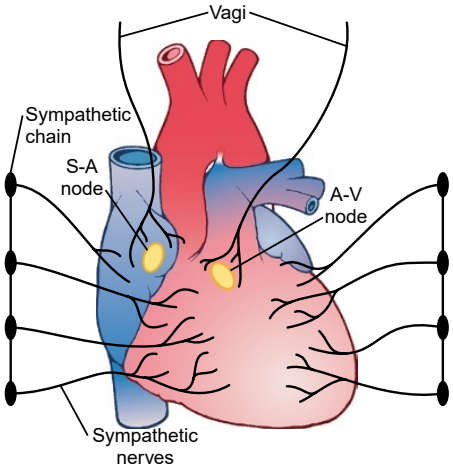

Figure 2.5. Autonomic innervation of the heart. Parasympathetic (vagi nerves) and sympathetic (thoracic and spinal nerves) excitation of the heart is represented (retrieved from [53]).

2.3.2. Cardiac Action Potential

The signal for contraction of the heart is originated in the autorrhythmic cells of the myocardium, which are noncontractile [57]. These cells are connected among them by intercalated disks which contain at the same time gap junctions that allow the rapid spread of depolarisation throughout a group of connected cells, including the contractile cells of the myocardium [58].

An action potential (AP) occurs when a threshold is reached entailing the quick depolarisation of the membrane potential of a specific cell, repolarising shortly af-

terwards. The resting membrane potential of myocardial contractile cells is closer to the equilibrium potential of K^+ (-90mV) than to the one of Na^+ (+60mV), being then more permeable to K^+ ion (see figure 2.6.A1-2). Thus, in the AP depolarizing phase, sodium ion entry is given by the opening of voltage-gated Na^+ channels, producing the cell depolarisation [58]. However, because of the low permeability of Na^+ in cardiac cells, the repolarisation is produced partially by transiently open K^+ channels, producing a characteristic plateau in the action potential of these cells. Autorhythmic myocardial cells are characterised by a pacemaker potential which is an unstable membrane potential due to the influx of positive charges caused by I_f channels [59]. The membrane permeability is in this way not constant for Na^+, K^+ nor for Ca^{2+} during this process, as represented in figure 2.6.A2.

In the case of myocardial cells, once membrane depolarisation occurs, voltage-gated Ca^{2+} channels (or L-type Ca^{2+} channels) open allowing Ca^{2+} ions to flow into the cell following their electrochemical gradient, balancing for a short period of time the flow of K+ ions out of the cell, entailing the previously mentioned characteristic plateau [60]. Finally, L-type Ca^{2+} channels are inactivated, and repolarisation occurs due to the K^+ efflux after the opening of K^+ channels in response to the previous depolarisation, stabilising the membrane AP shortly thereupon [59].

The force exerted by cardiac muscle when contraction occurs is not regular but graded depending on how much Ca^{2+} ions enter the cell. This process is regulated as Ca^{2+} entry triggers the release of more Ca^{2+} ions through the calcium-induced release in the sarcoplasmic reticulum [61, 62].

This AP directly depends on the cardiac innervation presented in the previous section, as the increase on the rate of the pacemaker depolarisation is caused by epinephrine and norepinephrine acting on β_1-receptors, leading to an increase on the heart rate. Conversely, a decrease in the heart rate is produced when muscarinic receptors are activated by acetylcholine, innervated by the vagus nerves of the parasympathetic system (see figure 2.5) [55].

Lastly, it is convenient to differentiate nodal cells of the conducting system from myocardium contractile cells in terms of their AP. These autorhythmic cells undergo a slow depolarisation in stead of a steady resting potential. This is known as a pacemaker potential, which continuously bring the membrane potential to the required threshold for the to occur (see figure 2.6.B1-2), reassuring a continuous heartbeat [60].

2.3.3. Heartbeat and Propagation of the Electric Signal

For an adequate pumping in both the pulmonary and systemic circulation, contraction of the atrium is required immediately before the contraction of the ventricle. This contraction is triggered by the depolarisation of muscle cells, connected by gap junctions that allow this AP to spread along the heart tissue [63, 64]. An initial

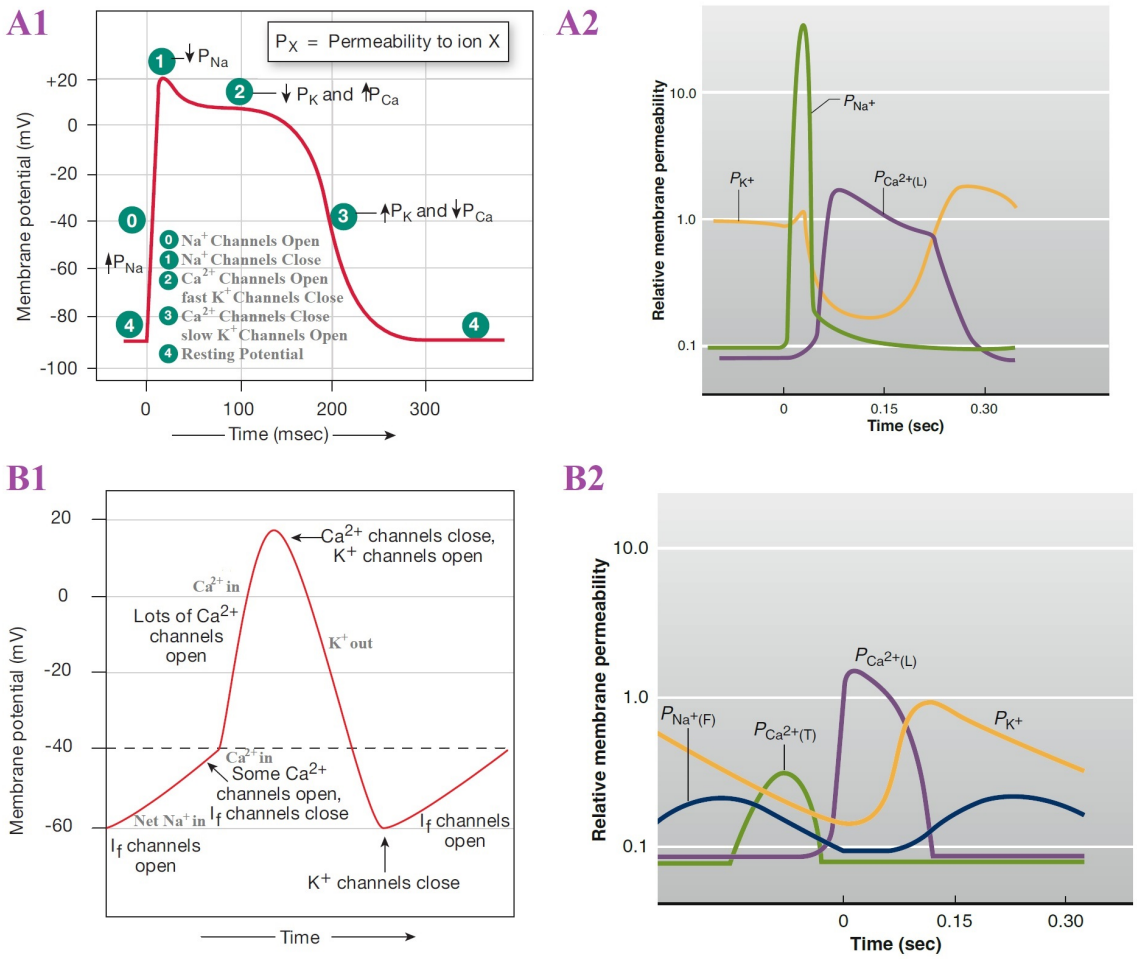

Figure 2.6. Membrane potential and ion permeabilities of cardiac autorrhythmic (A) **and contractile cells** (B). **A1**: Representation of the action potential of contractile cells of the myocardium and key changes of permeability of Ca^{2+}, Na^{+} and K^{+} ions. **A2**: Change of permeability of ions involved in the action potential of contractile cardiac cells over time. **B1**: Representation of the action potential of autorhythmic cells of the myocardium and key changes of permeability of Ca^{2+}, Na^{+} and K^{+} ions and in the funny current (I_f) channels. **B2**: Change of permeability of ions involved in the AP of autorhythmic cardiac cells over time. Created over figures retrieved from [37], [52] and [59]

depolarisation is required in order to spread the AP. The origin is the SN, from which the AP spreads over the atria and then into the ventricles.

The path that the AP conduction follows is important to understand physiopathologies of the heart [65] and how these bio-signals are detected and interpreted through the ECG and VCG, as it will be explained in later sections.

The pacemaker of the entire heart is, in healthy conditions, the SN, whose depolarisation entails the AP that generates the depolarisation of the other heart cells, coupled with the contraction of the myocardium – spread cell by cell through gap junctions [53, 66]. Thence, the heart rate, defined as the number of times that the heart contracts per unit of time, is determined by the SN's discharge rate [67].

Although the SN is located at the RA, the conduction occurs fast enough so that both atria are contracted at the same time. The spreading of such depolarisation continues to the ventricles from the atrioventricular node (AN), connecting both atria and ventricles. The conduction at this point is essential because it is characterised by an abnormally slow conduction of the AP, allowing atrial contraction to be accomplished before the excitation of ventricles. From the SN to the AN, internodal pathways serve for the AP conduction throughout the atria [64].

Right subsequent to the excitation of the AN, the propagation continues through the conducting-system fibres of the bundle of His along the interventricular septum. At the apex, it separates into left and right bundle branches, entering the pathways of low-resistance gap junctions through the Purkinje fibres, already in the walls of both ventricles [53, 64]. Rapid conduction at these fibres allows ventricles to contract synchronously, and a coordinated contraction of the heart overall. This whole process of the pathway of the AP is schemed in figure 2.7 in relation to the ECG signal that will be studied in the following section.

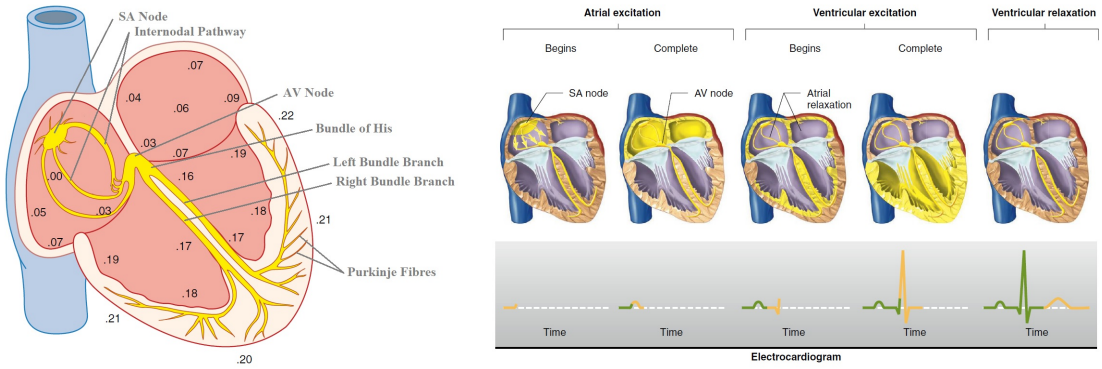

Figure 2.7. Scheme of the pathway that the AP follows in the process of activation of the heart. Left: Cardiac impulse transmission through the heart and time delay from the SN in fraction of seconds. SN, AN, internodal pathways, ventricular bundle branches and Purkinje fibres are depicted in a yellow path. **Right**: System of conduction of the heart in relation to the ECG signal formation and the phases of contraction and relaxation of atria and ventricles. Created over figures retrieved from [37] and [53]

2.4. Electrocardiography: Measuring the Electric Activity of the Heart

2.4.1. Historical Context and Fundamentals of the Surface ECG

By the end of 19$^{\text{th}}$ century, the fact that direct information about the heart could be obtained by measuring electrical activity through surface electrodes placed on the skin was discovered. The first ECG recorded from a human individual dates from 1887 [68], although the technique had to improve considerably before being used with clinical purposes.

One of the leading lights of this technique, well-known as the father of the modern ECG, is Willem Einthoven, who labelled the parts of the standard ECG signal and created the 'Einthoven's Triangle' [69], which is a hypothetical triangular geometry whose sides corresponds to the leads or pair of recording electrodes (an scheme is represented in figure 2.8). It would be located around the heart and where the electrodes are placed at both arms and the left leg. According to Einthoven's ECG system and his triangle, the leads are defined as [70]:

$$\begin{aligned} &\text{Lead } I: && V_I = \phi_L - \phi_R \\ &\text{Lead } II: && V_{II} = \phi_F - \phi_R \\ &\text{Lead } III: && V_{III} = \phi_F - \phi_L \end{aligned} \tag{2.1}$$

where,

$$\begin{aligned} V_I &= \text{Voltage of Lead I} \\ V_{II} &= \text{Voltage of Lead II} \\ V_{III} &= \text{Voltage of Lead III} \\ \phi_L &= \text{Potential at Left Arm} \\ \phi_R &= \text{Potential at Right Arm} \\ \phi_F &= \text{Potential at Left Foot} \end{aligned} \tag{2.2}$$

And, following Kirchhoff's 2$^{\text{nd}}$ law, the following relation can be established for Einthoven's limb leads:

$$V_{II} = V_I + V_{III} \tag{2.3}$$

Nonetheless, this was not conclusive. Goldberger added more limb leads by measuring the potential between a reference and a single lead, where the reference was the middle potential between the two other electrodes [71]. These leads are known as aVR, aVL aVF. Thus, the signal is augmented, reason why these three new limb leads are known as augmented leads. It has to be noticed that theoretically, Goldberger's augmented leads are completely redundant with respect to Einthoven's

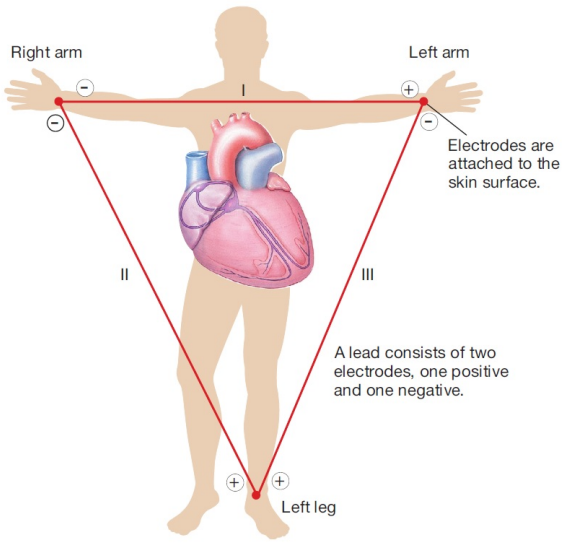

Figure 2.8. Representation of Eithoven's Triangle. ECG surface electrodes are placed in the three corners of the triangle, that is, both arms and the left leg. There are three leads: I, II and III, and each of them is comprised of a pair of ECG electrodes (retrieved from [59]).

limb leads (although they are useful because of their enhancement of the ECG signal), as the following relations are fulfilled:

$$\begin{aligned} aV_R &= \phi_R - \frac{\phi_L + \phi_F}{2} = -V_I + \frac{V_{III}}{2} \\ aV_L &= \phi_L - \frac{\phi_R + \phi_F}{2} = V_I - \frac{V_{II}}{2} \\ aV_F &= \phi_F - \frac{\phi_R + \phi_L}{2} = V_{III} + \frac{V_I}{2} \end{aligned} \tag{2.4}$$

It was in 1944 when Wilson, trying to measure the potential difference nearer to the heart, introduced the so-called precordial leads, represented as V1, V2, V3, V4, V5 and V6, located on the left area of the chest [72]. With these six and the previous ones, a system of 12-leads that is still used nowadays. Although some can be derived from the others, this system is still used as it improves the pattern recognition offering different projections of vectors in orthogonal planes.

2.4.2. Measuring the Electric Activity of the Heart: ECG Features

The standard ECG (see figure 2.9) is comprised of different features related to the cardiac activity that have been mentioned in previous sections. The three main components are the P wave, the QRS complex, composed of the Q, R and S waves, and the T wave.

Firstly, the P wave occurs during the event of atrial depolarisation, before the beginning of the atrial contraction. Right afterwards, caused by ventricles depolarisation, the QRS complex takes place, being both P wave and QRS complex, depolarisation waves. When ventricles recover, repolarisation or T wave takes place.

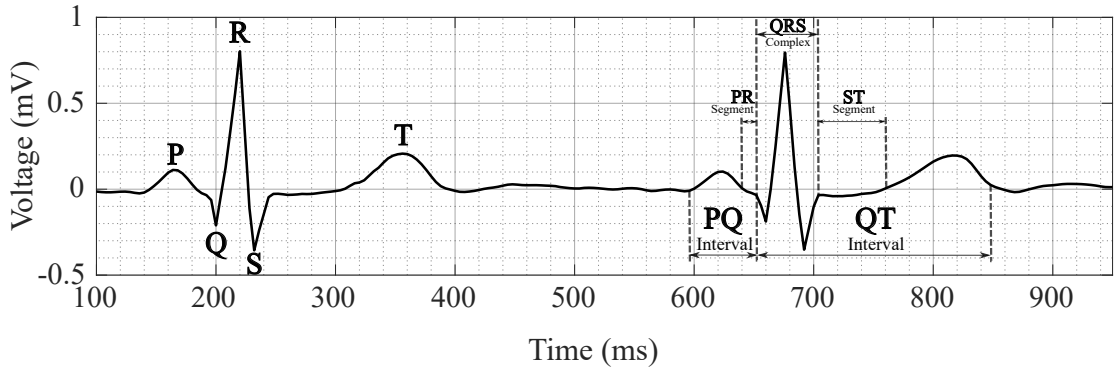

Figure 2.9. ECG Signal from a healthy patient. The representation is not ideal since it has been processed from a healthy patient (low and high pass filtered). P, Q, R, S and T waves are represented on the left beat and PQ and QT intervals, PR and ST segments and QRS complex are labelled on the right beat.

Depolarisation needs to be spread all throughout the atria or ventricle so that the muscle undergo contraction. Thus, the P wave occurs at the very beginning of the atrial contraction step, and similarly, the QRS complex takes place when ventricles begin contraction. Furthermore, the ventricles remain in this state until the end of the T wave, that is, the end of depolarisation, when they relax. In a similar way, the atria repolarise shortly after the end of the P wave. Hence, it overlaps to the time at which the QRS complex occurs, so in the standard ECG in normal conditions, the known as atrial T wave cannot be observed.

The value of the voltage in the output signal of the ECG depends on how the electrodes are attached to the body and how near they are placed with respect to the heart. This value oscillates for the QRS complex between 1 and 1.5 mV – measuring the amplitude from the lowest point at the R wave, to the highest as the S wave. In the case of the P wave, the voltage amplitude usually oscillates between 0.1 and 0.3 mV, and finally, for the T wave, it goes from 0.2 to 0.3 mV – note that these values are given for the surface ECG [53].

Another interesting region to mention is the P-Q or P-R interval, which consists of the signal for the time constrained between the very beginning of the P wave and the initial point of the QRS complex. This interval corresponds to the time between the beginning of the atrial and the ventricular excitation. This interval is well known as P-R interval because the Q wave is absent in a great number of cases.

Similarly, the Q-T interval is also known as the signal spanned from the beginning of the Q wave and the end of the T wave. Thus, it begins once the ventricular contraction is over. In cases in which the Q wave is absent or not well defined, this region can be taken from the R wave. The relation between the ECG signal and the cardiac cycle was already introduced in figure 2.7.B, but a more detailed illustration that painstakingly represents all the features described in this section in relation to the cardiac cycle is depicted in figure 2.10.

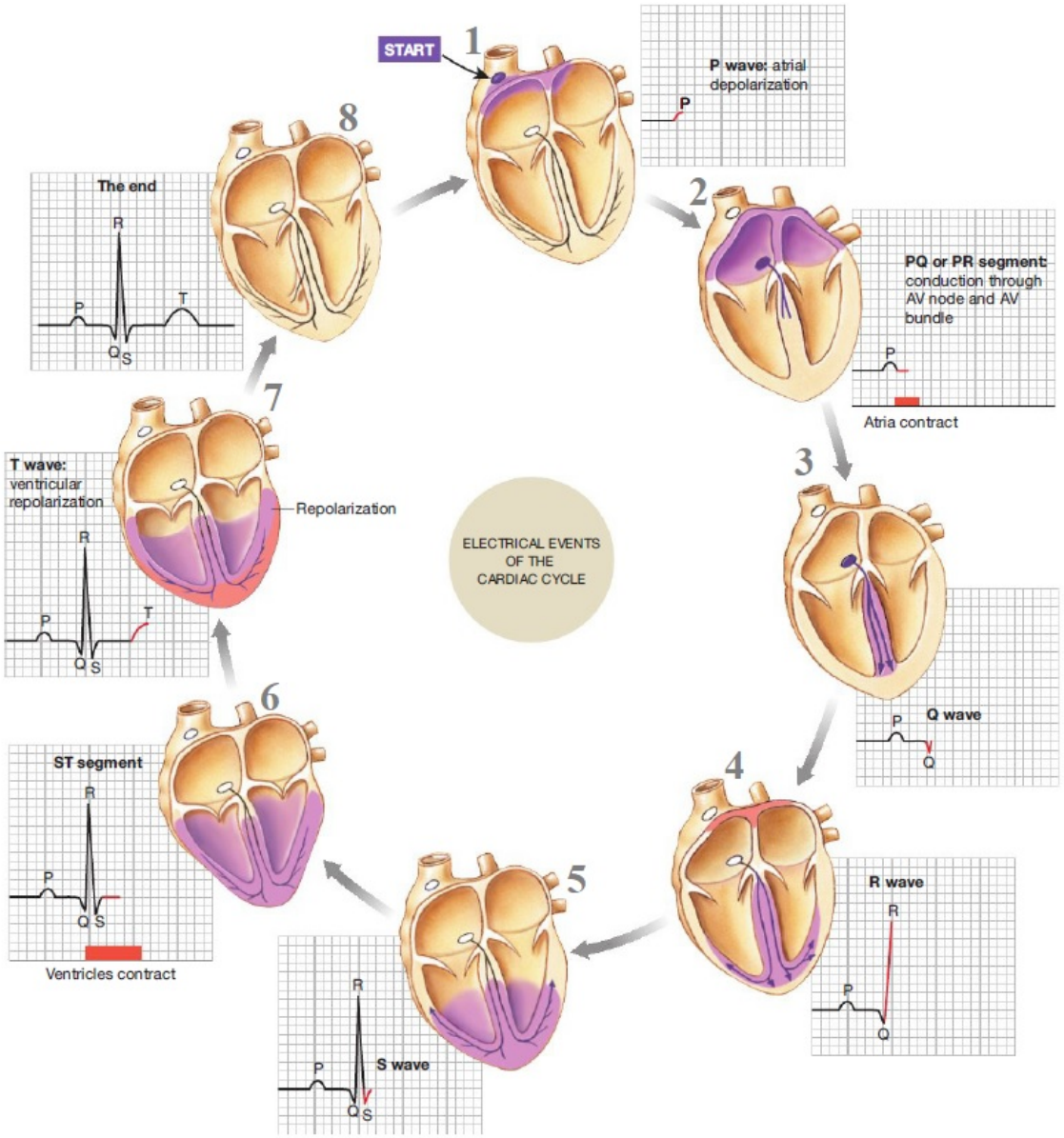

Figure 2.10. Illustration of the relation between the events in the cardiac cycle in terms of the electrical activity, and the principal features of the ECG signal. 1: Origin of the signal in the SN. **2:** Conduction throughout the atria and the AN, corresponding to the formation of the P wave, **3:** Conduction through the Bundle of His and Q wave, **4:** spread of the electrical signal through the ventricular walls, beginning of the R wave, **5** and **6:** spread of the signal throughout the ventricle, followed by ventricle contraction, finishing the QRS complex and the ST segment, **7:** Ventricles repolarisation and creation of T wave, and **8:** Recovering period between T and P waves (created from a figure retrieved from [59]).

2.5. Vectorial Analysis of the Electric Signal

2.5.1. A Vector that represent an Electric Potential

A vector is represented by an arrow that has a direction at which it points. In this case, the direction is given by the electric cardiac potential, which is generated by the current flow, and whose length is proportional to the magnitude of the voltage difference of the potential.

To understand how a vector can represent an exact moment in the cardiac cycle, an example is used illustrating the way it works. At the instant of heart excitation at which the depolarisation of the ventricular septum occurs (see shaded area in figure 2.11), electrical current is flowing from depolarised areas inside the heart to non-depolarised areas. As an overall, the current is flowing toward the apex, coming from the ventricular base. Therefore, the instantaneous mean vector, that is the result of the summation of vectors generated by this potential at the given instant, will go in the direction of that points the apex. This example is clearly illustrated in figure 2.11, where the vector is drawn large because of the considerable amount of current and the large potential. Note that there would also be an upward component, but it is not particularly noticeable taking into account the intense current flow in the downwards direction.

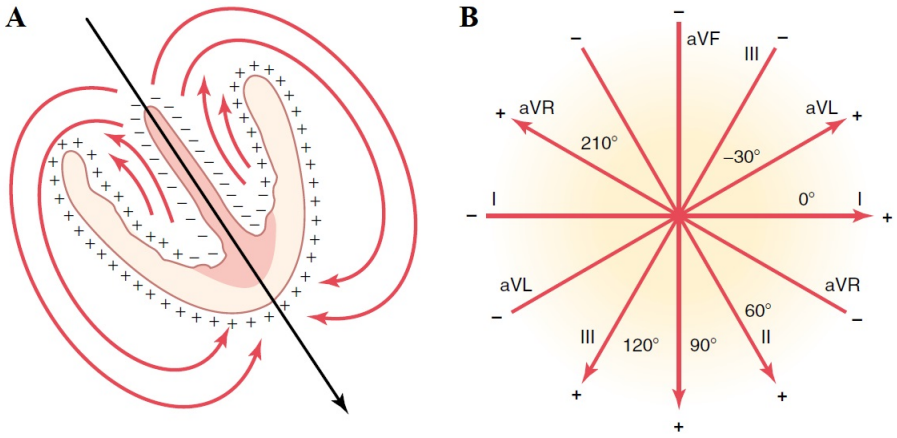

Figure 2.11. Mean vector representing the potential difference and current flow at the an instant of depolarisation and standard directions of mean potential vectors in relation to leads I, II, III, aVR, aVL and aVF A: Mean vector representing the potential difference and current flow at the the instant of depolarisation of ventricular septum and some parts of the apical endocardial walls in both ventricles. **B:** Standard directions of mean potential vectors in relation to leads I, II, III, aVR, aVL and aVF. Note that 0º corresponds to the left part of the chest as in anatomical drawings the standard is represented mirrored (created from figures retrieved from [59]).

These vectors are given a label according to their direction, which has been standardised and is worldwide used to better understand their meaning. Towards the individual's left side, the direction is 0 degrees, and downwards would correspond to positive 90 degrees, being upwards either positive 270 or negative 90 degrees (see figure 2.11.B). In this standard system, the mean QRS vector corresponds to the direction +59 degrees.

Thus, the leads can also be expressed in these directions, corresponding to 0º, +60º and +120º for leads I, II and III, and to +90º, +210º and +330º (or -30º), for leads aVF, aVR and aVL correspondingly. The mean QRS vector has almost the same direction as lead II, reason why this lead is usually used for the representation of the cardiac signal (as in figure 2.9). All these directions are summarised in figure 2.11.B. which illustrates the leads and representative directions (taking into account the sense of the vectors), being the left direction the right part of the body, as anatomical drawings are usually represented.

2.5.2. Vectorial Analysis of the Cardiac Cycle and Relation to the ECG Signal

In order to understand the VCG that will later be explained in this section, this subsection is used to understand the vectorial analysis of the first three leads in the ECG signal throughout the cardiac cycle. Figure 2.12, used as a reference and the golden standard to follow this subsection.

2.5.2.1. Vectorial Analysis of the QRS Complex

Beginning with the QRS complex that corresponds to the entrance of the electrical signal to the ventricles, there is a fast spreading of the depolarisation at the endocardial surfaces of the septum (see figure 2.12.A left). At this point, the instant represented by the vectors is approximately 0.01 seconds right after the beginning of the depolarisation of the AN. Since a small region of the whole ventricles is depolarised (just the septum), the voltages are low and small vectors appear in the first three leads. Vector in direction of lead II is considerably bigger as it coincides better with the direction of the current flow through the septum. The magnitude of the three vectors appears in the graph (figure 2.12.A right) as a positive voltage increment – positive because of the sense of the vectors.

After this event, the depolarisation spreads throughout the rest of the ventricles, more in detail, over the endocardial surfaces, as observed in the shaded region in figure 2.12.B-C. In this case, for the first part of the depolarisation of the endocardial surfaces, at around 0.02 seconds after the depolarisation's onset (figure 2.12.B), the mean vectors are longer because of the great increase in the coverage of the electric signal, related as a consistent increment in the voltage of the three leads, specially for lead II. By the second part (figure 2.12.C), at second 0.035, vectors are shorter and so is voltage increment because of the heart apex being electronegative, contributing to the neutralisation of the positive charges at the other epicardial surface. Also, there is a shift for the axis of the vector, in this case towards the left side, so the increment in lead I is significantly bigger than in lead III, and all of these increments are reflected as voltage increments in the ECG signal for the three leads (figure 2.12.C. right).

Finally, the impulse goes through the ventricular muscle to the outside of the heart, travelling through the muscle (see figure 2.12.C-E). Firstly, at about 0.05 seconds following the beginning of depolarisation (figure 2.12.D), the impulse goes towards the base of the ventricles generating a short vector due to the minor part of positive charges ongoing. The direction is then negative for both leads II and III and positive for lead I, so the ECG goes below zero for the second and third leads (figure 2.12.D right). In the last step of the QRS complex (figure 2.12.E), 10 after the last illustration, no current flows and no potential is generated due to the overall depolarisation. Thus, the vector becomes zero and all the three leads come to the baseline at 0 mV.

2.5.2.2. Vectorial Analysis of the T Wave

After the QRS complex and the consequent depolarisation of the ventricle, the repolarisation takes place, from about 0.15 until 0.35 seconds after the onset of depolarisation (figure 2.12.G).

The first area undergoing repolarisation corresponds to the outer surface of the ventricles, being the endocardial areas the last in repolarising. This sequence is given by the pressure that ventricles undergo during contraction, which decreases the endocardium's blood flow, slowing the depolarisation process in endocardial areas. Thus, given that the outer walls repolarise before the inner surfaces, the mean ventricular vector usually points towards the apex (see middle figure 2.12.G). The process of creation of the T wave can be divided in five steps (see figure 2.12.G right), where at each step, the vector is relatively small at the beginning because of the small area of repolarisation, and larger in the middle when increasing the repolarisation regions, becoming weaker again towards the end.

2.5.2.3. Vectorial Analysis of the P Wave and Atrial T Wave

As previously discussed, P wave comes as the result of the depolarisation of the atria, beginning the depolarisation in the SN and spreading in all directions until reaching the AN. Thus, the origin of the vector is the SN and the direction is approximately towards the AN (see figure 2.12.F left), being maintained as the average of conduction directions almost through the spread of the signal throughout the whole cavity. Besides, this direction is positive in the three leads, so it is registered in the ECG as positive voltage variation in all I, II and III leads – being in the latter the smallest as having the least contribution to the vector (see figure 2.12.F right).

The process of depolarisation and spreading of the AP through the atria is significantly slower than in the ventricles as the Purkinje fibres are missing in the first one. Thus, repolarisation occurs first in the SN, that was firstly depolarised. Hence, the vector in this case points backwards (as the SN would be positive with respect

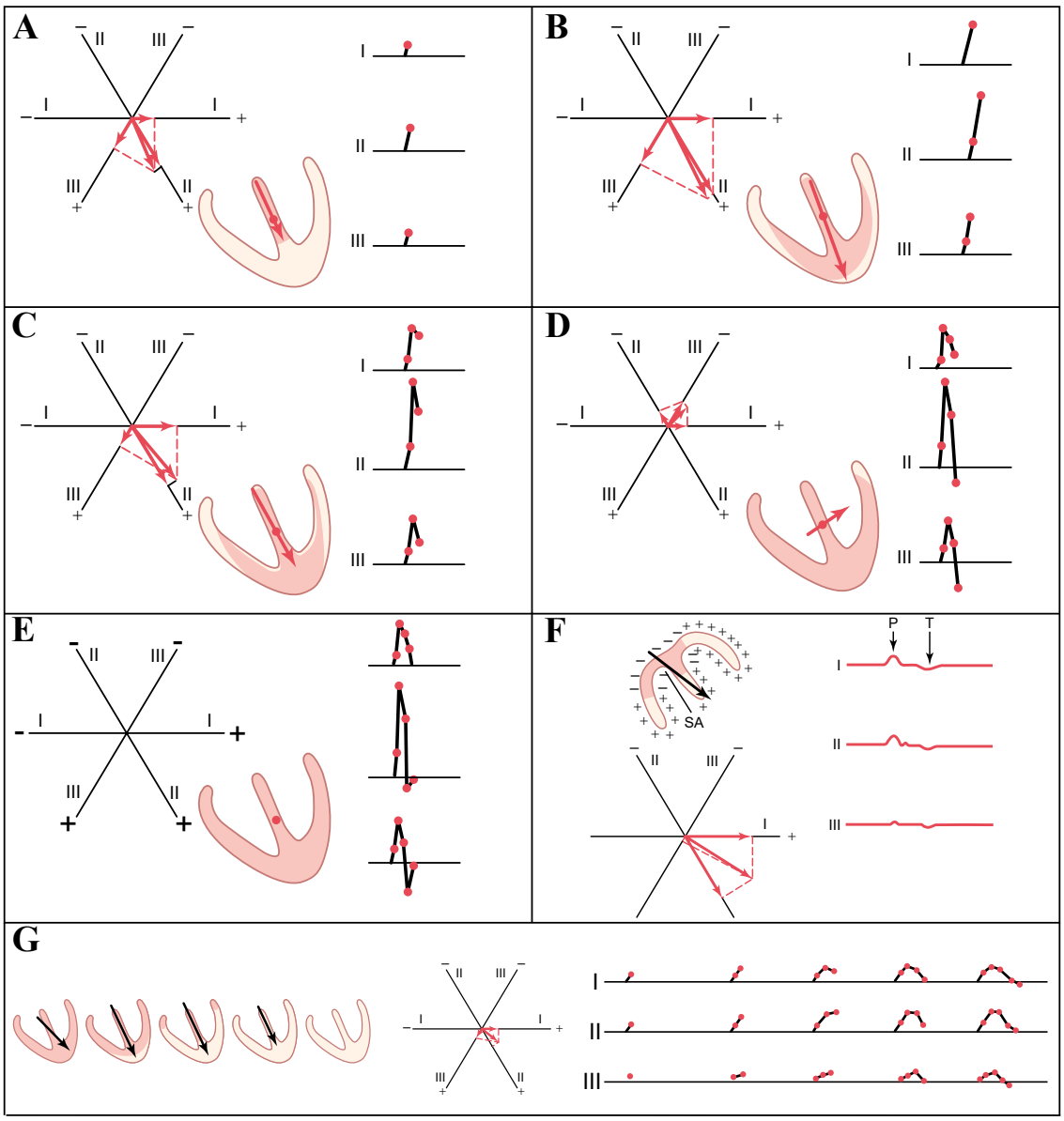

Figure 2.12. Evolution of the Vectorial representation and its corresponding voltage variation for lead I, II and III over the cardiac cycle. A: Beginning of the QRS complex that corresponds to the entrance of the electrical signal to the ventricles and the fast spreading of the depolarisation at the endocardial surfaces of the septum. **B-C:** Depolarisation spreads over the endocardial surfaces of the ventricles. **D-E:** The impulse travels throughout the ventricular muscle to the outside of the heart. **F:** Depolarisation of the atria (P wave) and repolarisation (atrial T wave). **G:** Repolarisation takes place, from about 0.15 until 0.35 seconds after the onset of depolarisation. (created from figures (adapted and complemented) retrieved from [59]).

to the atrial muscle at that moment), having the opposite effect than the one in the ventricles, so the contribution to leads I, II and III is a negative variation of the voltage (see figure 2.12.F right). However, this phenomenon is not observed in the ECG as it occurs at a similar time as the QRS complex, so in case of desiring to observe it, different techniques should be applied to extract the atrial contribution to the signal or suppress the ventricular one.

2.6. The Vectorcardiogram

2.6.1. Fundamentals

In the previous subsection of the section it has been described how the analysis of the mean vector representing the direction of the electric current is observed and corresponds to the voltage changes in the different leads.

It has been clearly observed how this vector of current flow changes in both magnitude and direction during the cardiac cycle. The VCG represents the changes in the direction and magnitude of this vector, creating a path that is not the path of the current flow [73], but the path of the changing vector created by the influence of this potential (see a scheme in figure 2.13).

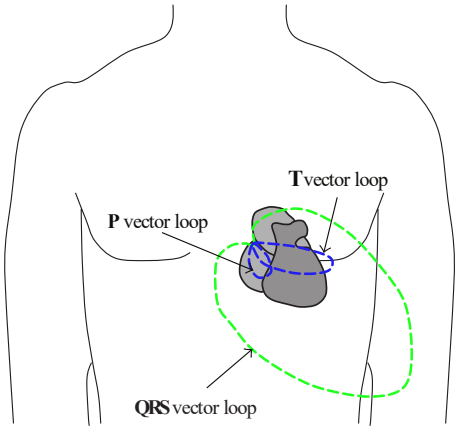

Figure 2.13. Illustration of the representation of the electrical potential variation of the heart through the VCG over a drawing of the heart and chest of a human individual. The small blue elliptical shapes illustrate the P and T waves VCG representation, and the green elliptical shape the QRS complex VCG representation (figure created over a figure retrieved from [74]).

The VCG of a normal cardiac cycle has a zero-reference point between beats since, although the cardiac muscle is still polarised, there is not vectorial electrical potential at this point [75]. Note that it will not stay long at this point because, as soon as the atrial depolarisation begins or lather the ventricular depolarisation, it will grow in the corresponding direction.

In the case of the QRS complex, as previously mentioned, the vector will quickly extend throughout the apex, growing towards left side, as represented in the vectors at figure 2.14.

Therefore, three loops are easily recognised in this representation of the electrical activity of the heart, corresponding to the P wave, the QRS complex and the T wave. The QRS complex is relatively bigger and has a characteristic elliptical shape. It is possible to record the VCG signal directly in an oscilloscope by connecting surface electrodes from the neck and lower abdomen regions to the vertical plates of the oscilloscope, and the chest electrodes to the horizontal [77].

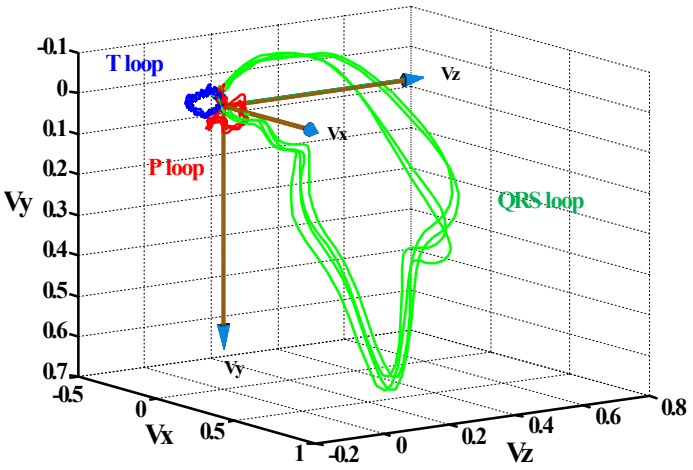

Figure 2.14. VCG representation of a healthy patient over several heart beats, highlighting the P and T waves VCG representations (red and blue respectively) and QRS complex VCG loop (green loops). The vectorial axis in brown with blue ends illustrate the standard representation of the VCG coordinated. (Figure created modifying a figure from [76]).

2.6.2. The derivation of the VCG: Frank's Leads System and The Inverse Dower Transform

It was in 1956 [78] when E. Frank published a VCG lead system with grounds on his previous works on this field [79]. The model was created based on a homogeneous thorax from a human individual and, to measure the dipoles, at least four electrodes were needed – being the fourth the ground or reference. In his model, Frank used up to seven electrodes to decrease the error – in terms of variation of anatomical sizes and locations. Hence, he designed a lead system (the well known 'Frank's lead sytem') yielding to corrected orthogonal leads.

As it has been previously explained, the VCG allows to record the direction and magnitude of electrical forces that lead the heartbeat in terms of a progression of vectors generating curved lines over a central point. Frank's leads provide a method to obtain the 3D representation of such electrical potential with the right-left axis (X), head-to-feet axis (Y) and anteroposterior axis (Z) [78].

Thus, the orthogonal projections generated over the cardiac planes obtained by Frank's method conduces to the frontal, horizontal and sagittal projections of the 3D VCG loop. The frontal corresponds to axes X and Y, the horizontal to X and Z and the sagittal to Y and Z (it is standardised to invert the Y axis for representation purposes) [78]. No figure is included to illustrate this as in the methods, results and discussion sections plenty of figures are depicted following this representation scheme.

To compute Frank's lead X, Y and Z from the standard lead system, that is, to compute the VCG from the ECG signal leads, the IDT is widely used, which follow the next expression [80]:

$$\begin{cases} \text{X} = - & (-0.172\text{V1} - 0.074\text{V2} + 0.122\text{V3} + 0.231\text{V4} + 0.239\text{V5} + 0.194\text{V6} + 0.156\text{DI} - 0.010\text{DII}) \\ \text{Y} = & (0.057\text{V1} - 0.019\text{V2} - 0.106\text{V3} - 0.022\text{V4} + 0.041\text{V5} + 0.048\text{V6} - 0.227\text{DI} + 0.887\text{DII}) \\ \text{Z} = - & (-0.229\text{V1} - 0.310\text{V2} - 0.246\text{V3} - 0.063\text{V4} + 0.055\text{V5} + 0.108\text{V6} + 0.022\text{DI} + 0.102\text{DII}) \end{cases} \quad (2.5)$$

Thence, the instantaneous cardiac vector is computed from these scalar coordinates, generating the VCG loop for each heartbeat.

2.7. Atrial Tachyarrhythmias and their Electrophysiological Foundations

There is a wide assortment of classifications for cardiac arrhythmias [81]. One common strategy is discerning according to their origin, finding atrial, ventricular and atrioventricular arrhythmias. The most interesting case for this dissertation is , but atrial tachycardia (AT) and atrial fibrillation (AF) will also be introduced to have a wider a more general contextualisation of the problem from the physiological and electrochemical point of view.

In general, atrial tachyarrhythmias occur when the electrical signal of the atria starts in an uncommon location and rapidly repeats the atrial beat, following or not a path or patron known as macroreentrant circuit MC [82].

2.7.1. Atrial Tachycardia

The mechanisms that originate the AT may be variegated, so two different types are well distinguished depending on this parameter: reentrant AT and automatic AT.

The MC variation is characterised by a repetitive response coming from a reentry, which is a region that permits the perpetuation of the reentrant circuit for the electrical signal along the atria. The other case is the automatic class, in which the AT is caused by at least one ectopic focus, whose automatism is more rapidly activated than in the SN [83].

There are different distinctive traits of AT that can be studied from ECG signals. Firstly, P waves tend to have uncommon shapes due to their dependence of the ectopic foci. The heart rate is usually elevated with respect to the normal state, existing the possibility of reaching 220 beats per minute (bpm). Normally P waves (either one or several) are followed by the QRS complex, except when blockages appear, and the ST segment is abnormal in some cases. An example of two leads of an ECG signal from a patient suffering from a multifocal atrial tachycardia is displayed in figure 2.15 [84].

2.7.2. Atrial Fibrillation

AF is the most frequent cardiac arrhythmia with a high prevalence nowadays specially in elder population. It has been during latter history one of the widest fields in research in cardiology. It is mainly characterised by an irregular cardiac

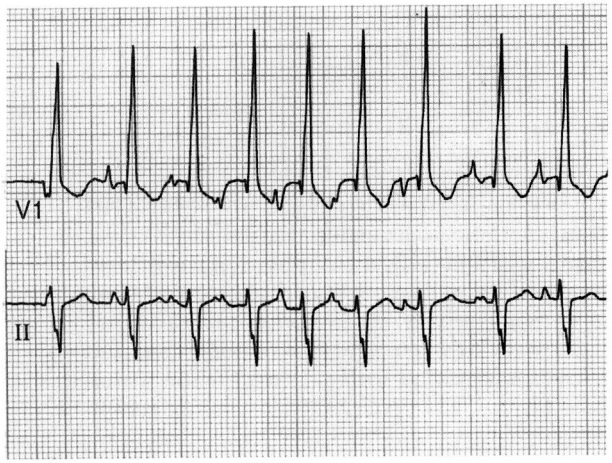

Figure 2.15. Representation of lead II and V1 from a patient suffering from multifocal AT (figure retrieved from a clinical study of multifocal AT [84]).

rhythm caused by a non-regular atrial activation.

In terms of pumping characteristics, bare active pumping from the atria would be recorded in a patient suffering from AF, although blood would passively flow through the atria to the ventricles, experiencing a decrease of about 25% in the output blood volume [37].

The electrocardiogram in AF is also interesting to study, being described by several minor depolarisation waves that spread in all directions in a chaotic manner. Because of the randomness of these waves, there is a high chance of them to cancel in couples, thus cancelling in many occasions the P waves. On the other hand, QRS and T waves would not be completely abnormal with just small variations as they are mainly produced by ventricular activation and repolarisation [85].

Furthermore, impulses arriving form the atrial muscle at the AN are rapid and irregular when atria are found to be fibrillating. Moreover, the AN will not send the impulse until 0.35 seconds after the previous one, an additional variable interval may occur before the following QRS complex appears, causing irregularities in the cardiac pace. See in figure 2.16 a representative example of the ECG signal of a patient suffering from AF [86].

2.7.3. Atrial Flutter

AFL has a very characteristic ECG waveform with uniform and regular wave shape. Physiologically, AFL is described by a MC, which consists of a circular or elliptical activation (known as reentry) conduction over a large obstacle (up to centimetres). Thus, it is not the same as the other tachyarrhythmias as the electrical signal advances in a particular direction over the path of the MC repetitively.

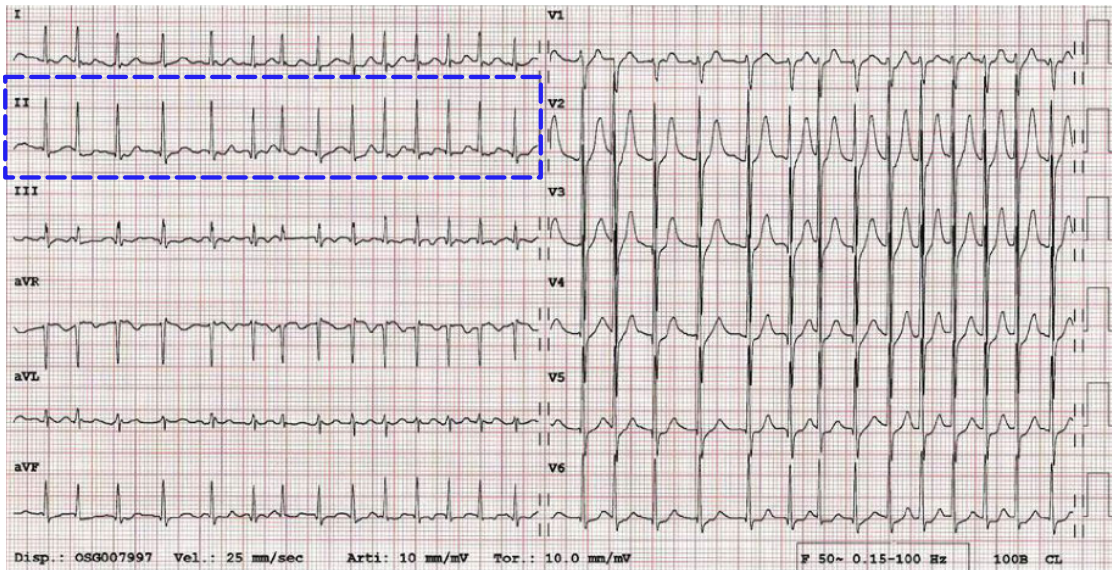

Figure 2.16. Representation of the 12-lead ECG from a patient suffering from AF. The most representative lead according to the explanation in this section is lead II, where it can be clearly seen how P wave does not appear and QRS complex and T wave are barely variant from the signal of a healthy patient (see figure 2.8). It can be observed (not only in II but in all the leads) how heartbeat is not constant – see for example the variant distance between QRS peaks. This figures has been extracted from a AF clinical study [86]

2.7.3.1. Electrocardiographic Signal of AFL

There is a classification scheme in AFL types which defines where the AFL occurs and the way in which the treatment would be applied to cure the condition. Typical or common AFL is the most frequent class, taking place in the RA [87]. It is also known as peri-tricuspid as is happens around the 'obstacle' of the tricuspid valve, which defines the MC. The rest of types are known as atypical, happening around a wide variety of obstacles along the atria, being the most common in this other type the perimitral AFL, whose obstacle defining the MC is the mitral valve [88].

Common AFL is physiologically caused by a rotational activation at the RA, occurring in about 80% of the AF cases. In anatomical terms, it is bounded by the venae cavae that happens to be the obstacle around which the MC is located, and the crista terminalis [89]. One of the key distinctions of this AFL type is that the electrical signal along the circuit necessarily passes between the lower tricuspid ring and the inferior vena cava, that is, it crosses the CTI, a key region for this type as will be seen later in this section.

The ECG signal of common AF is especially characterised by the 'sawtooth' pattern in leads II, III and aVF. The morphology of these waves consists of a complex segment that goes downward in a slowly manner, that continues with a negative deflection that quickly changes to positive linking to the next atrial cycle. The rate is usually in the range of 150 to 320 bpm. An example of a ECG signal from a common AFL case is depicted in figure 2.17 [88].

Figure 2.17. Leads I, II, III, aVR, aVL and aVF from an ECG signal recorded from a patient suffering from typical or common AFL. Ventricular activity has been blocked in the middle region to clearly observe the atrial wave. Leads II, III and aVG have been enclosed in a red box to highlight the characteristic 'sawtooth pattern'. Figure created over a figure retrieved from [90]

Sometimes, the pattern can be hardly recognised when atrioventricular conduction is 2:1, meaning two atrial beats per ventricular. In higher conduction ratios the pattern is more easily recognised.

In cases in which the sense is CCW, positive waves would be produced in lower leads, also with a 'sawtooth' pattern, in this case with a W shape, specially observed in lead V1 (Figure 2.18). These can also appear as obstacles. Other common obstacles are the pulmonary veins and the mitral ring.

For the cases of atypical AFL, the macroreentry occurs around a wide variety of obstacles in any of the atria. The AFL happening on the right atria is usually related to a structural disease at this chamber of the heart, either congenital or because of a previous surgery. For the cases of LA, the disease appears associated to an alteration of the atrial myocardium. In this case there are common regions known as electrically silent areas, where impulse is not transmitted. The latter is very common in atypical cases, producing the AFL type known as perimitral AFL [88].

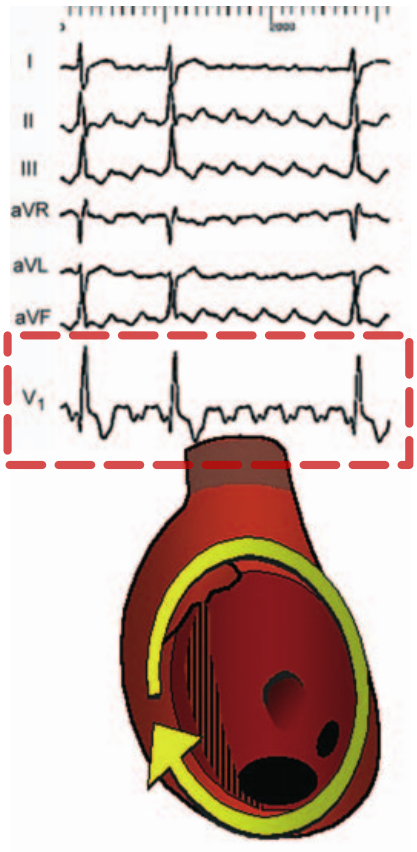

Figure 2.18. Leads I, II, III, aVR, aVL, aVF and V1 from an ECG signal recorded from a patient suffering from reverse or CCW AFL. V1 lead is placed inside a red box to highlight the double negative waves in an 'W' shape characteristic from this AFL type. In leads II, III and aVF, a similar 'sawtooth' feature as the one found in figure 2.17. is observed, although significant negative deflections are present. Figure created based on a figure extracted from [88]

For all these cases, both CW and CCW direction of conduction may appear. The ECG may be variegated for these cases, but always producing the characteristic repetition of atrial beats within QRS complexes as explained before for common or typical AFL.

2.7.3.2. AFL Treatment: Catheter Ablation

The most common treatment for AFL is the catheter ablation after mapping and performing an electrophysiological study of the atrium where the AFL occurs. The technique consists in ablating the tissue between two non-conducting anatomical structures via radiofrequency or cryoablation. In the case of typical AFL, the ablation is performed on the CTI, between the tricuspid valve and the venae cava, two non-conducting anatomical structures. Note that ablating means burning the tissue cells up to a point in which their structure is maintained at their place but no conduction occurs through them [79].

When the target is clear, the procedure takes place, being oriented by the reference multipolar catheter that records the activation sequence, and a steerable catheter used for mapping. Both serve as reference to perform an electrophysiological study and a map of the atrium with time reference and voltage difference in real time between the different poles of the catheters. For common AFL it may not be necessary, but when having several circuits at the same time because of anatomical abnormalities or previous surgeries, this process is necessary nowadays. The process of ablation is represented in two of its variations in figure 2.19. In most of the cases used in this dissertation, the first technique (radiofrequency ablation) has been performed.

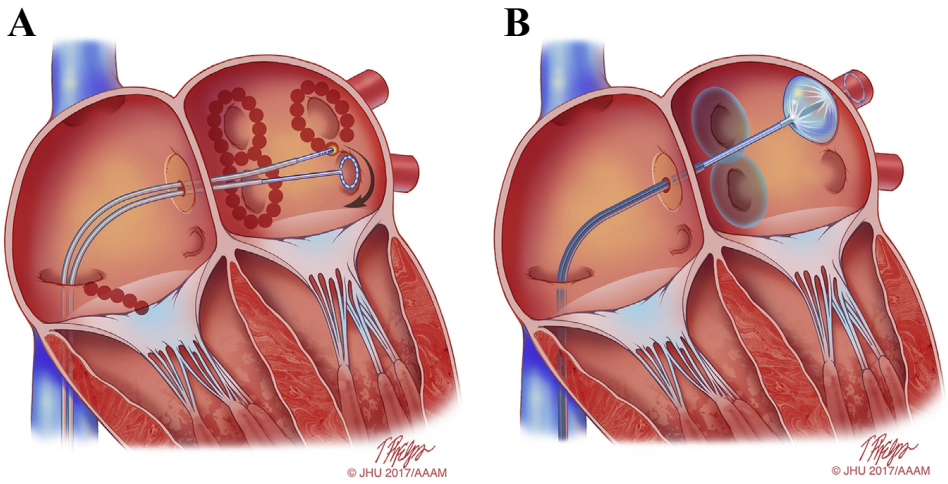

Figure 2.19. Schematic drawing illustrating catheter ablation of AF or AFL by radio frequency energy or cryoballoon ablation. A: Shows the lesion area after ablation in the CTI (RA, common AFL) and in circles around the left and right periveins. Note also that there is a multielectrode catheter to record and map the atria, located in the picture at the left interior perivein. **B:** In this case the ablation procedure is performed through a cryoballoon system. Here, the ablated area corresponds to the right periveins in the LA and the ablation catheter is placed by the left superior perivein. Illustration: TimPhelps © 2017 Johns Hopkins University ,AAM [79]

3. MATERIALS

In this study we used a geometrical model, which allows us for a full control and parametrisation of the 3D loop described by the vector and the location of the slow conduction regions. A synthetic VCG generator was designed base on this mathematical model to support the methods being used for the analysis and the hypothesis stated. This entails the creation of a large synthetic database which will be used as materials for the application of different methodologies.

With the objective of obtaining the vectorcardiographic representation of the atrial activity of patients suffering from different types of AFL, ECG signals from these patients were also needed.

Several cardiologists from 'La Paz' Hospital in Madrid collaborated in the project and provided ECG signals from 35 patients. From those, there were 11 patients suffering from common AFL of which 4 were characterised by a CCW direction and 7 by a CW - as both senses have been differentiated as different AFL modalities in previous studies [91]. The other 24 cases were atypical AFL from which peri-mitral and other atypical cases were acquired. In this case, 10 were CCW peri-mitral, 4 were CW peri-mitral and 10 were included in the miscellaneous variety were right and left peri-veins, anterior and posterior wall, cavo-tricuspid isthmus and superior vena cava flutters were placed.

Nonetheless, to have an accurate signal coming from the influence of the disease of a specific AFL, cases from patients suffering for other illnesses that could affect the atrial signal were rejected. Thus, after this analysis, 2 cases of common CW AFL, 2 cases of peri-mitral CCW AFL, one case of peri-mitral CW AFL and one case of anterior mural wall belonging to the atypical miscellaneous group, were discarded.

All in all, four common CCW AFL, five common CW AFL, eight peri-mitral CCW AFL, three peri-mitral CW AFL and nine atypical miscellaneous AFL were considered for the analysis and production of results.

4. METHODS I. VCG ANALYSIS

4.1. Acquiring and Processing the ECG Signal

Various methods to suppress ventricular activity have been developed in research [92]. One of the latest and most common nowadays consists of the analysis of Blind Source Separaction (BSS) using the principal component analysis (PCA) or independent component analysis (ICA) from the ECG signal, extracting the atrial contribution to the signal [93, 94]. Although these methods have been quickly developed and its robustness has been proved [95], for this experiment a physiological treatment has been included in the protocol that has been established in the data acquisition.

Adenosine was administrated to the patients during the physiological treatment by the cardiologists to suppress ventricular activity and record ECG signal during various seconds without ventricular influence. The representation of the standards 12-lead ECG signal of a patient suffering from common CW AFL is presented in figure 4.1. The heart is under the influence of adenosine from time 2 seconds until shortly after time 10 seconds (see figure 4.1.A). During that time, the ECG signal corresponds exclusively to the contribution of the atria (see figure 4.1.B).

ECG signals were processed with a 50 Hz notch filter to cancel out mains interference and a band-pass filtering process consisting of a high-pass Butterworth filter and a low-pass Chebyshev filter of eighth order. The band-pass was defined by cut-off frequencies of 0.5 and 60 Hz were used to reduce thermal noise and get rid of base line wandering [96]. Chebyshev filter is implemented bidirectionally to minimise transients of the filter.

4.2. Computation of the Patient's Representative Vectocardiogram

A VCG is created for every single patient. There are several mathematical transformations for the reconstruction of a VCG – in a conventional VCG Frank's orthogonal lead system - from a 12-leads electrocardiogram (ECG), including Kors quasi-orthogonal transformation, Kors regression transformation, linear regression-based transformations and IDT [97]. Due to its widespread trials to enhance vascular [98] or other clinical [99] diagnosis, in this study the IDT has been chosen with the purpose of deriving the VCG signal from a 12-leads ECG for each patient. This method is used to calculate the Frank's leads in a Cartesian space X, Y and Z (see eq. (2.5)) using the standard leads system [80].

From these scalar coordinates, the instantaneous cardiac vector is computed,

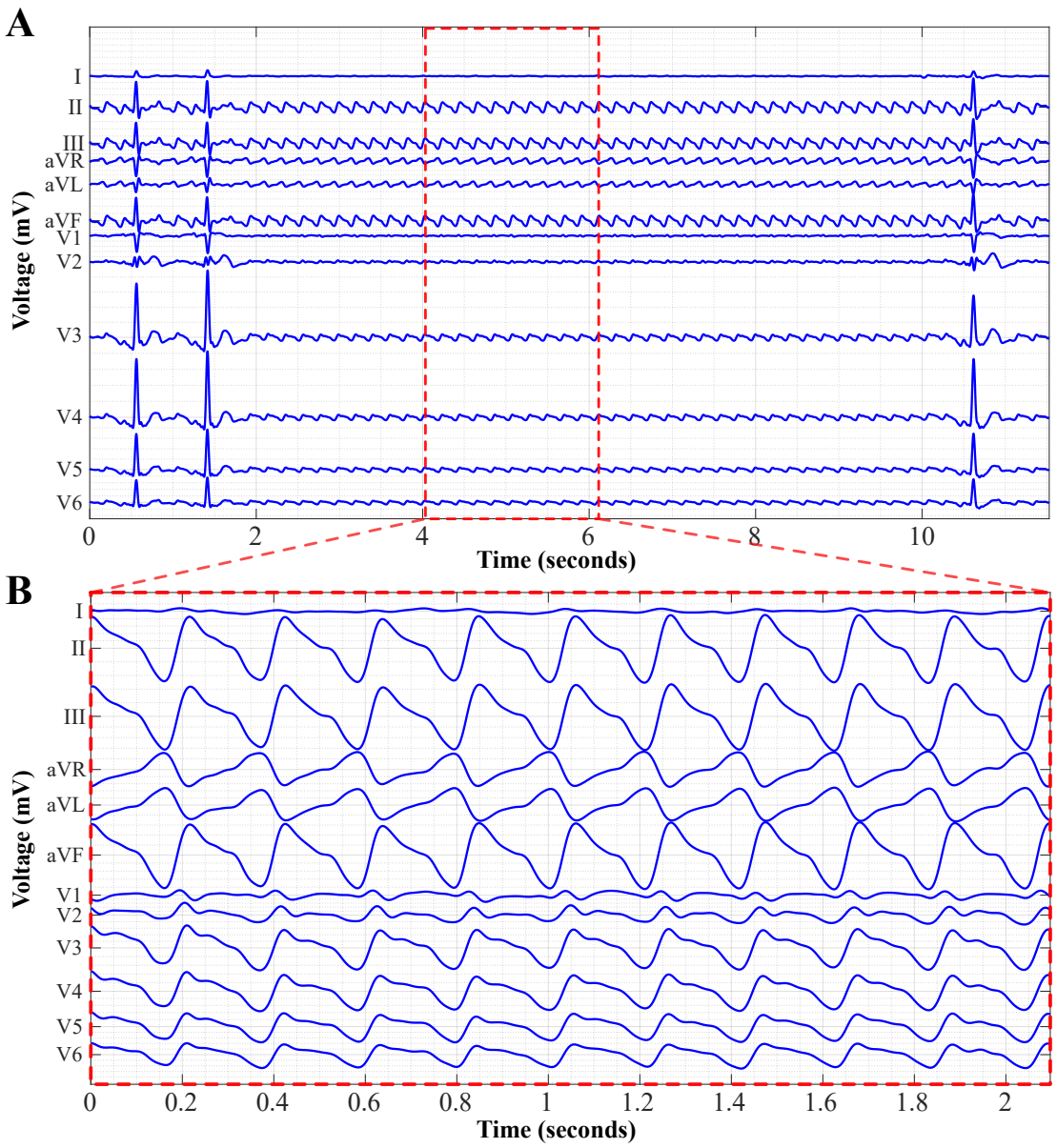

Figure 4.1. Representation of the ECG signal of a patient suffering from common CW AFL under the influence of adenosine. A: Representation of 11 seconds of the ECG signal where from second 2 to shortly after second 10, only the atria are activated and contributing to the ECG signal. **B:** Section of 10 repetitions (or beats) of the atria under the influence of adenosine, extracted from section A. Loops represent an almost identical voltage variation, as characteristically in AFL.

building a VCG loop as the spatial addition of the points generated by those vectors.

The VCG of interest is taken from the unique contribution of the atria. Thus, the previous mathematical transformation is applied to a section of the ECG where adenosine is actively blocking ventricular activity and contribution to the ECG signal. Thus, several VCG loops representing the atrial signal are derived (see figure 4.3.A). In order to follow a standard protocol for all the patients, ten atrial beats are used to create 10 VCG loops in every case.

Because of the fact that the interest signal to obtain as the representing VCG

of a patient and in order to have the most accurate and precise representation, the ten VCG loops are spatially and temporally averaged. The spatial and temporal information of these loops is stored in a four-dimensional matrix where the three first dimensions are the Frank's X, Y and Z lead in a 3-dimensional space coordinate system, and the fourth is the temporal dependence in that system of coordinates.

The time length of one loop is found through a simple technique based on a correlation function that returns a vector of lag indices measuring the delay of two correlated signals. In this case, both signals are the same, so the maximum values of the returned vector correspond to the points at which the maximum correlation exists when displacing one signal over the other in time (see figure 4.2 left). Uncommon patterns can appear when the ECG signal is not regular. Those are addressed with a variant of this algorithm that will select the maximum corresponding to the definition of the beginning of a new atrial wave, that is, the real peaks avoiding possible false ones (see figure 4.2 right).

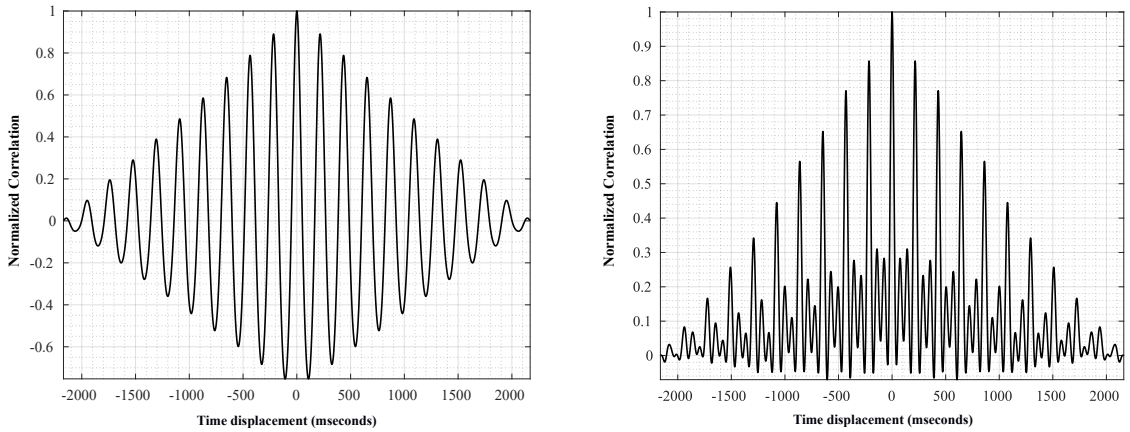

Figure 4.2. Left: Regular AFL ECG Correlation. Result of the correlation of a regular signal of a patient suffering from common CCW AFL – same patient as in figure 4.1. The distance between two peaks is 224ms, representing the length of an atrial beat (and of a VCG loop when transforming the signal). **Right:** Irregular AFL ECG Correlation. Result of the correlation of an irregular signal of a patient suffering from perimitral CCW AFL. The distance between two main peaks is 215ms, corresponding to the length of an atrial beat (and of a VCG loop when transforming the signal). The algorithm is prepared to avoid false peaks as the two intermediate peaks between two real ones in this signal.

Thus, the time length that it takes for a VCG loop to take place is computed and, over this value and in the temporal dimension of the 10-loops VCG, an average is performed so that a representative 1-loop VCG is obtained from each patient (see figure 4.3.B-D). Because of the possibility of a displacement in the Cartesian axes in different measurements of patients' signals and to focus on the morphology of the VCG, this representation is centred so that the origin belongs to the geometrical centre of the VCG. Then, further computations can be performed in a normalised way.

Besides, since the average is computed from a discretised signal, the beginning and end of the loop may not coincide. Consequently, an interpolation and smoothing over the beginning and end of the VCG is computed so that a closed loop is finally

obtained (see figure 4.3.B).

Once all VCGs are computed, the analysis to go through the characterisation process that allows to determine common features in VCG signals belonging to the same AFL variant analysis is performed. This will be later explained in this section.

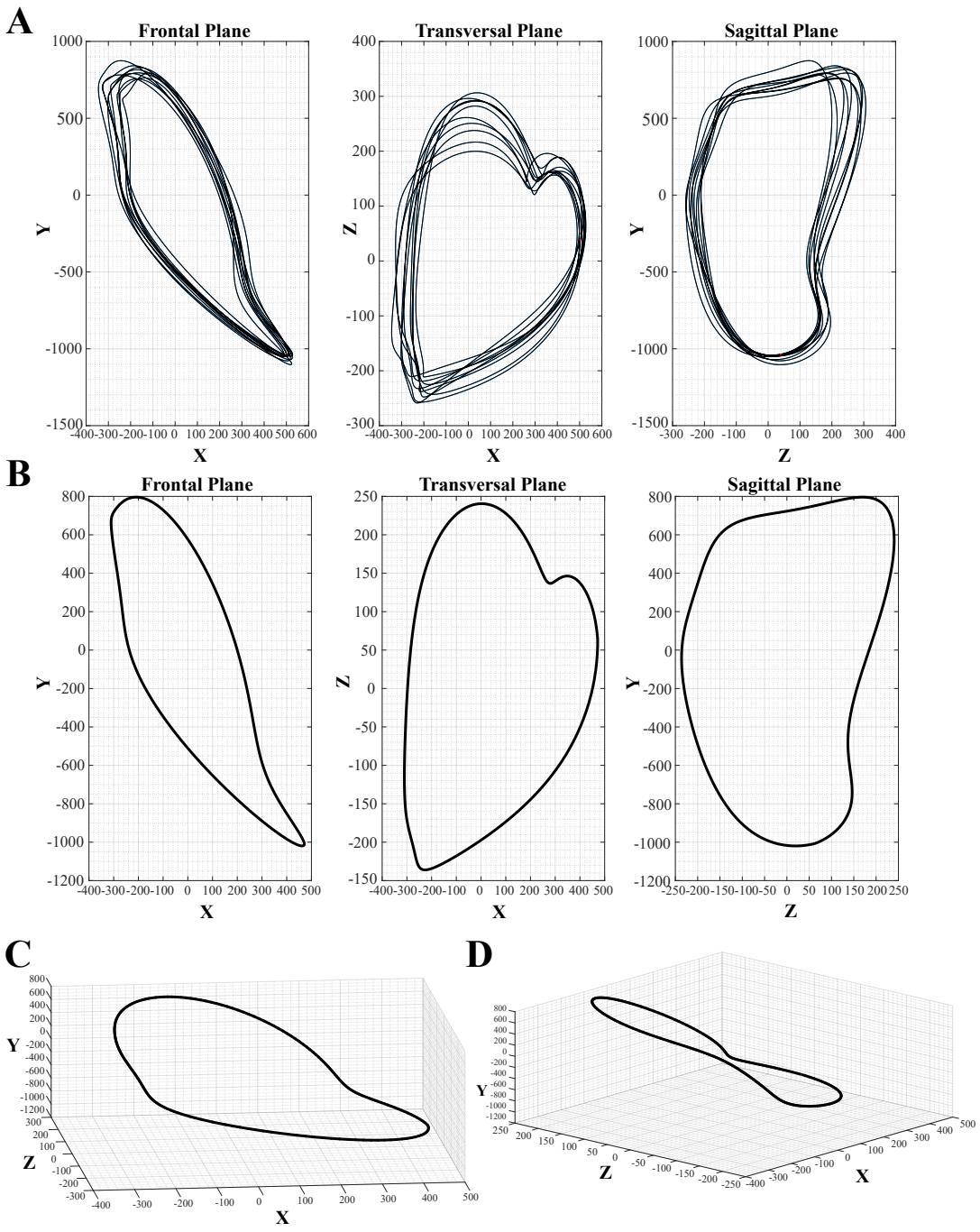

Figure 4.3. Reconstruction of a VCG from 10 loops under the adenosine effect blocking the ventricle contribution to the signal (**A**) and average in the temporal dimension of the spatial vectorcadiographic loop, representing the VCG signal of a patient in 2 dimensions (**B**) and in 3 dimensions (**C** **D**). The patient from which the ECG is processed suffers from common CCW AFL. The two-dimensional axis of the views of the VCG for the frontal, transversal and sagittal planes follow the standards in classical literature.

4.3. Analysis of the VCG features

Once the representative VCG has been computed, different methods have been developed and implemented to analyse the features of the VCG loops in the different categories, to analyse, not only the importance of slow conduction regions along the re-entrant circuits in AFL, but also shape and other geometrical features to characterise more accurately the VCG loop types.

4.3.1. Slow Conduction Velocity Regions

After the analysis of plenty of research articles in the classic literature (i.e. H.W. Draper's et al [100] or L. Edenbrandt's et al [99]) and in actual literature (i.e. C.A. Pastore's et al [101] or T.A. Sakhnova's et al [102]) it has been concluded that a discretisation of time in a VCG loop to analyse low velocity regions has never been found to be studied.

The nearest approach was provided by Jason Ng et al. [103], but our methodology steps forward and discretises the time over an average of loops to have an accurate representation of the VCG in the 3D space (see figure 4.5.A). Discretising the signal for equal time frames shows a direct relation between the observed space in the figure and velocity (see equation (4.1))

$$V = S/\Delta t \rightarrow S = V \cdot \Delta t \text{ Where } \Delta t \text{ is a constant} \tag{4.1}$$

A relatively short distance among two points will be then translated as a lower velocity over that region, although a higher number of points will make a more accurate idea of the variation of conduction velocity possible.

The velocity along the loop is calculated by computing the distance of the reconstructed trajectory between two points and setting the constant discretisation time (see figure 4.4.A). Velocity is referred as conduction velocity or velocity of the transmission of the electrical impulse along a macroreentrant atrial loop (or MC). As the ECG has a time dependence over the voltage variation, the distribution of slow velocity regions along the VCG loop will be fundamental characterise the VCG of the patients according to our hypothesis of the importance of such property.

An algorithm has been designed to compute a profile of the velocity along the averaged VCG loop, and to stablish a threshold which provides information about the slow frames in the VCG -slower than this threshold. In order to normalise the analysis and find a coherent relation on the shapes and slow frames of the VCGs for different patients, the threshold is fixed as a dependence of the maximum transmission velocity in the VCG loop, that is, the peak in the velocity graph. The dependence has been settled in our analysis to one fourth of this maximum velocity (see figure 4.4.B). These regions are represented in different colours to identify the correspondents in the VCG and ECG plots (see figure 4.4.B-C).

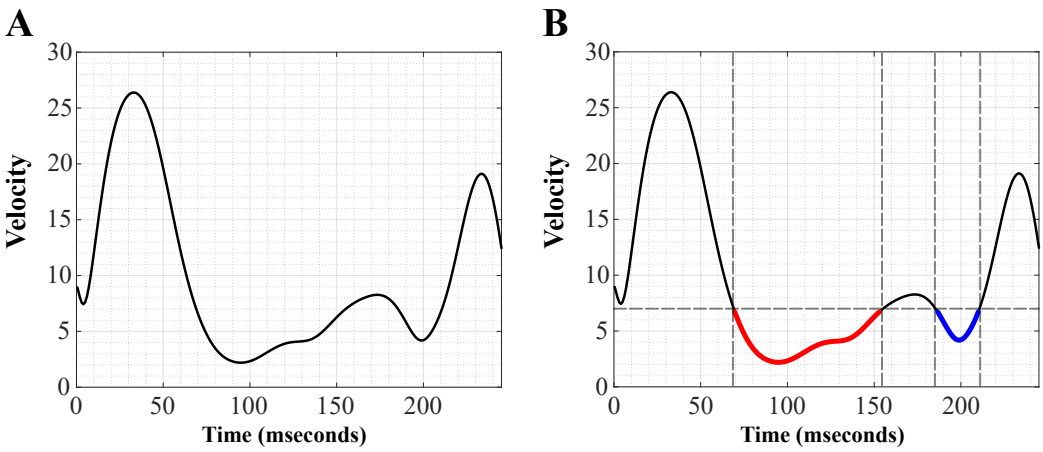

Figure 4.4. Velocity profile (in V/s as a potential difference over time unit) **of the transmission of electrical impulse in the trajectory in a MC from a patient suffering from perimitral CCW AFL. A:** Velocity over the trajectory vs time. **B:** Slow regions under the threshold of one fourth of the maximum velocity (6.60 units) are represented in red and black over the profile. The red region occurs first in time in the established frame and the black one occurs later in the loop, being correspondent to coloured regions in figure 4.5.B-C.

Thus, a tool is created to identify the velocity profile of the electric impulse, and the relation to the regions of the VCG and ECG. Hence, further characterisation can be provided with the utilisation of this feature. In addition to this, the concept is very important to evaluate the VCG as a weighted trajectory where slow areas take more importance due to the accumulation of data points. This weighting is essential in the correlation parameter (CP) that will be later explained, being fundamental to prove the hypothesis.

4.3.2. Quantisation of Slow Velocity Regions: SVPOT, SVPOD and their Rate.

The previous tool is designed to represent slow conduction velocity regions along the signal, but a quantisation needs to be performed to obtain quality data to analyse the variation of these slow regions among signals from patients suffering from different AFL groups.

4.3.2.1. Slow Velocity Percentage Over Time (SVPOT)

The SVPOT parameter allows to quantify the percentage of time at which the conduction velocity has been under the threshold defined by one fourth of the maximum velocity. The SVPOT is simply computed by dividing the time from the velocity profile computed from the average VCG loop of the patient by the average time that it takes to complete a VCG loop in that patient. This parameter oscillates between zero, meaning no velocity under the threshold, and one, although this value can never be reached since at least the value for the maximum velocity will be over the threshold, computed as a fraction of that value.

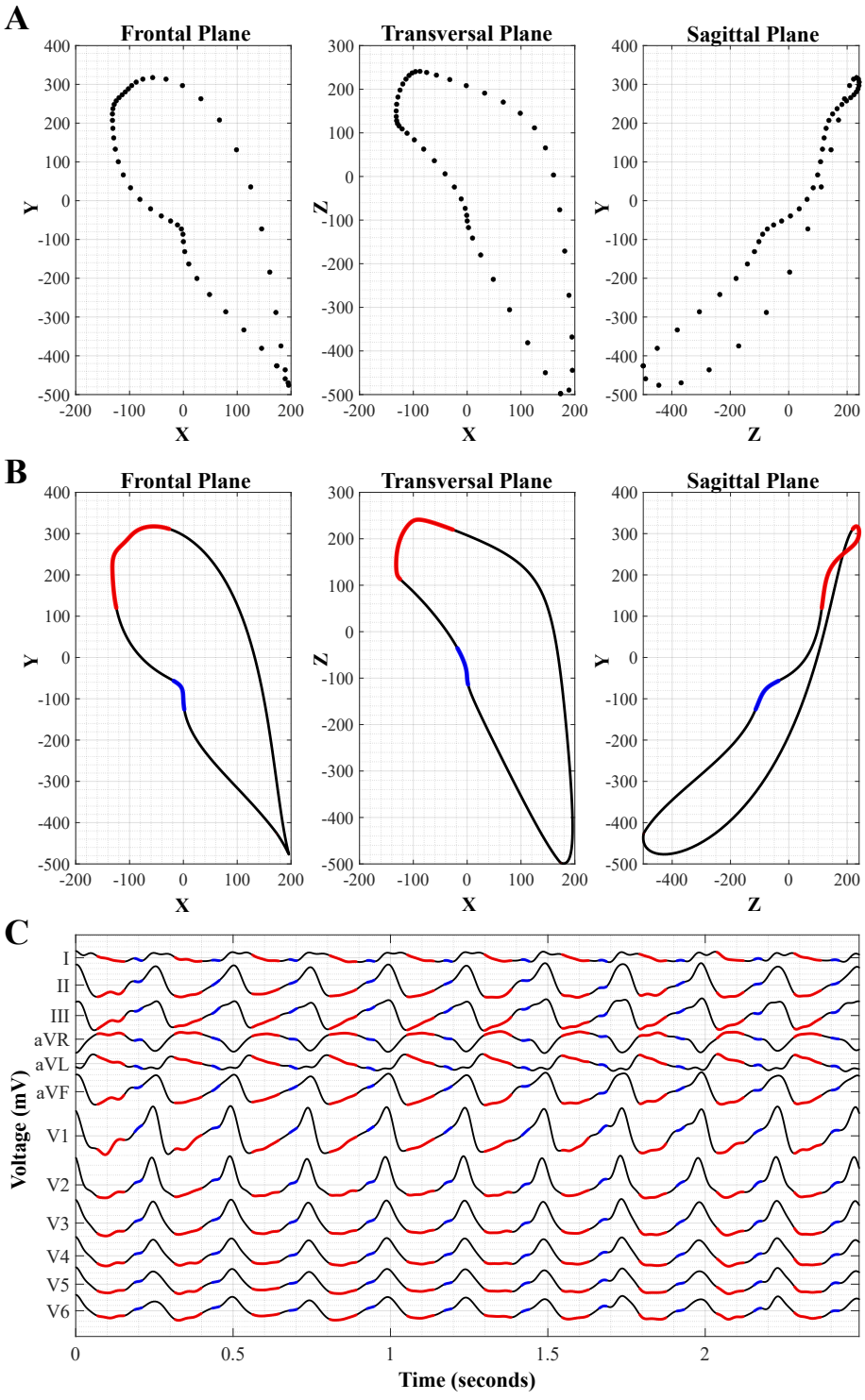

Figure 4.5. VCG reconstruction from a ECG atrial signal, highlighting slow velocity regions in both the VCG and ECG representation from which the atrial VCG loop is averaged. A: VCG reconstruction with a sampled on time so that the phenomenon of concentration of points leads to the idea in which the tool of slow-frames velocities is found; **B:** representation of the VCGs with the slow regions corresponding to velocities under a settled threshold, related to those in the velocity profile found in figure 4.4; and **C:** representation of the 12-leads ECG of the patient from which the IDT has been applied to find A and B, with the slow frame velocities marked in every lead, corresponding to both B and figure 4.4.

4.3.2.2. Slow Velocity Percentage Over Distance (SVPOD)

The SVPOD parameter allows to quantify the percentage of distance that has been travelled with a conduction velocity less than one fourth of the maximum velocity. The SVPOD is calculated from the distance covered by the signal over the arch of the VCG average loop under the velocity threshold, and then dividing that number by the total perimeter of the VCG loop. The value of SVPOD is different to the value of SVPOT since the first is highly influence by how low the velocity is when it is under the threshold -as well as how fast the signal travels when being over the threshold.

4.3.2.3. Rate SVPOT/SVPOD

The previous parameters are meaningful themselves, but additional information can be obtained when relating them. For example, in a case in which the velocity under the threshold is very low, less distance will be travelled and less would be the SVPOD, although SVPOT may be maintained. Thus, only a lower SVPOD will be seen, while if we see that the SVPOT is relatively high, it would mean that we have a region with a very low velocity. SVPOD is expected to be lower than SVPOT since when a fraction of time is covered under the velocity threshold, the distance travelled will usually be smaller in percentage. For instance, if 50% of the time the velocity is below the threshold, less than 50% of the arch of the VCG loop will be covered since velocity is lower at this region. Thus, the higher the rate SVPOT/SVPOD is, the slower the regions under the threshold would be, while in cases where short periods of time are in a relative high conduction velocity and the rest in a continuous low velocity, the rate SVPOT/SVPOD will be lower (see figure 4.6).

Hence, using SVPOT, SVPOD and their rate, the slow velocity regions will be quantised. **Despite the fact that the core point of our hypothesis is not related with an overall quantisation of the slow velocity regions (but with the weight that they impose over the correlation parameter that will later be explained), these parameters are useful to have extra information and characterise the behaviour of VCG loops from different AFL types.**

4.3.3. Angular Velocity Profile

A different approach to the velocity profile can be studied from the angular velocity profile. The previous analysis has limitations that the angular velocity can solve, such as the fact of expressing a profile velocity in units of potential increment over time from the projection of the vector of such potential increment (i.e. the VCG), which is complicated to understand although directly related to the conduction velocity over the atria.

In this case, the units are simpler since the angular velocity can be expressed in radians over time unit (seconds). Furthermore, the physical meaning is clearer: for

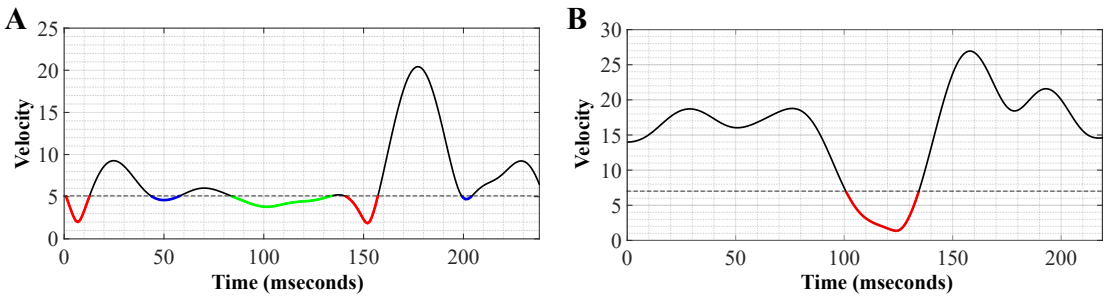

Figure 4.6. Velocity profile (in V/s as a potential difference over time unit) **of the transmission of electrical impulse in the trajectory in a macrorreentrant atrial loop from two patients suffering from perimitral CW AFL.** The dashed line represents the threshold for low conduction velocity. Colours follow the Red-Black-Green order in case that a correlation is needed with VCG or ECG plots. **A:** The distribution of the profile velocity is characterised by a short period of time with a high velocity and the rest with a continuous low velocity profile -low SVPOT/SVPOD rate of 1.56. **B:** The velocity profile is characterised by a short period of time with a noticeable low conduction velocity - high SVPOT/SVPOD rate of 4.64.

an average period of approximately 250ms (the average time it takes to complete a VCG loop), a frequency of 4Hz is found, that multiplied by the angle increment that it takes to complete an ellipse, i.e. 2π radians, an average velocity of 25.12 radians per second is expected. VCG loops would tend to be slightly more complex than an ellipse, so the average angular velocity is expected to be from 25 to 30 radians per second.

This profile is computed from the point discretised VCG loop, computing the vectors of the VCG loop at the i-th and the (i-1)-th point and their module. The discretisation time Ts is computed by dividing the number of points in which the average VCG loop is discretisd over the time that it took to travel this distance. The appropriate formula to compute the angular velocity for each point is expressed in (4.2).

$$\omega_i = \frac{\arccos\left(\frac{(v_i)^T(v_{i+1})}{||v_i||\,||v_{i+1}||}\right)}{Ts} \tag{4.2}$$

This parameter provides an supplemental value to the previous velocity profile since some specific features would be highlighted such as the slow velocity regions where an obstacle is being surrounded. Despite showing similar slow/fast regions, some regions would be emphasised when surrounding an obstacle because of previous ablations, dysfunctionalities in the heart tissue or other anatomical of physiological features that can be studied through this representation. See an example displayed figure 4.7 for a patient suffering from perimitral CW AFL. The highest conduction velocity does not correspond with the highest angular velocity, so that region is giving us clues to investigate the physiological reasons behind that behaviour.

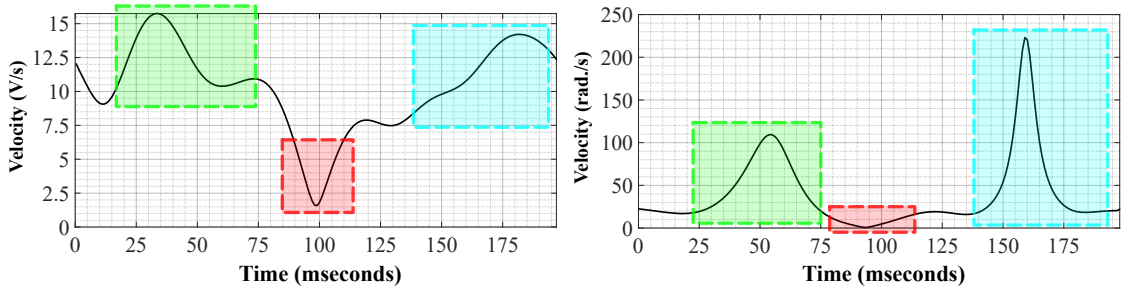

Figure 4.7. Conduction velocity and angular velocity profile from a patient suffering from perimetral CW AFL. A: The velocity profile shows an almost continuous high-speed region and a tight very slow velocity, corresponding to a high SVPOT/SVPOD of 3.49. **B:** The angular velocity profile of this case in rad./s, showing additional value to the left plot. The second fast region (blue) experiments a higher angular velocity although the conduction velocity is slower to the first fast region (green), indication characteristic physio-anatomical features to be studied. The slow region (red) shows a very low angular velocity, corresponding to an almost straight region. In fact, in the low region of the angular velocity, there is a place where it reaches almost zero, located in a similar region to the slowest conduction velocity (left red), indicating that the slowest conduction is happening trespassing a tissue with very low conduction velocity probably because of pathophysiological issues characteristic from that tissue. The mean in this case is higher than usually expected (38.805 rad/sec) due to the shorter time length of the VCG loop corresponding to a higher frequency of 5.04 Hz and the higher complexity of the VCG loop which correspond to a total rotation of more than 2π radians.

4.3.4. Variability or Consistence of the VCG

Since the process of analysing the ECG waves and creating the VCG is automatised once the atrial-depending region under adenosine effect is manually selected, a new parameter has been developed to assess the similarity among the atrial waves or VCG loops. This parameter is named as 'consistence' or 'variability' since it evaluates the way each of the 10 VCG loops is similar to each other in the 3-dimensional space. It also considers the time discretissation, delivering the precise weight to the place where more time frames occur, considering the four dimensions of the problem.

Hence, the consistence parameter is computed in an intra-patient mode, determining the quality of the signal of the patient, been a high coefficient convenient since it means a low variation from loop to loop in the VCG, or from wave to wave in the ECG, defining more precisely the path that the MC is traversing throughout the atria. An inter-patient version of this parameter is also defined in later sections, understood as a correlation parameter (CP) and used to quantify the similarity of two average patient loops, or to compare how similar a single average patient VCG loop is to an archetype of a type of AFL.

In order to perform the analysis of the variability of the VCG loops, they are created as single different VCGs, each one corresponding to one wave of the ECG signal. Applying the IDT to each of the repetitions of the atrial wave, all the loops are created separately. Once having the loops, they are aligned to the centre of coordinates in the Frank's Leads system.

Once all the loops of VCGs corresponding to each of the consecutive ECG waves are created and aligned in the 3D space, the correlation is performed as the average

of the scalar product [104] of each of the points of both loops (see equation (4.3)).

$$\mathrm{C}_t = \frac{1}{\mathrm{N}} \cdot \sum_i \frac{x_i^T \cdot y_i}{||x_i||||y_i||} \forall i \in \mathbb{N}, i \in [1, \mathrm{N}] \tag{4.3}$$

Nonetheless, it is not possible to claim that all loops are temporally aligned. Thus, the consistence will be the maximum coefficient obtained from all the possible temporal situations of both loops, since in such case, the different regions and frames will coincide or have the highest similarity. Hence the consistence (or CP when inter-patient) C, is temporally aligned when following the expression at equation (4.4).

$$\mathrm{C} = \max\left(\mathrm{C}_t\right) \forall t \in \mathbb{N}, t \in [1, \mathrm{N}] \tag{4.4}$$

Consequently, equation (4.5) computes the appropriate computation of the C considering spatial and temporal alignment, combining both eqs. (4.3) and (4.4).

$$\begin{aligned} \mathrm{C} &= \max\left(\tfrac{1}{\mathrm{N}} \cdot \textstyle\sum_i \frac{x_k^T \cdot y_i}{||x_k||\,||y_i||}\right) \forall i \in \mathbb{N}, i \in [1, \mathrm{N}] \\ \text{where,} \quad k &= \begin{cases} i+j \quad , i+j \leq N \\ i+j-N, i+j > N \end{cases} \quad \forall j \in \mathbb{N}, j \in [0, \mathrm{N}-1] \end{aligned} \tag{4.5}$$

In the previous analysis, $\mathrm{x_i}$ and $\mathrm{y_i}$ are the 3 spatial components (X, Y and Z in the Cartesian system) of the i-th points of both AFL loops. N is the total number of points after discretising over a constant time frame. $\mathrm{C_t}$ is the coefficient constant for a single temporal situation, and thus, C evaluates all possible $\mathrm{C_t}$ configuration, depending on the N possibilities. For each $\mathrm{C_t}$ each of the k-th points are the first occurring in time while i-th parameter does not variate on time, so that adding any j-th number from 0 to N-1, all possible time situations relating both loops are considered and in consequence, spatial and temporal alignment is performed.

Hence, if the global trajectory of a pair of AFL loops match when being temporally aligned, both x and y vectors would be coincident for every point, reaching the upper bound of the consistence parameter which is 1.

4.3.5. Arc or Circumference Parameter

The arc parameter consists of the summation of angular changes in the direction that the VCG undergoes through the loop point by point. Given that the archetype for a group of patients and the VCG of a patient are computed from the average of several loops, it is expected to have a smoother trajectory. Thus, a lower angle variation is expected to be found in those than in the VCG loops coming from the reconstruction of a single atrial activity wave.

Taking this into account, the arc parameter permits performing an analysis on an overall variation of the trajectory of the path along the MC, more than negligible

small variations along its general path. It is also important to contemplate again that the slow regions are particularly significant since they offer a more detailed description of the path, contributing to this parameter with a detailed summation of the angle variation along such regions.

The angle variation ϑ_i for a consecutive set of points p_i, is determined by equation (4.6).

$$\cos(\theta_i) = \frac{(p_i - p_{i-1})^T (p_{i+1} - p_i)}{\|(p_i - p_{i-1})\| \, \|(p_{i+1} - p_i)\|} \tag{4.6}$$

The angle variation of the whole loop is then determined by the summation of all the angle increments ϑ_i. In order to define a unitless normalised circumference parameter, the lowest summation of angle variation (that is, 2π radians given by the simplest path) is divided over the actual angle variation of the particular VCG, being defined the arc parameter A by equation (4.7).

$$A = \frac{2\pi}{\sum_i \arccos\left(\frac{(p_i - p_{i-1})^T (p_{i+1} - p_i)}{\|(p_i - p_{i-1})\| \|(p_{i+1} - p_i)\|}\right)} \tag{4.7}$$

As parametrised in this way, where the minimum summation of angle increments ϑ_i is 2π radians, the maximum value of this parameter is 1, corresponding to the simplest trajectory of the VCG loop, and the minimum will tend to 0 as the loop angle can increase with no limit as complexity in the shape increases. Hence, this parameter is inversely proportional to the complexity of the VCG -i.e. a single planar ellipse will have A=1 while a very complex VCG will have a very low A, near to 0.

4.4. VCG Archetypes of AFL Variants

Approaches based on parameters extracted from ECG have been studied with the aim of characterising of AFL [105, 106]. However, the novelty of these methods consists on establishing the grounds on the VCG as an approach to identify the AFL variant non-invasively. From all the previous parameters, analytic data can be obtained intra-patiently which is useful to identify similarities among VCG loops from patients belonging to the same AFL group. This can help to identify to which archetype a single unknown VCG is more alike. Nonetheless, the main approach is based on the creation of archetypes for each AFL variant so that correlating the new unknown signal to all of them would provide the higher correlation or similarity parameter to the archetype of the AFL group to which it belongs.

Archetypes for each of the main AFL variants are created from the average of time aligned VCGs from those patients suffering from each type of AFL. The diag-

nosis is performed by a group of physicians through conventional and contemporary invasive diagnosis techniques [91, 107]. Thus, a record of the full record of the patients is created before selecting them to be part of the archetype.

It is noteworthy to mention that a deep analysis on the symmetry of a VCG has been performed, proving that CW VCGs are not the same as CCW VCGs just changing the direction of the current flow. Anatomically it may make sense, but physiologically it does not, as demonstrated through trials with this model obtaining different results which do not make sense when assuming this symmetry. Hence, different archetypes are created for both variants, making the model to work in a more precise and accurate way. Similar conclusions were assumed in previous studies [103, 104].

4.5. Similarity among VCGs and Characterisation

Once archetypes are created, the previously mentioned techniques are used in order to evaluate the similarity between a new case which is not known or labelled and each of the archetypes. In this case, the main parameter determining to which group the new case belongs to is the consistence or variability parameter, not intra-patient as explained in 4.3.4, but between the new individual and the archetype. The average representing VCG of the patient is compared through an algorithm based on equation (4.5) to each of the archetypes. The highest CP will determine which AFL variant it belongs to.

Another way of checking the efficiency of the algorithm is found by using the Leave One Out (LOO) algorithm, where the patient of study is excluded from the design of the experiment. Thus, it can be considered as a non-identified case, and since we have the complete record of the patient, it is possible to evaluate the result given by the algorithm.

As previously mentioned, there is a greater accumulation of points in slow regions when discretising with a constant time. Thus, the concentration of points can represent a large percentage of time in a very small region of the path. Given this circumstance, the contribution of those regions is crucial for the correlation parameter, and that the shape of the MC is not that important in faster regions that weigh less in computational terms. Consequently, those regions would play a very important role in the quantification of parameters regarding the analysis of VCGs, and in the process of characterisation of a patient with unknown record, according to the hypothesis presented.

4.6. Statistical Analysis

With the purpose of including a valuable discussion for the results obtained from the different parameters and from the synthetic VCG generator, which is explained

in next chapter, some statistical methods have been utilised. As a reminder note, it was not my role in this project to choose the tests, program the algorithms or compute the parameters with the appropriate formulas. My role was based on the interpretation of the results and outcome of the statistical analysis and the creation of representative figures that helped with the elaboration of a detailed discussion of the different results and methods. The statistical methods that are used to obtain data that will be presented in the results are introduced here.

For the statistical analysis of the patients, non-parametric tests are used, as they do not assume a specific distribution of the parameters - given that we have a relatively low number of patients. In this case, the Kruskal-Wallis test is used as the non-parametric alternative of the parametric analysis of variance (ANOVA) test. This test consists of an extension of the Mann-Whitney test for more than two groups, with the same function as the T-test but comparing ranges in stead of averaged.

In the case of the large database created by the synthetic VCG generator, the ANOVA test was used. This parametric test is used to compare among groups in terms of a quantitative variable. It is a generalisation of the equality contrast for two independent samples, and it is applied to contrast the average equality of three or more independent populations with normal distribution. The statistical distribution being treated is the F of Snedecor, which helps to decide whether the variable is statistically significant. Hence, ANOVA is similar in some way to t-student test, but it compares the averages of three or more groups, together with an associated probability determining if the differences among groups is statistically significant.

In order to take decision when interpreting the outcome of the test and rejecting the null hypothesis or not we will look at the p-value. When having $p<0.05$, the null hypothesis would be rejected confirming differences among groups, while in the opposite case (i.e. $p>0.05$) the null hypothesis would be accepted. Furthermore, ANOVA tests is complemented with the well-known post-hoc tests determining in which groups the differences are found when having statistical significance. In this study the Bonferroni test is the one employed - for 'a priori' planned hypothesis, either simple or complex.

Finally, the Receiver Operating Characteristics (ROC) curve is a method that allows us to illustrate visually the efficiency of some parameters. The further the curve is from the diagonal, the higher the predictive capacity of the test is. The Area Under the Curve (AUC) is the most important evaluation metric of the ROC, verifying the performance of any classification model. It evaluates the efficiency in the classification process and represents the degree of separability among the groups. The higher the AUC, the better the predictive capacity of the model is.

5. METHODS II. VCG GENERATOR: A MATHEMATICAL MODEL

5.1. Introduction to the Mathematical Model

The purpose of this model is to generate a large database of geometrical figures having a similar shape to natural VCG signals reconstructed from MC of AFL. Thus, they will have similar characteristics and behaviour to the ones obtained after applying the to ECG signals from patients suffering from AFL. The purpose is to consolidate the initial hypothesis by providing the figures with a characteristic 'slow velocity region' that will allow to distinguish among the different types when producing unlabelled figures.

There will be eight different categories according the main parameter of the spatial location of the clustered distribution of points. Thence, the fact that the algorithm that being used to classify VCG loops considering this parameter as the imperative one works appropriately, will be proved. Later, the exemplification through the analysis of signals coming from a sample of patients from the Hospital 'La Paz' suffering from AFL will be performed under the LOO principle.

The fundamental property of this model is the existence of a wide variety of randomised variables including the path taken by the geometrical figures, the location and rotation in the 3D space or their shape. Each of the groups has exclusively one characteristic in common: the distribution of clustered points in a similar region in the 3D space.

Thus, the algorithm will be able sort all the figures from a big database created by the VCG generator, in four groups, without the information about how they were created. The success of this analysis would prove the efficiency in the algorithm when applied to the signals retrieved from patients from the hospital, classifying them according to the geometrical shape of their VCG and the slow velocity regions, sorting them out in groups that will correspond to the diagnosis given by the physicians about the AFL type they correspond to. Further proofs will be taken to evaluate the influence of slow regions in the CP or consistence.

It is important to underline that the ellipses created by this mathematical model do not show a physiological behaviour but an approximation of the shape from ranges of parameters approximated from real atrial VCG signals. Note also that the clusters of points are related to a low conduction velocity in the atria, being that one indispensable requisite in the hypothesis that we expose for categorising AFL subgroups.

5.2. Grounds of the Synthetic VCG Generator

5.2.1. Definition of an Ellipse

The basis of our geometrical figure is an ellipse that will be processed to become randomly, amorphous and asymmetrical. The equation of a circle in 2 dimensions in a Cartesian system of coordinates comes from the equation of an ellipse (see equation (**??**)) for the case in which the major (a) and minor (b) semi-axes are both equal. Thus, a and b define a property that will be called orientation of the ellipse all through this section, being defined by whether a>b or b<a.

$$\frac{(x-x_o)^2}{a^2}+\frac{(y-y_0)^2}{b^2}=r^2 \tag{5.1}$$

x_0 and y_0 describe the displacement of the centre of the ellipse along x and y axis. Nonetheless, when processing VCGs, centring at the origin of coordinates is necessary for the computation of some parameters. Thus, x_0 and y_0 are equal to zero, having equation (5.2) as the initial expression in the mathematical model (i.e. an ellipse centred on the origin of coordinates, see 5.1).

$$\frac{x^2}{a^2}+\frac{y^2}{b^2}=r^2 \tag{5.2}$$

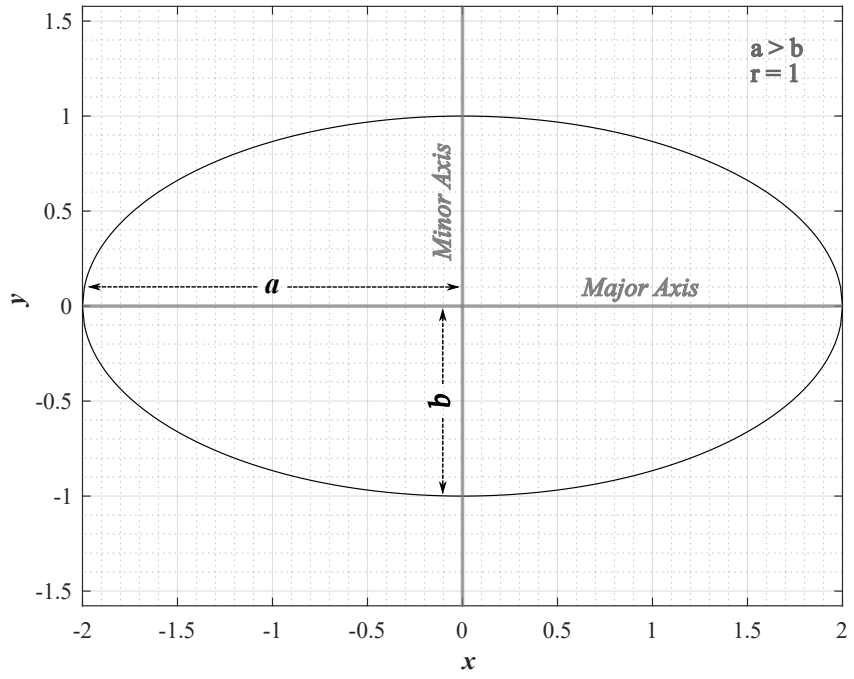

Figure 5.1. Definition of an ellipse for a major axis a greater than the minor axis b. In this case a=2b and r=1.

5.2.2. Perimeter of an Ellipse

The perimeter of an ellipse has been approached through different formulations along history [108, 109]. One of the most famous implementations was stated by Ramanujan [110], who expressed the perimeter P as:

$$P = \pi \left\{ (a+b) + \frac{3\,(a+b)^2}{10\,(a+b) + \sqrt{a^2+14ab+b^2}} + \varepsilon \right\} \quad \text{where } \varepsilon \approx \frac{3ak^{20}}{68719476736}, \tag{5.3}$$

being a and b the semi-major and semi-minor axes of the ellipse and k the value of the eccentricity.

Despite being aware of the existence of more accurate formulations of the perimeter of the ellipse, in this model computational time is more valuable than the exact value for this perimeter. Hence, a the expression provided by Euler in 1773 [109, 111] is the one chosen to approximate this value (see equation (5.4)).

$$P = 2\pi \cdot \sqrt{\frac{a^2+b^2}{2}} \tag{5.4}$$

This expression provides the model with a simple relation among the semi-axes of the ellipse and its perimeter, something very useful to define the parameters in certain ranges as discussed later in this section.

5.2.3. Polar Coordinates

The expression of the ellipse is more convenient in polar coordinates for defining angular and radial parameters, so Cartesian's axes X and Y are expressed in terms of radial and angular components as:

$$\begin{aligned} x &= r \cdot \cos\theta \\ y &= r \cdot \sin\theta \end{aligned} \tag{5.5}$$

Equation (5.1) is expressed as follows (the constant which was previously called r is now called k to avoid possible misunderstandings):

$$\frac{(r\cdot\cos\theta)^2}{a^2} + \frac{(r\cdot\sin\theta)^2}{b^2} = k^2 \tag{5.6}$$

Thus, the radius is defined as a function of the angle and semi-axes a and b as:

$$r(\theta) = \frac{a\cdot b}{\sqrt{(a\cdot\cos\theta)^2 + (b\cdot\sin\theta)^2}} \tag{5.7}$$

5.3. The Semi-axes of the Projections

With the aim assigning random values between a range that would lead to shapes similar to the VCG loops obtained from patients, relations are established between the semi-axes and the perimeter as function of constants assigned with values within a range, calculated as explained in this section.

5.3.1. Relations among a and b

Perimeter P is defined as a constant which will variate randomly among a set of values, similar to the ones obtained in real patient VCG loops.

The geometrical figure will be constituted by the projection of two 2D ellipses, creating a 3D loop with random variations in X, Y and Z direction. Thus, to have an appropriate shape, a relation between radius a and b is defined so that clear 'non-physiological' shapes are avoided. From the two possible orientations, the range needs to be reduced to one of them to work in a controlled environment, so a needs to be greater than b. Furthermore, semi-axis b is defined as a function of perimeter P multiplied by a constant c.

$$b = c \cdot P \tag{5.8}$$

This constant c is a coefficient that will be defined according to the relation of a with b. Combining equation (5.4) and equation (5.8), an expression for a as a function of P and c is found:

$$\boldsymbol{a} = \sqrt{\frac{P^2}{2\pi^2} - b^2} = P \cdot \sqrt{\frac{1}{2\pi^2} - \boldsymbol{c}^2} \tag{5.9}$$

Given the previously mentioned orientation, for a>b, and combining equations (5.7) and (5.9), the next expression is obtained:

$$P \cdot \sqrt{\frac{1}{2\pi^2} - c^2} > c \cdot P \tag{5.10}$$

And for P>0,

$$\sqrt{\frac{1}{2\pi^2} - c^2} > c \tag{5.11}$$

So, solving the inequation, c is expressed as:

$$c^2 > \frac{1}{4\pi^2} \begin{cases} c < \frac{1}{2\pi} \\ c > \frac{-1}{2\pi} \end{cases} \tag{5.12}$$

The negative value has no significant meaning in this model, so for any c<1/2π and greater than zero, a will be higher than b.

Nevertheless, to maintain an elliptical shape similar to the ones coming from cardiac patients, limits should be established for the relation of the values of a and b. If coefficient c were very small, almost a line would be created while if a=b, a circle will be found.

At the same time, when discretising an ellipse in terms of a constant angle increment with respect to the origin, there is a natural cluster because of the different distance of the points to the centre. The two symmetrical areas nearer to the centre, nearby r=b, will have points closer to each other than the further ones, nearby r=a. Thus, this would be something characteristic of the synthetic VCG, but a cluster would be forced somewhere else as a distinction parameter of a type of VCG -as, stated by the main hypothesis, occurs in real patients. Nonetheless, this would be discussed in the angular and radial parameters definition. The reason to be mentioned here is something to take into account when defining the restrictions among the relations between the semi-axes, since the natural clustering would be influenced by such relation.

Therefore, the restriction is established as follows:

$$\frac{3}{2}b < a < 2b \tag{5.13}$$

Thus, both inequalities have to be studied to define the limits of c that would permit the above relation among the semi-axis of the synthetic VCG. For a>2b, combining equations (5.7) and (5.9),

$$P \cdot \sqrt{\frac{1}{2\pi^2} - c^2} > 2 \cdot c \cdot P \tag{5.14}$$

and similar to the derivation in eqs. (5.10)-(5.12), c is found to be expressed as:

$$c^2 > \frac{1}{10\pi^2} \begin{cases} c < \frac{1}{\sqrt{10}\pi} \\ c > \frac{-1}{\sqrt{10}\pi} \end{cases} \tag{5.15}$$

The negative value has no significant meaning in this model, so for any c<1/10π and greater than zero, a will be higher than b.

In a similar way, for a>3/2b, combining equations (5.7) and (5.9),

$$P \cdot \sqrt{\frac{1}{2\pi^2} - c^2} > \frac{3}{2} \cdot c \cdot P \tag{5.16}$$

and similar to the derivation in eqs. (5.10)-(5.12), c is found to be expressed as:

$$c^2 > \frac{2}{13\pi^2} \begin{cases} c < \frac{\sqrt{2}}{\sqrt{13}\pi} \\ c > \frac{-\sqrt{2}}{\sqrt{13}\pi} \end{cases} \tag{5.17}$$

The negative value has no significant meaning in this model, so for any c<$\sqrt{2}/(\sqrt{13}\pi)$ and greater than zero, a will be higher than b.

Hence, for constant c to fulfil equation (5.13), it must be contained in the next range of values:

$$\frac{1}{\sqrt{10}\pi} < c < \frac{\sqrt{2}}{\sqrt{13}\pi} \tag{5.18}$$

The area in 2D that allows this constant c allows can be observed in figures 5.3 and 5.4.

5.3.2. Definition of c in Terms of a Normalised Random Variable in Matlab

The previous constant c needs to be expressed in terms of a variable between zero and one because Matlab, which is the software being used to design the synthetic VCG generator, allows the creation of a variable with a random number between 0 and 1. In order to create that expression, a straight line is defined as:

$$y = mc + d \tag{5.19}$$

where y is this random variable going from 0.0000 to 1.0000, m is the slope and d the y-intercept. In this case the abscissa displacement is equal to zero and the slope m and displacement ordinate displacement *(c_0)* are defined as:

$$m = \frac{\Delta y}{\Delta c} = \frac{1-0}{\frac{\sqrt{2}}{\sqrt{13}\pi} - \frac{1}{\sqrt{10}\pi}} = \frac{\sqrt{130}\pi}{2\sqrt{5} - \sqrt{13}} \tag{5.20}$$

$$c_0 = -\frac{1}{\sqrt{10}\pi} \tag{5.21}$$

Thus, y is defined as:

$$y = \frac{\sqrt{130}\pi}{2\sqrt{5} - \sqrt{13}} \cdot \left(c - \frac{1}{\sqrt{10}\pi} \right) \tag{5.22}$$

And solving for c, as a function of random variable y, we get:

$$c = \frac{2\sqrt{5} - \sqrt{13}}{\sqrt{130}\pi} \cdot y + \frac{1}{\sqrt{10}\pi} \tag{5.23}$$

Giving 10,001 values for c, in the range defined by equation (5.18), for all:

$$0.0000 < y < 1.0000 \tag{5.24}$$

5.4. Angular and Radial Variables

5.4.1. Angle Variation: Irregular Discretisation

With a constant angle increment ($\Delta\vartheta$), a 'natural' and symmetrical cluster of points occurs in an ellipse at both regions near to the origin (at the minor semi-axis), since further away, there will be a larger distance between points - see red dots in comparison to blue and yellow ones in figure 5.3 and 5.3. Furthermore, in the simplest case of a circle, this constant increment would be equivalent to a constant time discretisation at a constant velocity when computing a VCG of a patient. However, velocity is not constant, and thus, discretised points at a constant time interval are not equidistant (see figure 5.2)

The purpose of the model is to define different types of 3-dimensional elliptical shapes, based on the principal criteria of a characteristic cluster of points in a predefined region. Consequently, the angle variation must be defined so that this discretisation is performed in a way in which there is a section where $\Delta\vartheta$is smaller and more points are plotted. It is convenient that this region is located in a further

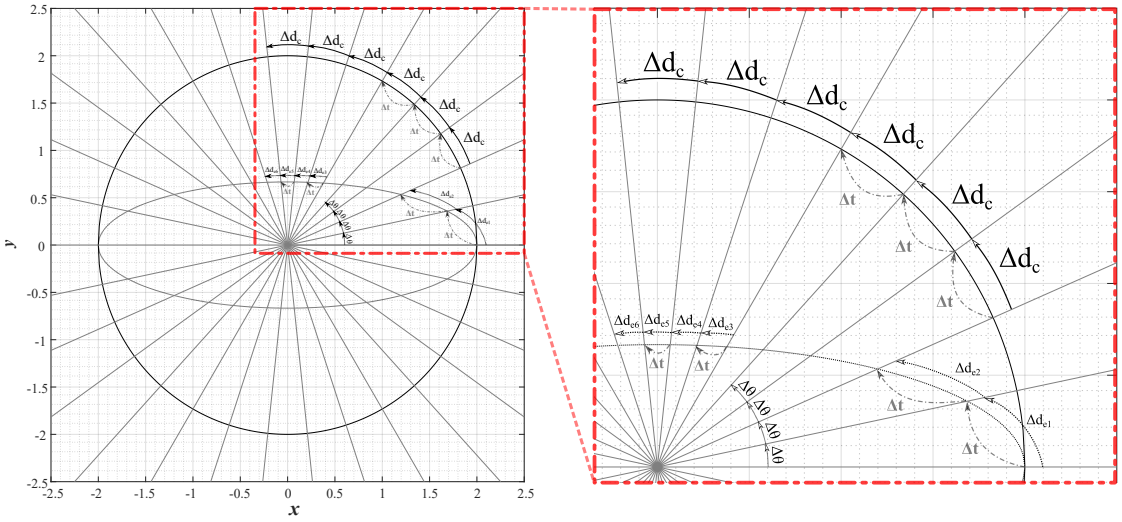

Figure 5.2. Representation of a circle (continuous line) **and an ellipse** (dotted line) **over a constant discretisation time illustrating a 2D signal increasing through angle ϑ.** As there is a continuous time increment (Δt) corresponding to a constant $\Delta\vartheta$. In the case of a circle after a period of time Δt there has been a displacement Δd_c which is constant over the whole circle in any angular variation, that is, during any Δt. Nevertheless, in the ellipse, the angle increment after a time period Δt entails different travelled distance depending on the spatial position and orientation. Thus, Δd_{e1} is greater than Δd_{e2} which is greater than Δd_{e3} and so on. Hence, if computing the velocity (v) travelled over this path by a signal, in the case of the circle it would be constant as both Δd_c and Δt are constant. However, for the elliptical pathway, it will be faster near the abscissa axis and slower when approaching the coordinate axis.

region from the centre so that it is something characteristic of the ellipse that we create, avoiding it to happen in the 'natural' symmetrical clusters near the origin. Note that these 'natural' condensations of points nearby the region by the minor semi-axis will produce oscillations in the velocity profile similar to the ones found in real VCG, being this feature of special interest for the model (figure 5.4B).

To create this 'forced' cluster of points, characteristic for the synthetic VCGs, the absolute value of the cosine is a very suitable shape because it allows a concentration of points in a very specific region with respect to the geometrical figure, that is, around π radians from the first point of the figure.

The variation of the angle is defined by an equation of the form:

$$\Delta\theta_n = K_{\max}\left|\cos\left(n\frac{\pi}{N}+\phi\right)\right| + K_{\min}, \tag{5.25}$$

where $\Delta\theta_n$ is the angular increment at each n sample, being N the total number of samples of the loop, K_{min} the minimum angle increment, which sets up the minimum velocity, K_{max} + K_{min} is maximum angle variation, which stands for high velocity regions, and phase argument phi determines the location of rapid and slow regions. The angular increment is going to decrease until it reaches the minimum value of K_{min}, having a cluster of points around the region 180º separated from the origin. The angular increment per discretisation point is represented in figure 5.3.A.

However, in order to implement this expression, the sum of all $\Delta\vartheta$needs to be equal to 2π to close the loop. Although it may be trivial for some readers, the expression of the summation of eq. (5.25) is developed next. A simpler expression is taken as initial step to later implement the whole expression. The summation of the angular increment is represented in figure 5.3.B, where the last point is 2π, closing the ellipse. Hence, an initial expression is defined as:

$$\sum_{k=1}^{n}\cos(\alpha\cdot k), \tag{5.26}$$

where α represents the angular increment and k the number of times that this increment is performed (in figure 5.3, k is represented in the abscissa axis). To solve that expression, the following relations are needed:

$$\begin{aligned}\cos(kx) &= \mathrm{Re}[\cos(kx)+i\sin(kx)]\\ \sin(kx) &= \mathrm{Re}[\cos(kx)+i\sin(kx)]\end{aligned} \tag{5.27}$$

It will also be useful to use the formulas of De Moivre and Euler, in this order shown next:

$$\cos(kx)+i\sin(kx) = (\cos(x)+i\sin(x))^k = \left(e^{ix}\right)^k \tag{5.28}$$

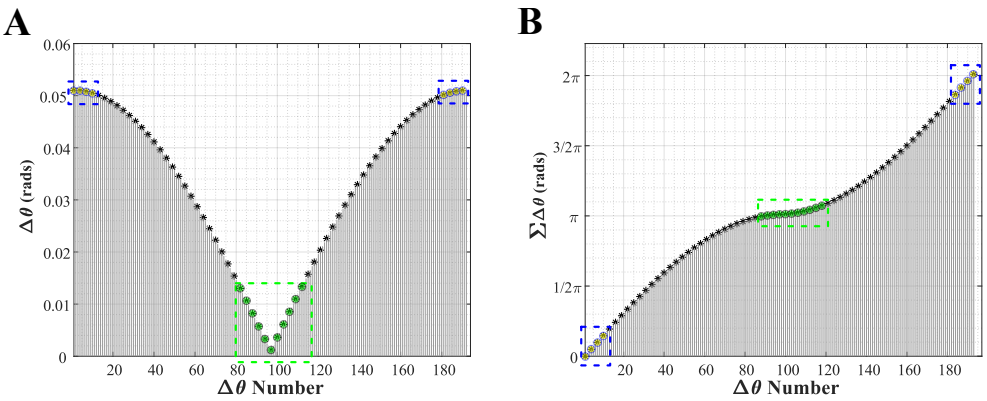

Figure 5.3. Representation of the angular discretisation design in the VCG generator in relation to synthetic VCGs and slow conduction regions. A: Representation of the angle increment ($\Delta\vartheta$) over number of increments needed to complete 2π radians with the absolute cosine formula expressed in eq. (5.25) where K_{min}= 0.001 rad and K_{max}= 0.05 rad. Each angular increment consists of the vertical grey line, so over a constant time discretisation the magnitude of such line is incremented in radians. The sum of all grey lines, that is the summation of all angle increments, correspond to 2π, and the number of increments is computed by numerically solving eq. (5.50). Asterisks represent a sampling of the angular increments corresponded in B and 5.4.A. **B:** Summation of angular increments over time, or in this case, $\Delta\vartheta$ number. X-axis illustrates the time increment which in this case corresponds to the number of angular increments needed – similarly to A. Each grey line correspond to the summation of all the previous grey lines in that $\Delta\vartheta$number in A. In both A and B green regions correspond to 'forced' slow regions in the synthetic VCG and blue to fast regions. All subfigures in figure 5.4 and here are related and consequential, being the colour code related in all of them.

With this, introducing equation (5.26) (in terms of variable x) and equation (5.28):

$$\sum_{k=1}^{n}\cos(kx)+i\sum_{k=1}^{n}\sin(kx)=\sum_{k=1}^{n}(\cos(kx)+i\sin(kx))=\sum_{k=1}^{n}\left((\cos(x)+i\sin(x))^k\right)=\sum_{k=1}^{n}\left(e^{ix}\right)^k, \tag{5.29}$$

where, according to equations (5.27), the solutions for the expressions of interest are defined as:

$$\begin{cases} \sum_{k=1}^{n}\cos(kx)=\mathrm{Re}\left[\sum_{k=1}^{n}\left(e^{ix}\right)^k\right] \\ \sum_{k=1}^{n}\sin(kx)=\mathrm{Im}\left[\sum_{k=1}^{n}\left(e^{ix}\right)^k\right] \end{cases} \tag{5.30}$$

Therefore, the next sum must be solved:

$$S=\sum_{k=1}^{n}\left(e^{ix}\right)^k, \tag{5.31}$$

which can be rewritten as,

$$S=e^{ix}+e^{2ix}+e^{3ix}+\cdots+e^{nix}, \tag{5.32}$$

and multiplying both sides by the first term of the sum:

$$e^{ix}\cdot S=e^{2ix}+e^{3ix}+\cdots+e^{nix}+e^{(n+1)\cdot ix} \tag{5.33}$$

Subtracting the second to the first, all the terms disappear except for the first and last ones:

$$S\left(1-e^{ix}\right)=e^{ix}-e^{(n+1)\cdot ix}=e^{ix}\left(1-e^{nix}\right) \tag{5.34}$$

And the expression of the sum S can be expressed as:

$$S=\frac{e^{ix}\left(1-e^{nix}\right)}{1-e^{ix}} \tag{5.35}$$

So that the equation (5.30) can be rewritten as:

$$\begin{cases} \sum_{k=1}^{n}\cos(kx)=\mathrm{Re}\left[\frac{e^{ix}\left(1-e^{nix}\right)}{1-e^{ix}}\right] \\ \sum_{k=1}^{n}\sin(kx)=\mathrm{Im}\left[\frac{e^{ix}\left(1-e^{nix}\right)}{1-e^{ix}}\right] \end{cases} \tag{5.36}$$

In order to simplify the expression of the sum, Euler's formula (eq. (5.37)) can be used.

$$\begin{cases} e^{ix}=\cos(x)+i\sin(x) \\ e^{-ix}=\cos(x)-i\sin(x) \end{cases} \tag{5.37}$$

Working with Euler's formula, adding both terms and later multiplying numerator and denominator by e^{ix}, the following expression is found:

$$e^{ix}+e^{-ix}=2\cos(x), \tag{5.38}$$

rewritten in terms of the cosine as:

$$\cos(x)=\frac{e^{ix}+e^{-ix}}{2}=\frac{e^{2ix}+1}{2e^{ix}} \tag{5.39}$$

Similarly, subtracting both terms from equation (5.36)

$$e^{ix}-e^{-ix}=2i\cdot\sin(x), \tag{5.40}$$

rewritten in terms of the sine as:

$$\sin(x)=\frac{e^{ix}-e^{-ix}}{2i}=\frac{e^{2ix}-1}{2i\cdot e^{ix}} \tag{5.41}$$

Taking equation (5.41), the terms of the sum expressed in equation (5.35) can be found when rewriting as:

$$1-e^{2ix}=-2i\cdot e^{ix}\cdot\sin(x) \tag{5.42}$$

From the equation (5.42), variable x can be defined as x/2:

$$1 - e^{ix} = -2i \cdot e^{\frac{ix}{2}} \cdot \sin\left(\frac{x}{2}\right), \tag{5.43}$$

or as nx/w:

$$1 - e^{inx} = -2i \cdot e^{\frac{inx}{2}} \cdot \sin\left(\frac{nx}{2}\right) \tag{5.44}$$

Thus, introducing equations (5.43) and (5.44) into the sum expressed in equation (5.35):

$$S = \frac{e^{ix}\left[-2i \cdot e^{\frac{inx}{2}\cdot\sin\left(\frac{nx}{2}\right)}\right]}{-2i \cdot e^{\frac{ix}{2}\cdot\sin\left(\frac{x}{2}\right)}} = e^{\frac{(n+1)}{2}x} \cdot \frac{\sin\left(\frac{nx}{2}\right)}{\sin\left(\frac{x}{2}\right)}, \tag{5.45}$$

and converting the first term by Euler's formula (eq. (5.37)):

$$S = \left[\cos\left(\frac{n+1}{2}x\right) + i\sin\left(\frac{n+1}{2}x\right)\right] \cdot \frac{\sin\left(\frac{nx}{2}\right)}{\sin\left(\frac{x}{2}\right)} \tag{5.46}$$

Separating real and imaginary part we find:

$$S = \frac{\cos\left(\frac{n+1}{2}x\right) \cdot \sin\left(\frac{nx}{2}\right)}{\sin\left(\frac{x}{2}\right)} + i\frac{\sin\left(\frac{n+1}{2}x\right) \cdot \sin\left(\frac{nx}{2}\right)}{\sin\left(\frac{x}{2}\right)} \tag{5.47}$$

Hence, equation (5.26) is solved as:

$$\sum_{k=1}^{N} \cos(k\alpha) = \mathrm{Re}[S] = \frac{\cos\left(\frac{n+1}{2}\alpha\right) \cdot \sin\left(\frac{n\alpha}{2}\right)}{\sin\left(\frac{\alpha}{2}\right)} \tag{5.48}$$

The expression of interest for the stated problem (neglecting φas phase is not the point summation), equation (5.25) can be expressed as follows considering a range in which cosine is always positive:

$$\sum_{k=0}^{N}\left(K_{\max}\cos\left(n\frac{\pi}{N}\right) + K_{\min}\right) = K_{\max} + K_{\min} + \sum_{k=1}^{N}\left(K_{\max} \cdot \cos\left(n\frac{\pi}{N}\right) + K_{\min}\right) \tag{5.49}$$

Rewritten with (5.48) in terms of the same variables (substituting α), as the final expression of the sum variation. Note that, as the absolute sum was computed for the cosine, the absolute value is taken up to π radians, so the expression needs to be multiplied by 2.

$$\boldsymbol{\sum_{n=1}^{N}(\Delta\theta_n) = 2\left[K_{\max} + \frac{N}{2}K_{\min} + K_{\max}\frac{\cos\frac{\pi}{4}\sin\frac{\pi}{4}}{\sin\left(\frac{\pi}{2N}\right)}\right] = 2\pi} \tag{5.50}$$

All the above information and the fundamentals of angle variation and its effect on velocity along the synthetic VCG path are summarised in figures 5.3 and 5.4, which represent the proposed problem through eq. (5.25) (figure 5.3.A), the solution expressed in eq. (5.50) (fig 5.3.B), the visual illustration of the theory developed (figure 5.4.A) and the corresponding velocity profile (figure 5.4.B).

5.4.2. Variation of the Radius: Creating Random Geometries

The radius of an ellipse in polar coordinates as a function of the angle depends on the constants of radius a and b as expressed in equation (5.7). – which depends on randomised parameters equations (5.4), (5.8) and(5.23).

Note that the definitions being designed until now are described for 2-dimensional shapes, and that the synthetic VCG path was defined when introducing the model as a line in a 3-dimensional path. Thus, these paths will be created from the projection of two 2-dimensional ellipses with variant radius and different spatial dispositions.

In 2D, the increment of the angle (for each of the ellipses to be projected) is performed as explained in previous sections. Now, to create a wide variety of random elliptical shapes with loops and variation in the curvature in 3D, some the components in the denominator will randomly variated (within a range) as a function of a the continuous expression of a chirp.

In this way there is going to be an oscillatory increment and decrease of the radius for points which are next to another (note that the frequency is going to be smaller to the shown in the figure).

The frequency of the chirps oscillates from 0 to a random value from 0 to 1 Hz, in the context of the following variables: target time is settled to 10s, sweep time to 100s, sample rate to 50 and finally, the number of samples in the signal is the length of our discretised ϑ(see figure 5.5). This will allow variations in the radius of the ellipse when multiplying the chirp by a constant and by the radius (matching the samples of the chirp to the ones of the synthetic VCG path).

Hence the final expression of the radius as a function of the angle is:

$$r(\theta) = \frac{a \cdot b}{\sqrt{(a \cdot \cos\theta + K_1 C_1)^2 + (b \cdot \sin\theta + K_2 C_2)^2 + K_3 C_3}}, \tag{5.51}$$

where K_1, K_2 and K_3 are random constants in the following ranges: K_1 and K_2 C [0,150] and K_3 C [0,15]. Note that C_1, C_2 and C_3 oscillate from 0 to 1 with the above conditions.

It also needs to be considered that 2 radii are defined for the two projections of XY and ZY, so that both random oscillations together generate variations in the curvature in 3 dimensions.

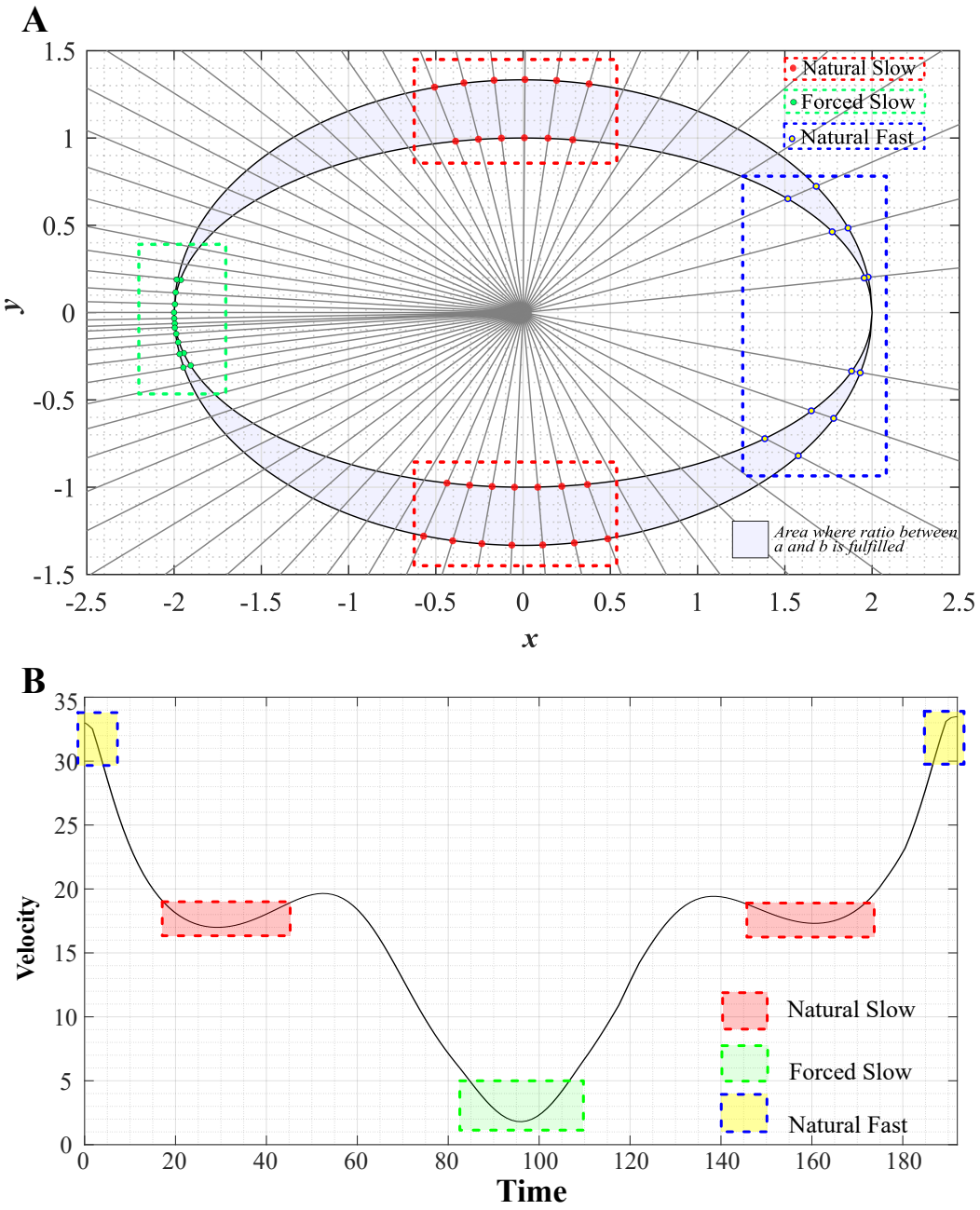

Figure 5.4. Representation of the angular discretisation design in the VCGs generator in relation to synthetic VCGs, slow regions, and their velocity profile. A: Representation of a synthetic 2D ellipse following the theory developed and figure 5.3. Angular discretisation are sampled to illustrate clearer the result. Blue shaded area represents the allowed area when fulfilling the semi-axes relation expressed in eq. (5.13) **B:** Velocity profile over the path generated by the ellipse in A and with the angular discretisation defined by plots in figure 5.3. Velocity and Time are unitless in this case because of being an illustration over a hypothetical time discretisation over a unitless spatial representation in A. Green slow region is defined as 'forced' because it is defined by small angular increments deliberately designed with this purpose. Red slow areas are of the geometrical uniqueness of the ellipse, which has been chosen in this orientation to provide this profile, similar to the one obtained when analysing real VCGs. Fast yellow areas are presented at the beginning and end of the profile since the initial and final point are located in the middle of the fast region. All subfigures in figure 5.3 and here are related and consequential, being the colour code related in all of them.

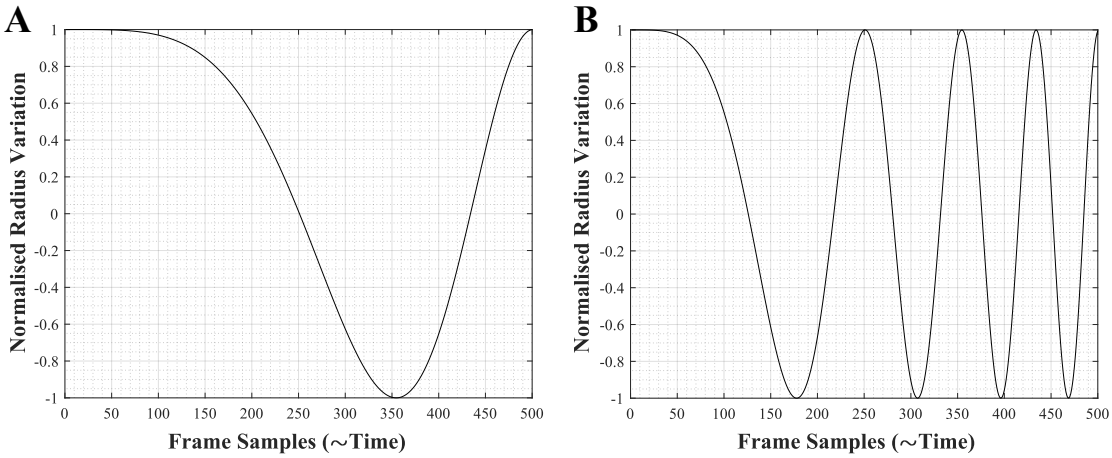

Figure 5.5. Representation of two chirp signals with normalised radius variation and two examples of target frequencies over 500 samples (equivalent to time if it was a real signal, not simulated). Target time is fixed to 10s, sweep time to 100s, sample rate to 50 and final or target frequency to 0.2Hz (A) and 0.8Hz (B). The generated chirps are randomised so that the target frequency can acquire any of 10.001 values from 0 (no chirp) to 1Hz (a slightly higher frequency to the represented in B).

5.5. Definition of the Cartesian Coordinates of the Ellipsoidal Loop

The definition of the coordinates in the 3-dimensional pathway is computed in the Cartesian space as follows:

$$\begin{cases} x = r_1(\theta) \cdot \cos(\theta) \\ y = r_1(\theta) \cdot \sin(\theta) \\ z = r_2(\theta) \cdot \cos(\theta) \end{cases} \tag{5.52}$$

With the above definition the ellipsoidal figure may not be closed because:

- r_1 and r_2 are not have according to the same random parameters and the perimeter of the ellipse in ZY plane depends on P_2 (which may be a different perimeter) slightly smaller than P_1 (in which the XY ellipse is defined) with the only purpose of finding the ellipsoidal figure as a projection of both.
- The contribution of the chirps may not end at zero increment in the radius (since individually they may finish in a normalised increment between +1 and 1), and as there are 6 chirp variables depending on 6 random constants, it may be that the initial modification of the radius is not the same as the final one at 2π degrees.

To solve this issue, the last points of the ellipse and the first ones are interpolated in the 3-dimensional path to create a closed ellipse. Note also that the ellipse is centred at the centre of coordinates by subtracting the average of all points in a translation placing it at that position.

5.6. Smoothing the Synthetic VCG and Velocity Profile

Because of the wide variety of shapes and the variegated variability of changing parameters, the angular discretisation can seldomly present peak that would not appear in natural VCGs coming from patients. Thus, a low pass filter can be applied over the 3-dimensional path. An adaptation of the Savitzky–Golay filter over the three axis has been implemented to slightly smooth the trajectory avoiding these possible peaks. A final synthetic VCG is represented in figure 5.6.A. (the three main projections are illustrated), and the difference between being filtered or not is observed in figure 5.6.B-C.

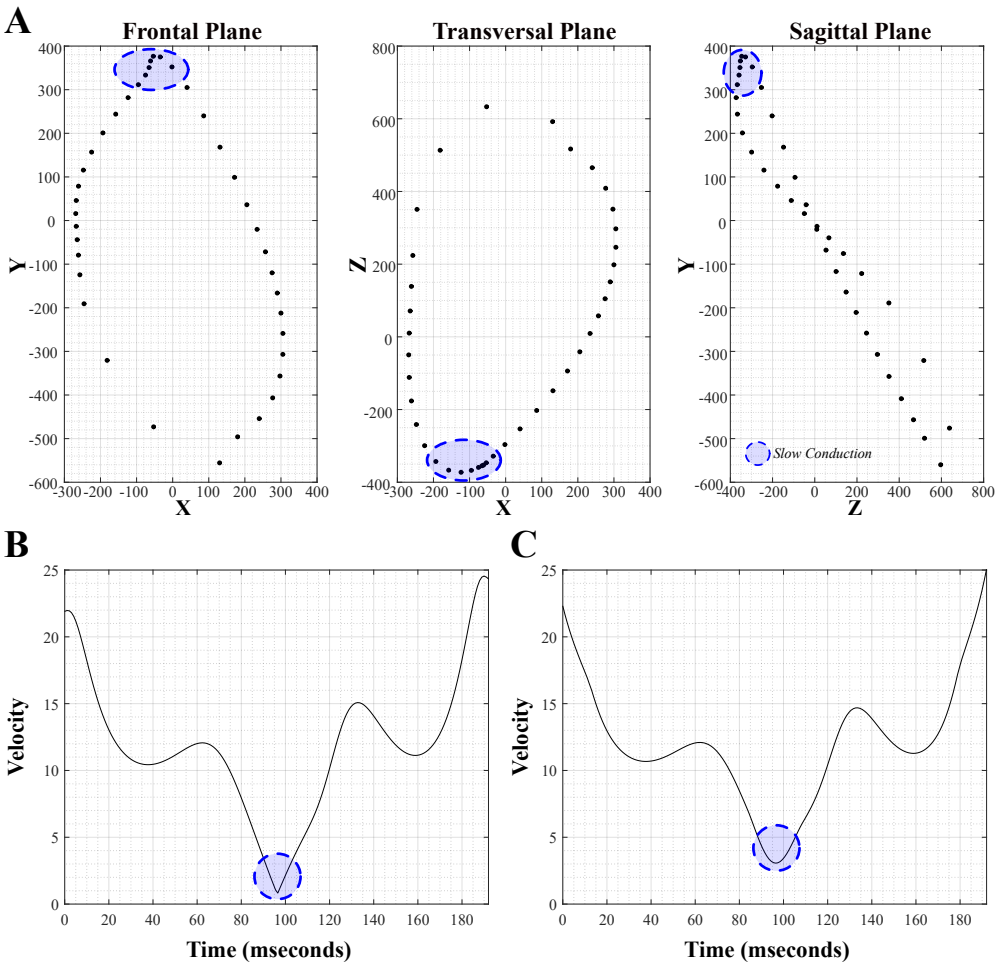

Figure 5.6. Synthetic VCG created by the mathematical model (A)**, represented after sampling, and velocity profiles before** (B) **and after** (C) **having applied an adapted low pass Savitzky–Golay filter over the 3-dimensional VCG loop. A:** Representation of the 3 standard VCG projections (frontal, transversal and sagittal) of the synthetic VCG created by the mathematical model. **B:** Representation of the velocity profile before applying the designed low pass filter over the synthetic VCG, which is not represented in this figure because no changes are observable in the figure with respect to the loop after being filtered. Unnatural peaks are observed at the minimum velocity and at the beginning and end. **C:** Velocity profile after applying the adapted low pass Savitzky–Golay filter, implemented in the model, which corrects the unnatural shaped peaks observed in B. Slow regions are highlighted in A, B and C with a dotted blue shaded circular shape.

5.7. Modalities: Subgroups of Ellipsoidal figures

The main parameter to define the subgroup of the ellipsoidal figures or synthetic VCGs is the region where the minimum of the absolute cosine function in the angular discretisation appears (see figure 5.3.A) that is, the agglomeration of points (see green regions in figure 5.4). This is equivalent to the slow regions of the VCG representation. In this way, if the algorithm works properly identifying the figures in their correspondent group by this parameter of slow velocity, the efficiency of the algorithm we are testing will be proved.

The mathematical model creates the same number of 8 different types of figures. As they are rotated in different ways, the slow velocity regions appear in different spatial locations. In the same way, there are two groups in the same range of planes. In those, the initial point would be defined in opposite regions, varying where the slow region would appear. Plane A is defined as the plane corresponding to the projection of Planes XY and ZY. Thus, the four first groups are defined as depicted in table 5.1

β_{pq} is a random angle between -15 and 15 being p and q indexes indicating the type and coordinate to which this constant is being added. Thus, the slow region in the same group is at the same position with respect to the initial point of the figure, which is always the same. However, there is a variation of 30^o per coordinate so that the slow region is not exactly in the same, so that it relates more to real life VCGs, where anatomies are not exact.

For groups 5 to 8, the same conditions as in groups 1 to 4 are considered, but the opposite sense is being evaluated. Calling groups 1 to 4 as synthetically CW, groups 5 to 8 would be the correspondent CCW. Although slow regions would be located in similar spatial regions, this provides the mathematical model with a more accurate representation of the VCG possibilities considering also the sense of the current transmission in electrophysiological terms. Table 5.1 summarises the definition of the eight possible groups that the VCG generator creates. The included parameters are only the ones modifying the sense or slow region spatial distribution, since the rest of parameters are randomised within the aforementioned ranges among all the groups.

Synthetic VCG Type	Sense	Plane Rotation	Initial Angle
Type I	CW	$60^o \pm \beta_{11}, 90^o \pm \beta_{12}, 40^o \pm \beta_{12}$	0 radians
Type II	CW	$30^o \pm \beta_{21}, 60^o \pm \beta_{22}, 10^o \pm \beta_{22}$	0 radians
Type III	CW	$30^o \pm \beta_{31}, 60^o \pm \beta_{32}, 10^o \pm \beta_{32}$	π radians
Type IV	CW	$60^o \pm \beta_{41}, 90^o \pm \beta_{42}, 40^o \pm \beta_{42}$	π radians
Type V	CCW	$60^o \pm \beta_{11}, 90^o \pm \beta_{12}, 40^o \pm \beta_{12}$	0 radians
Type VI	CCW	$30^o \pm \beta_{21}, 60^o \pm \beta_{22}, 10^o \pm \beta_{22}$	0 radians
Type VII	CCW	$30^o \pm \beta_{31}, 60^o \pm \beta_{32}, 10^o \pm \beta_{32}$	π radians
Type VIII	CCW	$60^o \pm \beta_{41}, 90^o \pm \beta_{42}, 40^o \pm \beta_{42}$	π radians

Table 5.1. SYNTHETIC VCG TYPES AND CHARACTERISCTISATION

6. RESULTS AND DISCUSSION

6.1. Introduction and Organisation of Results and Discussions

Conventionally, in scientific literature (papers, thesis, dissertations...), results are organised in one section so that the results when applying the methodology are well presented to later be commented in the discussion section. Nonetheless, because of the technical nature of this dissertation and the wide amount of methods being used, I consider more appropriate to group results and discussions. In this manner, I can better expose the different results for all the parameters used to quantify VCG features and discuss each of these results sequentially.

The possibility of expressing the results in one section and discussion in a different one exists, but I find more convenient to write both together so that the discussion is better understood having the tables and figures in the same section. Furthermore, there is a wide assortment of schemes and results for the broad and varied methods utilised, so this approach is found to be more convenient.

Finally, due to the two main groups of methods used in this study (for patients and synthetic VCGs), it is convenient to separate the analysis of results and discussions in two sections.

As a brief comment on the organisation of the two main analysis performed, I will talk firstly about the synthetic VCG generator and then about the actual results of the signals coming from patients. The first allow me to test my hypothesis in a controlled manner and reach meaningful conclusions about the variation of parameters and about the appropriateness of the methods that I use to evaluate the patients. Having made tests and analysis in a controlled environment with a big quantity of synthetic signals, I will present the results computed from the signals coming from the patients, acquired and processed as described in the methods section. The discussion for each of the parameters will be performed after displaying the results for each of the sections, as well as how each influence the hypothesis and objectives proposed at the beginning of the dissertation.

6.2. Analysis of the Synthetic VCGs Results

The efficiency and contribution of the synthetic VCG generator are addressed from different perspectives. It is convenient to remind that the only parameter characterising each of the groups is the location of the slow region defined by an initial point for discretisation and plane position of the synthetic VCG, allowing the slow region to be located within an area in the space.

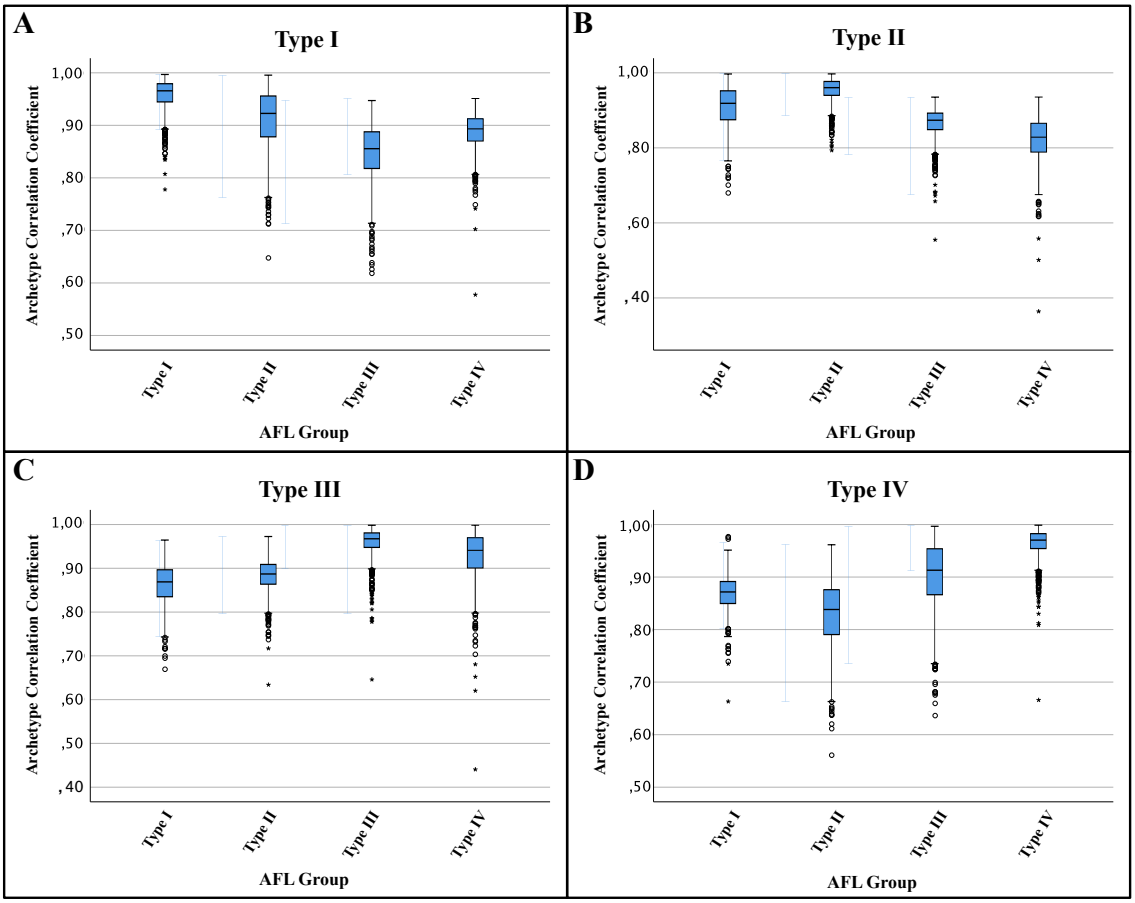

Figure 6.1. Box plot of the correlation coefficient of types I to IV with their representative archetypes (A to D correspondingly). Each subfigure represents the correlation of one archetype (created from the 'training' synthetic cases) with all the patients from groups I to IV (the 'real' population)

Also remember that for the correlation, an archetype was created for each group from 25 synthetic cases of each type, and then 1000 synthetic cases were created to be correlated with all archetypes. The results of the correlation of these 8000 patients with each of the archetypes is displayed in figure 6.1 – note that only groups 1 to 4 were included as groups 5 to 8 are the opposite-direction version of groups 1 to 4, offering a similar results among them as the depicted on this figure.

The results corresponding to the average correlation and standard deviation for each of the archetypes is displayed in table 6.1.

	Type I Patients	**Type II Patients**	**Type III Patients**	**Type IV Patients**
Type I Arch	0.96±0.03	0.91±0.05	0.85±0.05	0.80±0.04
Type II Arch	0.91±0.05	0.95±0.03	0.86±0.04	0.82±0.06
Type III Arch	0.86±0.05	0.88±0.04	0.96±0.03	0.92±0.05
Type IV Arch	0.89±0.04	0.82±0.06	0.90±0.06	0.96±0.02

Table 6.1. AVERAGE CORRELATION COEFFICIENT OF THE PATIENTS FROM EACH GROUP THE ARCHETYPES

Figure 6.1 and table 6.1. illustrate the differences in the CP when patients

belonging to a specific group are correlated with the archetype of its group of to others. In all the subimages, the highest and most concentrated correlations are found in the synthetic VCGs being correlated to their archetype, demonstrating the differentiating capacity of the concentration of the slow region in a constrained area, rather than other features in the shape or other parameters that tend to have a Gaussian distribution in all the types.

The fact that there is some overlapping between the groups is noticeable for all the types (note that types 5-8 show the same distribution than 1-4). The reason is that in order to perform later a statistical analysis to understand the significance for the different correlations in such a big group, a considerable freedom was given to the location of slow areas when allowing rotation of the planes of $\pm 15^{o}$ per coordinate. Even if this variability was allowed, the results showed a clear difference among the groups.

The ANOVA test shows statistical significance for all the cases with a p-value $p<0.001$ for all the types. The F corresponding to the ANOVA test for the 8 correlation tests are for each of the archetypes in order: F=1050.68, F=1456.28, F=973.85, F=1215.12, F=959.20, F=1288.73, F=1191.51, F=1371.81. Thus, although overlapping among groups occurs, statistical tests show difference among the types from the evaluation of the correlation parameter. Furthermore, when evaluating through multiple comparisons using Bonferroni's test, a high significance is found for all groups when compared to any other ($p<0.001$ for all of them).

To evaluate how accurate this method would be for classification purposes and evaluating how precise the mathematical model is in terms of differentiating among groups, ROC curves are created for each of the types (see figure 6.2).

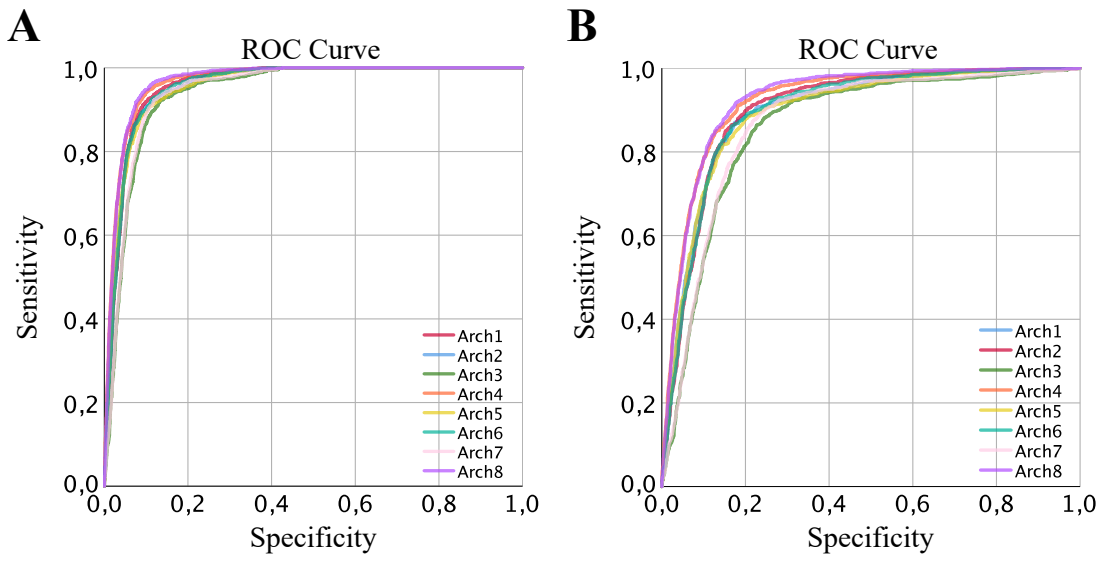

Figure 6.2. ROC curves for all patients corresponding to each of the groups when taking into account all the 8000 synthetic patients (A) or the first 4000 in one subgroup (with types I-IV) and the rest in the other (types V-VIII).

The first ROC curve (figure 6.2.A) represents all the curves for each of the group of patients and their archetype. The second one (figure 6.2.B) represents the same analysis but comparing on one side the first four groups and on the second the four last groups. The results of each AUC for both types of analysis is represented in table 6.2.

	Type I	**Type II**	**Type III**	**Type IV**	**Type V**	**Type VI**	**Type VII**	**Type VIII**
AUC (8)	0.957	0.958	0.941	0.967	0.955	0.957	0.945	0.968
AUC (4vs4)	0.899	0.902	0.863	0.923	0.895	0.899	0.872	0.926

Table 6.2. AUC FOR ALL PATIENTS IN TWO MODALITIES

As observed in both, figure 6.2. and table 6.2, the AUCs are higher for the groups in which the 1000 patients have been compared to the other 7000, as the difference between groups 1-4 and 5-8 is very noticeable. Thus, a more accurate model would be presented by the ROC curves in which only 4000 patients are taken into account and the 8 groups are analysed as if they belonged to two subgroups. Even in this case, the high area under the curve and the very positive shape of all the curves demonstrate a high precision in the determination of whether the patients from each group belong to the group defined by their archetype. This strengthen the hypothesis of the correlation coefficient as a crucial parameter to discriminate among AFL groups, based in this model just (as previously mentioned) on the location of predefined slow regions.

Hence, something of a great interest to asses in the model is based on a controlled variation on the parameters of a synthetic VCG model. With this purpose, for different slow conduction concentrations (redefining K_{max} and K_{min} eq. 5.50), rotations on two directions of the VCG and on the position of the slow conduction area are performed, as depicted by figure 6.3 (A and B respectively).

For the figure in which the synthetic VCG is being rotated as a whole (figure 6.3.A), two groups of four-colour lines can be distinguished. The change in colour means a 'slower' slow conduction region through the decrease of K_{min} in eq. 5.50. In order black, red, blue and green the conduction velocity is decreased for the characteristic area.

The first type of rotation consists of turning the synthetic loop around an axis that links the slowest region to the fastest in the VCG (that is, the major semi-axis of the irregular ellipse). The variation with the change in K_{min} is very slight, and it is attributed to the fact that, although the slow region is more concentrating contributing to a better CP, the faster region is gaining speed at the same time (increase in K_{max} to maintain the number of discretisation points). Thus, the slight improve in correlation from the higher concentration is counteracted by the reduction of points in the fast region, that are placed in semi-slow regions or along the trajectory, slightly decreasing the correlation. Something similar would happen in the order of the lines when rotating with respect to the minor semi-axis (lower

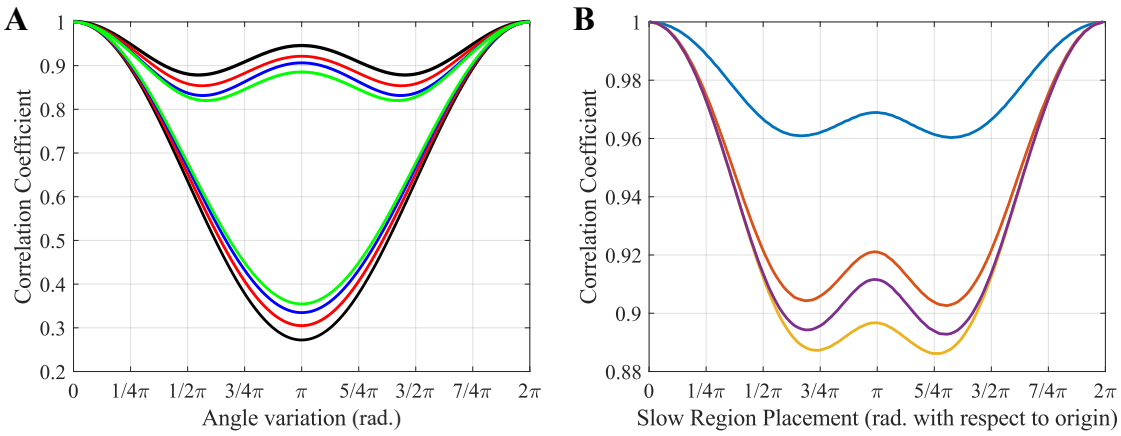

Figure 6.3. Variation of correlation coefficient under the modification of parameters having the rest fixed in the synthetic VCG Generator. A: Rotation over the major semi-axis (higher correlation coefficients) and minor semi-axis, entailing the movement of the slow conduction region, located at one extreme of the major semi-axis (lower correlation coefficient). **B:** Correlation coefficient of a synthetic loop with itself, changing the position of the slow region over the whole trajectory in one of them. For A, $\mathbf{K_{min}}$>K_{min}>K_{min}>K_{min}. For B, K_{min}>K_{min}>K_{min}>K_{min}. The lower the K_{min}, the slower the conduction area (and correspondingly, the higher the velocity in the fast conduction region and higher K_{max}, as number of discretisation points is maintained, see eq.5.50).

correlations coefficients).

Nevertheless, this is not the point of discussion. The interesting quality to asses is the significant decrease in the correlation parameter when performing a rotation involving the movement of the slow region, in comparison with the slight decrease when moving all the loop except for the synthetic loop. This reinforces the great contribution of the placement of the slow region to the correlation coefficient.

The other figure in this scheme (figure 6.3.B), represents the variation of the placement of the slow conduction region along the whole trajectory. This demonstrates that in exactly the same trajectory the coefficients that contribute to the correlation tend to overlap although the slow region is varying, and even if the trajectory is exactly the same, up to higher values than 0.1 can be affected by this position. This figure is illustrative to study the properties of the model.

Finally, an interesting result to discuss, related to the difference of both ROC curves (figure 6.2) is the contribution to the correlation coefficient when changing the direction of conduction. The significant change in the correlation from groups 1-4 to 5-8 determines that, although sharing the rest of parameters, the direction of conduction is well distinguished by this analysis (see figure 6.4).

6.3. Analysis, Interpretation and Discussion of the Patient's Results

In this section, the result of the analysis of the signals coming from patients after being acquired and processed according to the first sections of methods I is presented. With this purpose and following the techniques presented in the aforementioned section, results are arranged in four divisions. The first describes the

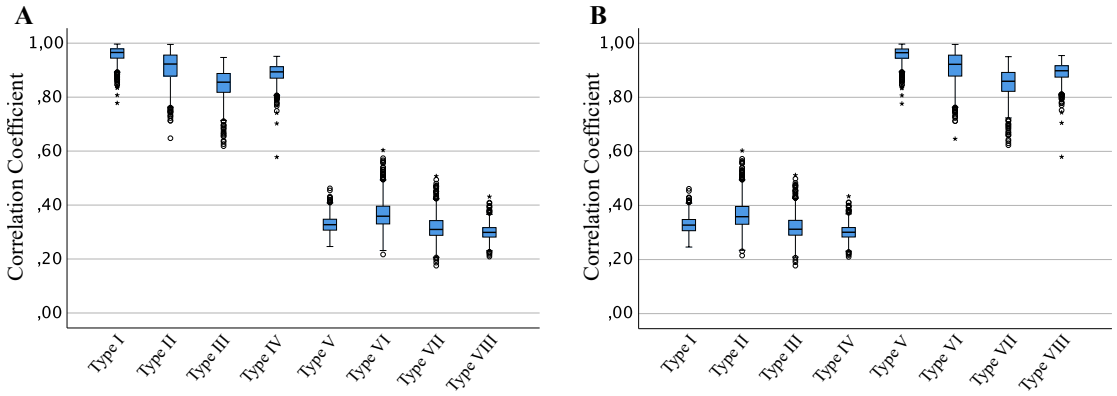

Figure 6.4. Box plot of the correlation coefficient of all synthetic VCG types with two archetypes. Correlation of all VCGs (8000) with archetype I. **B:** Homologous with type V. The purpose of this figure is to highlight the difference between groups I-IV and V-VIII in terms of correlation coefficient, cause by the change of direction (I-IV would be the CW version and V-VIII the homologous CCW).

general characteristics of the groups, stating differences or common features that characterise the acquired signals. The second focuses on the parameters related to the distribution of slow velocity frames. The third evaluates the simplicity or complexity of the signals through the arc or circumference parameter. Finally, the fundamental section that tests the hypothesis is depicted, showing whether the parameter of correlation significantly influenced by the location of slow velocity regions allows the distinction of AFL types or not.

The AFL types are presented in the figures as C.CCW, C.CW, P.CCW, P.CW and misc., being common CCW AFL, common CW AFL, perimitral CCW AFL, perimitral CW AFL and the miscellaneous of atypical AFL cases not belonging to the previous groups, respectively.

6.3.1. General VCG Features: Number of cycles, Loop Time Length Consistence Intra-Patient

The results for the number of cycles that were feasible to be analysed to later compute the average of the waves having a representative averaged VCG loop for the patient is as described in table 6.3.

Number of Cycles	2	3-4	5-6	7-8	9-10
Number of VCGs	1	3	0	2	23

Table 6.3. NUMBER OF VCGS VS NUMBER OF CYCLES FROM WHICH THEY WERE AVERAGED

The objective was to compute the average over 10 loops for each of the patients in the region affected by adenosine, that is, the ECG region with the exclusive contribution of the atria, where the AFL was taking place.

Patients were filtered for this study, choosing only the one appropriate for the study, that is, without an inconvenient medical history or the record of previous

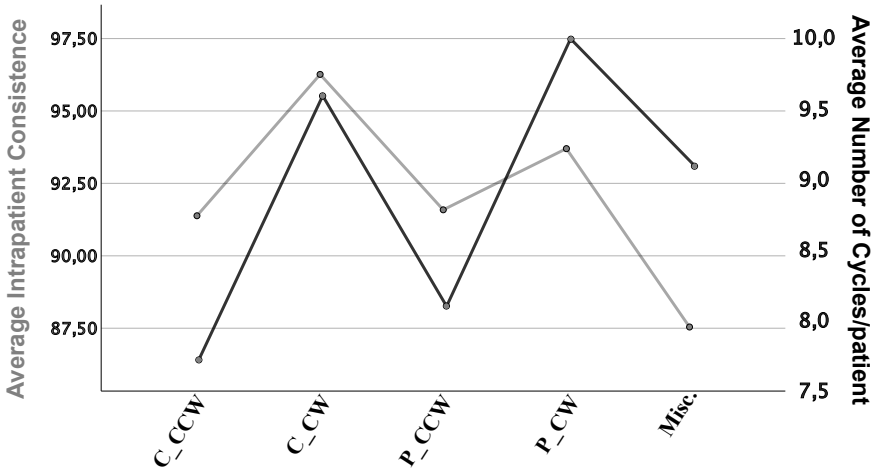

Figure 6.5. Representation of the average consistence intra-patient (grey) **and the average number of cycles** (black) **for all the patients belonging to the different AFL groups.** None of these parameters present statistical significance to distinguish among groups, but they follow a similar tendency and allow enclosing the signals among ranges and evaluating their appropriateness for the study.

cardiac pathologies. Therefore, it was expected that most of the cases were on the last group, having a clear signal to obtain 10 atrial loops.

The consistence intra-patient is more meaningful in this case since it shows how similar were the atrial loops before computing the average. The results for this parameter for each of the AFL groups is displayed in figure 6.5, together with the average number of cycles per group.

The results for the average and variance of these two parameters for each of the groups is displayed in table 6.4.

	C.CCW	**C.CW**	**P.CCW**	**P.CW**	**Misc.**	**Overall**
Cycle Number	7,75±1,65	9,60±0,40	8,13±1,23	10,00±0,00	9,11±0,77	8,83±0,47
Intra-pat. CP	91,38±8,60	96,26±2,87	91,58±10,29	93,70±1,89	87,54±13,85	91,32±10,01

Table 6.4. AVERAGE CYCLE NUMBER AND CONSISTENCE INTRA-PATIENT

The CP is above 90% in average for all the groups except for the atypical miscellaneous an in the overall average. The more similar the cycles are among them, the more credible the signal is as coming from a characteristic from an AFL. Thus, this parameter allows to discriminate whether there is influence of other cardiac arrhythmias. Hence due to the high consistence coefficients intra-patient found in all the cases it can be stated that all of them are representative and that, in general, if more loops are feasible to be extracted from the signal of the patient, a higher CP is obtained. Note that this is not always true as the miscellaneous group should have the worst CP intra-patient, but it does not. This can be attributed to the complexity that these cases usually show in the MC of the signal.

Finally, the average time length for each of the patients is summarised in table

6.5.

Time Length (ms)	<200	200-300	>300
Number of VCGs	2	23	4

Table 6.5. NUMBER OF VCGS VS AVERAGE TIME LENGTH

Note that almost all the cases are in the range described by literature, that is, between 200 and 300 ms per loop. Furthermore, 18 of them agglutinate in the tight range of 200-250 ms. From the abnormal values our of these range, four belong the the miscellaneous group, that present the highest variation of velocities ranging from below 200ms to over 300ms. Furthermore, commons are always constrained to this range, and common CW cases are always between 200 and 250ms. This result makes sense as the obstacle of the tricuspid valve around which the macrorreentry is formed in the common cases does not have a wide variation between patients. The distribution per AFL group is presented in figure 6.6.

All in all, these parameters allow to contextualise the quality and overall characteristics of the group of signals we are working with, and to complement the information given by other tests, but it does not allow to completely characterise or define all the AFL groups. The non-parametric Kruskal-Wallis test performed over the number of cycles, intra-patient CP and time length for each group present a p-value of p=0.659, p=0.513 and p=0.098 respectively, demonstrating no statistical significance to distinguish among groups.

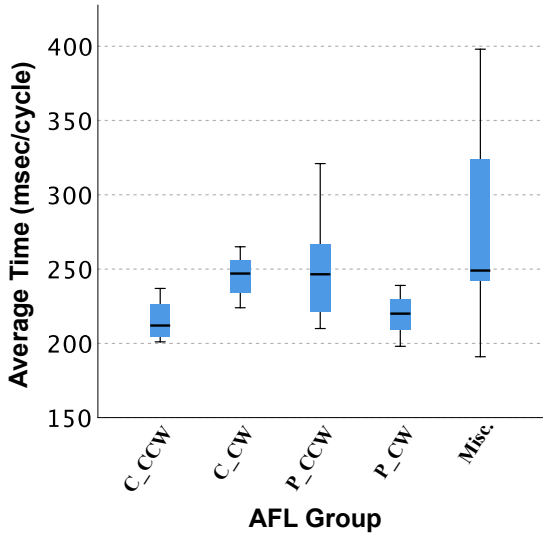

Figure 6.6. Representation a box and whiskers plot for the parameter of Average Time per VCG loop (in msec/cycle) from the Kruskal-Wallis test showing non-statistical significance to discriminate among groups (p=0.098). The highest dispersion is observed in the miscellaneous group with an average of 275.89 ±69.03 ms.

6.3.2. Slow Conduction Region Distribution Analysis: SVPOT, SVPOD and Rate

The results for the SVPOT, SVPOD and their rate are summarised in table 6.6.

	C.CCW	**C.CW**	**P.CCW**	**P.CW**	**Misc.**	**Overall**
SVPOT	0.41±0.05	0.18±0.12	0.30±0.14	0.21±0.19	0.43±0.18	0.32±0.17
Range SVPOT	[0.36,0.48]	[0.08,0.35]	[0.06,0.44]	[0.06,0.42]	[0.20,0.75]	[0.25,0.39]
SVPOD	0.20±0.03	0.08±0.06	0.12±0.06	0.10±0.14	0.17± 0.06	0.14± 0.08
Range SVPOD	[0.17,0.24]	[0.03,0.18]	[0.02,0.22]	[0.02,0.27]	[0.07,0.24]	[0.01,0.26]
Rate	2.09±0.17	2.30±0.26	2.47±0,37	3.23±1,54	2.46±0,40	2.46±0.59
Range Rate	[1.97,2.34]	[1.98,2.57]	[1.93,3.10]	[1.58,4.64]	[1.68,3.17]	[1.58,4.64]

Table 6.6. RESULTS OF SVPOD AND SVPOT PARAMETERS

To have a better illustration of the distribution of the values for the different parameters for each of the AFL groups, a box plot has been created and the non-parametric Kruskal-Wallis test is used to later evaluate the significance in these variables. Before continuing with the discussion on these results, see figure 6.7 representing these values in a box plot and contrasting averages in the last sub-image.

For the interpretation of this data, it has to be remembered how these parameters were designed in the materials I section and what they represent. The SVPOT allows us to identify what is the percentage of time at which the conduction signal travels under the threshold velocity. Thus, the lower this parameter is, the lower the time the velocity is under this threshold, and vice versa. Thus, it can be observed how in average, common cases spend more time under this threshold than perimitral, although there is a great difference between both senses. In both cases, common and perimitral, CCW direction shows a higher time travelling in low velocity (see table 6.6 and figure 6.7). These results provide us with clues for physiological and clinical studies about the reasons for the AFL to spend more time in low velocity when travelling in one direction or in another. This may help to understand better the physiochemical mechanisms of AFL that are currently under study.

In the case of the parameter, it helps to understand what percentage of distance of the MC where the conduction velocity travels under the given threshold. Thus, this parameter provides a more direct relation with the anatomy and physiology of the tissue where the conduction occurs. In this case parameters follow a similar tendency as svpot for every group but are significantly lower (see figure 6.7.D). This indicates a very clear topic of discussion: the slow regions are located in specific and probably well-defined regions of the MC spending a high percentage of time in a very specific region. Thus, SVPOT is higher than SVPOD for every case. Again, for this parameter, higher values are obtained on average in CCW direction than in CW, reinforcing the previous statement about the importance of direction in terms

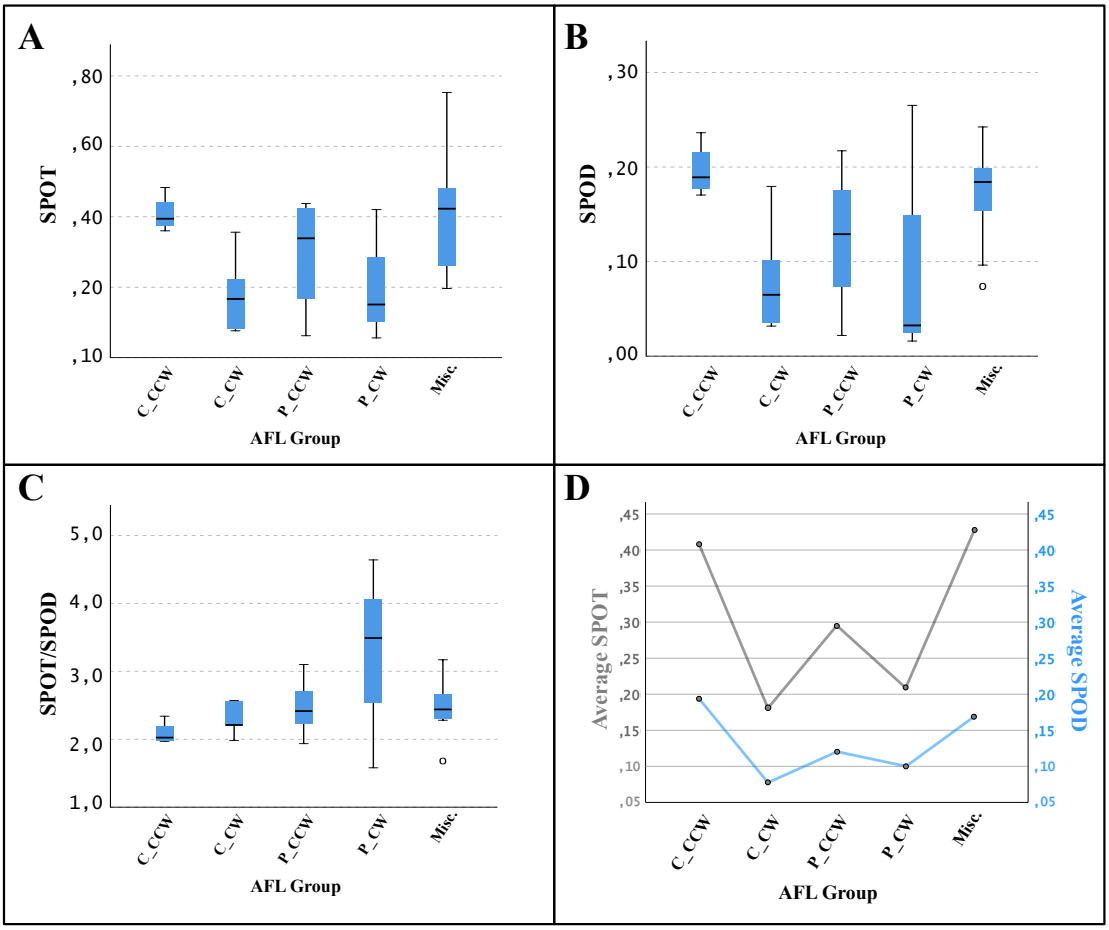

Figure 6.7. Representation a box and whiskers plot for the parameter of SVPOT, SVPOD and SVPOT/SVPOD rate. A, B and **C:** Representation the box plots from these variables showing no significance for B and C (p>=105) and statistical significance for A (P=0.045). **D:** Representation of the averages of SVPOT and SVPOD in the same scale to observe the same tendency but significantly different values.

of slow velocity distributions. For both SVPOT and SVPOD the highest average values are found in the miscellaneous group, indicating that these cases where the MC is not located around the mitral nor the tricuspid valve present broader slow conduction regions.

It is also noticeable that the cases that present more variability (a higher range between the maximum and minimum value found) are perimitral for SVPOD (specially perimitral CW), and the miscellaneous group for the SVPOT. Nevertheless, as this would not be completely meaningful if the relation among SVPOD and SVPOT is maintained among the different groups. For this analysis, the rate SVPOT/SVPOD can be used, complementing the previous discussions and providing some more meaningful information.

As a quick reminder, the rate SVPOT/SVPOD provides information about how slow regions are for a given AF case. In case of having a low rate, the percentage of time were the conduction velocity is slow would be similar to the percentage of loop distance at which the velocity under the threshold. On the opposite side, a

high parameter describes a case where there is a long time at which the conduction velocity is very low, travelling over a small distance of tissue.

Thus, this rate has a direct relation with physiological problems related with the tissue. The slow activation regions in AFL are being studied constituting a fundamental topic of research nowadays, and this parameter directly states the existence of very slow regions over the MC.

Analysing the data (see table 6.6 and figure 6.7.C), the fact that the average values for this rate is over 2 in all the AFL cases need to be highlighted, as it describes the existence of considerably slow regions in all the cases. Furthermore, there is a noticeable difference between common and perimitral AFL cases, as common AFL normally present a lower rates than perimitral, indicating slower or more concentrated regions around the MC around the mitral valve.

Moreover, for the clockwise direction in perimitral AFL a very wide variety is found, offering a new perspective: although slow conduction is generally slower and concentrated for these cases, there is a wide variability with possibility of finding cases with faster or less concentrated conduction velocities. This fact indicates the relation of slow conduction with the tissue over which the MC is located. Hence, it orients physiological studies to focus on characterising the tissue where slow conduction happens over these cases and observe the differences when these rates happen to be different. Perimitral CW AFL would be convenient for this analysis as a relatively big variation appears from the minimum to the maximum value for this rate, ranging from 1.58 to 4.64, which are the absolute minimum and maximum of all the AFL cases analysed, including the miscellaneous group.

Finally, it is important to notice how these parameters are used to analyse, evaluate and understand better the physiological mechanisms of AFL, but it does not provide us with statistically significant information to discriminate among AFL groups. The non-parametric Kruskal-Wallis test over these parameters provide a slightly relative significance for SVPOT (p=0.045) and no statistical significance for SVPOD (p=0.105) or SVPOT/SVPOD rate (p=0.330). Thus, despite the fact that this was not the purpose when defining these parameters, SVPOT could be used to help the identification of flutter type. The SVPOT/SVPOD rate unveils that there is in the end a high similarity among groups for this parameter in statistical terms, describing the common fact that all AFL types share a relatively slow region that may be characteristic for each group.

6.3.3. Arc or Circumference Parameter

The results for the arc parameter in each of the groups are summarised in table 6.7

*Outliers are not taken into account to define ranges

	C.CCW	C.CW	P.CCW	P.CW	Misc.	Overall
Arc Param. (rad)	8.28±.59	10,08±1.97	12,66±5.30	10,52±2.18	15,97±7.42	12.42±5.62
Range (rad.)	[7.64,8.97]	[7.62,12.92]	[7.83,14.55*]	[9.17,13.03]	[8.41,32.51]	[7.62,32.51]
Norm Arc. Param	0.76±.05	0.64±0.12	0.55±0.17	0.61±0.11	0.46±0.18	0.57±0.17
Range (norm.)	[0.70,0.82]	[0.49,0.82]	[0.25,0.80]	[0.48,0.68]	[0.19,0.74]	[0.19,0.82]

Table 6.7. RESULTS OF ARC PARAMETER FOR ALL AFL GROUPS

The result for the arc parameter is representative not only for the characterisation of the VCG loops but also for the discrimination among different types, as it will be later explained in this section. For a better picture of the data, a box and whiskers plot is depicted in figure 6.8 In both, table 6.7. and figure 6.8, two representations of this parameter are shown: in radians and in the normalised parameter. The distribution for the different groups is the same and so is the statistical significance found when performing a non-parametric test over the data. However, the one described in radians may help for the understanding of the interpretation of the parameter. For the final discussions the unitless would be used as found to be more appropriate to illustrate the result as it is constrained between 1 and zero.

The arc parameter describes how complex a VCG loop is by computing the summation of all the angular increments in the three directions of the Cartesian space. Thus, it allows to identify how complex is the path that the MC is following around an obstacle in the atria. Notice that the VCG does not reflex the exact path but the projection of the main vector of the conduction potential, so it is not an actual map of the MC but of its vectorial projection (see the state of the art).

The higher the arc parameter is in radians, the lower it would be in its normalised correspondent expression as 1 would be the simplest possible path and an infinitely

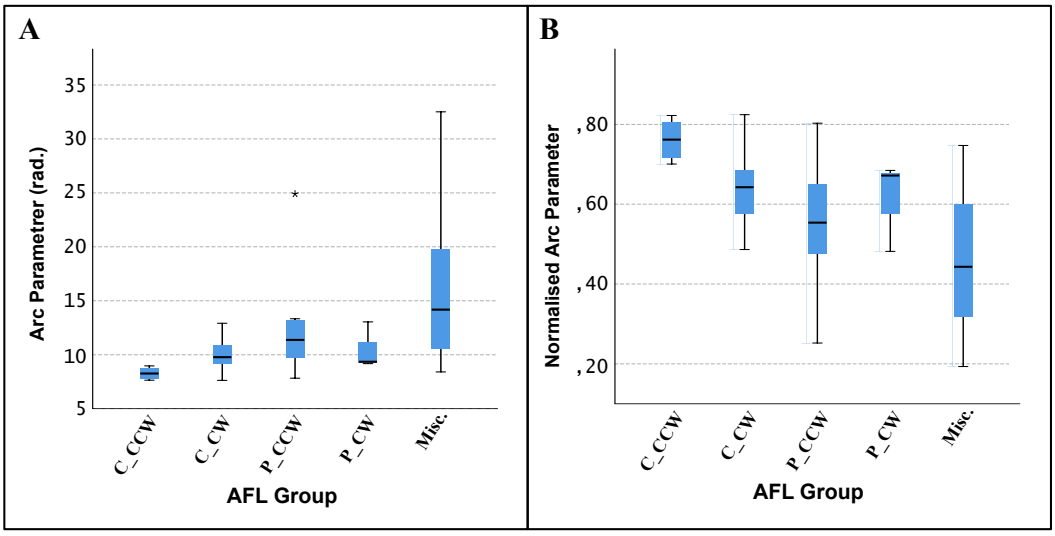

Figure 6.8. Representation a box and whiskers plot for the arc or circumference parameter in radians (A) **and in a normalised unitless version** (B)**.** The representation of this variable shows statistical significance (p=0.035) when performing a non-parametric Kruskal-Wallis test. This can be predicted when observing the box plot as groups are conspicuously separated or around different ranges of values.

complex loop would tend to 0. Thus, in general terms, common AFL types tend to be simpler than perimitral as they present a higher normalised arc parameter. On the other hand, the miscellaneous group has the lowest coefficient, being defined as the most complex. Thus, not only the obstacles that define the macroreentrant pathway are variate, but also defined by more complex anatomies in general terms (see table 6.7 and figure 6.8).

In terms of variability, common cases present the smallest variation (and CW perimitral, but I do not consider mentioning its variability accurate due to having the smallest number of patients). Thus, the anatomy where the MC is described appears to be very similar among common AFL cases. On the other hand, CCW perimitral and miscellaneous cases present the wider variability. However, there is an outlier that contributes to this variability (see figure 6.8.A), and when removing it from the analysis, the range of values is more constrained, being consequently more variant for the miscellaneous group – which makes sense because of the broad variety of AFL subtypes enclosed there.

It is also necessary to consider the other important contribution of the arc parameter. All the above permits a useful characterisation of the physiology and anatomy unveiled under the AFL types. Nevertheless, when performing the non-parametric Kruskal-Wallis test over the set of patients grouped as previously described, statistical significance is obtained with a p-value of p=0.035. Thence, it proffers a good possibility to discriminate among different AFL subtypes, fulfilling one of the objectives of being able to discriminate between AFL types or at least intuit about the characteristics of the MC through the mere analysis of the VCG signal.

This parameter is essential with the correlation one (that is explained in the forthcoming section) to discriminate among AFL types through the VCG signal and to establish a new perspective on the analysis of the AFL condition from VCG features. Furthermore, it provides interesting clues about the characterisation of the MC defining the conduction of the AFL.

6.3.4. Archetype Correlation: Fundamental Results Supporting the Hypothesis

The has been used as follows in an inter-patient modality. Although a more detailed explanation was written in the methods I section, a brief reminder of how this data is computed is written next, due to the importance of this parameter. Firstly, the archetype for each of the groups was created and then compared to all the VCG loops from the patients inside its group and from the other groups. Notice that when comparing with the patients belonging to the groups from which the archetype has been created, the LOO is used. This consists of creating an archetype to compare with each one of the patients, that contains the averaged VCG loop from all the patients of this groups except the one it is being compared with. Thus,

one archetype is created to compare with each of the loops of the patients from the group, and one with the average VCG from all these patients to compare with the other groups. In this manner, the bias of a comparison with an archetype having the influence of the loop it is being compared with is avoided.

The results from the average correlation of each archetype with all the patients from each of the groups is depicted in table 6.8

	C.CCW Patients	**C.CW Patients**	**P.CCW Patients**	**P.CW Patients**	**Misc. Patients**
C.CCW Arch.	0.85±0.01	0,69±0.04	0.79±0.09	0.79±0.11	0.68±0.15
C.CW Arch.	0.73±0.09	0,95±0.03	0.64±0.12	0.77±0.03	0.58±0.12
P.CCW Arch.	0.79±0.04	0,67±0.01	0.87±0.04	0.75±0.15	0.59±0.19
P.CW Arch.	0.81±0.08	0,74±0.05	0.69±0.11	0.91±0.03	0.66±0.16

Table 6.8. RESULTS OF CORRELATION OF ARCHETYPES WITH PATIENTS FROM AFL GROUPS

The correlation coefficient found when comparing archetypes from different groups among them is displayed in table 6.9 Only the lower half is expressed as it is diagonally symmetric.

	C.CCW Arch.	**C.CW Arch.**	**P.CCW Arch.**	**P.CW Arch.**
C.CCW Arch.	1			
C.CW Arch.	0.6921	1		
P.CCW Arch.	0.8655	0.6989	1	
P.CW Arch.	0.8652	0.7556	0.7401	1

Table 6.9. CORRELATION AMONG ARCHETYPES

The results for the correlation of VCG loops coming from patients with each of the AFL archetypes created considering the LOO algorithm is expressed in a box and whiskers plot in figure 6.9 Each plot depicts the correlation for one of the AFL archetypes: common CCW AFL (figure 6.9.A), common CW AFL (figure 6.9.B), perimitral CCW AFL (figure 6.9.C) and perimitral CW AFL (figure 6.9.D).

The main objective that this parameter was meant to illustrate is the importance of slow regions in the VCG representation of a patient to characterise the AFL type. The concentration of points in the discretised version of the VCG loop produce a weight in the CP, giving more importance to slow regions as they entail a higher number of points concentrated in a specific area. This highly contributes to the correlation parameter performed point by point. Thus, the hypothesis was based in the fact that averaging VCG loops from patients suffering from the same AFL type would produce archetypes with a representative slow region in a specific area. This would lead to the possibility of discriminating among AFL types by focusing on this characteristic and on this correlation parameter. The archetype to which the new unlabelled case presents the higher correlation would determine what group it does belong to.

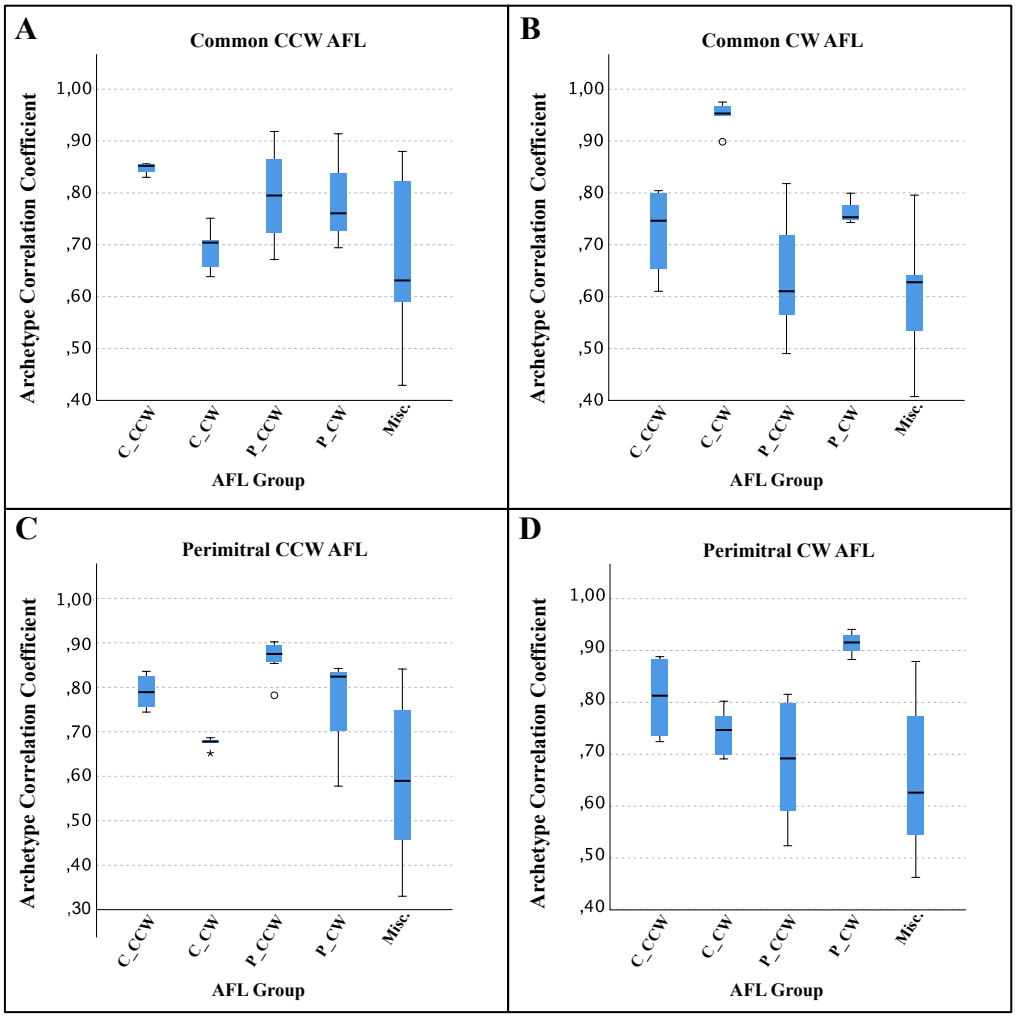

Figure 6.9. Representation in a box plot for correlation coefficient from the archetype of each AFL type with the patients from its group (using the LOO algorithm) and the rest of patients. The representation of this variable shows statistical significance for groups common CW AFL (B), p=0.003; perimitral CCW AFL (C), p=0.001; perimitral CW AFL (D), p=0.038, when performing a non-parametric Kruskal-Wallis test.

The results support favourably this hypothesis. In table 6.8, it can be observed how the highest average correlation coefficient is found for each archetype with the components of its AFL group (corresponding to the diagonal of the table). Furthermore, the differences in the correlation are relatively high for all the cases except for the first one, where there are differences, but some overlaps could be intuited from the values on the table. These results demonstrate the similarities among the VCG signals from patients from similar groups and the noticeable differences with patients from other groups. The archetype technique based on the representative signal for each AFL group could be a successful approach that needs to be studied with a higher number of AFL cases. Furthermore, the influence of the slow regions on this parameter is crucial, as shapes are variable from VCGs coming from different patients form the same AFL type (as will be discussed later based on figures 6.10, 6.11, 6.12 and 6.13.

On the other hand, AFL archetypes present significant differences in this parameter as observed in table 6.9. The highest correlations are found with respect to archetype one, but not definitive conclusions should be taken for this group as the number of patients was considerably low, and the tendency for the other cases indicate differences among archetypes. In addition, the archetypes are averaged loops from different patients, so smoother trajectories might be found, contributing to the increase of this parameter in general terms. Even though, favourable results are depicted by the table as correlation coefficient is below 0.87 for all the cases and below 0.76 for all cases not related to common CCW AFL archetype.

Analysing figure 6.9, the distribution of the correlation values for each or the archetypes is displayed. In the case of the commonCCW AFL archetype (figure 6.9.A), a high narrow range of values is obtained for the patients from this group, which is positive for our conclusions. Nevertheless, the whiskers of boxes from patients suffering from perimitral or miscellaneous AFL types reach this high range of values. This indicates that in case of discriminating, some AFL types from these groups could be identified as common CCW AFL as false positives for this case. This result is not convenient for discriminating nor for demonstrating our hypothesis, but it may be given by the small quantity of patients from this group in comparison with perimitral or miscellaneous. It is not a baffling result as it happens only for this case and with a low number of patients from broad groups as perimitral and miscellaneous AFL, indicating that the model should be improved and the main limitation, in this case the low number of patients, should be corrected for further studies.

For the cases of common CW AFL, perimitral CCW AFL and perimitral CW AFL, the results are doubtlessly, successful. The highest correlation coefficients are found when comparing the archetype with the AFL cases from the same group. No overlapping is found among other types with the high values of correlation from patients from the archetype's class. Hence, these cases favourably support the hypothesis of how this correlation parameter significantly influenced by slow conduction regions allow discrimination and characterisation of AFL types.

Furthermore, the discrimination capacity of this method has been evaluated performing a non-parametric Kruskal-Wallis test for the correlation distribution with each of the archetypes. In the case of the common CCW AFL, the results are not completely ideal as previously commented, and no possibility of rejecting the null hypothesis in statistical terms is found with this method, although the result is not far from statistical significance ($p=0.078$). For the rest of the cases, a high discriminating capacity is unveiled by this statistical analysis that shows clear statistical significance and the rejection of the null hypothesis for all the cases with a p-value of $p<0.05$ of all the cases and $p<0.01$, common CW AFL archetype and perimitral CCW AFL archetype. Note that the least significance is found for common CCW AFL and for perimitral CW AFL (although the latter shows

significance: p=0.038). These two were the ones with the smallest number of cases, so it may be intuited that increasing the number of signals from these conditions would improve the results (and more in case of increasing the number of cases for all the patients).

Some interesting conclusions can be obtained when analysing in couples through variants of the Kruskal-Wallis test. For the common CCW archetype, this analysis cannot be performed as $p>0.05$, so no significance is analysed between pairs. For the common CW archetype, it is interesting the discriminating capacity from this group with respect to the perimitral CW and miscellaneous, showing a high significance in pairs for all of them ($p<0.002$). For the perimitral CCW, the case to be highlighted where the most noticeable discrimination occurs is in relation with the CW common and miscellaneous group ($p<0.002$). For the Perimitral CCW, high significance stands with respect to the perimitral CW and miscellaneous group ($p<0.009$), and also a noticeable significance is highlighted with respect to group common CW (p=0.033).

Finally it is necessary to accentuate the explanation on why the slow regions are thought to be that important. Tests have been performed to VCG loops showing similar shapes but belonging to different groups and with slow regions in different places, demonstrating a low CP. Naturally, a similar shape contribute to a higher CP, but if slow regions were located in different areas for different cases, when averaging point by point in the creation of the archetype, this concentration of points would not be found in a specific place. As a finale demonstration of the results, the archetypes for all AFL groups have been plotted together with the VCG loops for each of the patients from the same group of the archetype. Common CCW AFL is represented in figure 6.10,common CW AFL in figure 6.11, perimitral CCW AFL in figure 6.12 and perimitral CW AFL in figure 6.13. These figures demonstrate that the slow region is maintained and also that variations occur in the 3D representation, especially for the fast regions. Nevertheless, when displaying the three components for each of the VCGs (after temporal alignment), similar trajectories appear among them.

These figures are an illustration of the possibilities that this method offers to the possibility of discriminating among AFL types through the characterisation of their VCG signal, as it depicts a profound visual resemblance among VCGs from the same AFL type. As being subsampled for the illustration and the archetype is displayed in a black pattern, the slow regions can also be clearly observed to be in similar areas in the different perspectives. The coordinates representation also demonstrates a similarity on the shape of VCGs from the same groups.

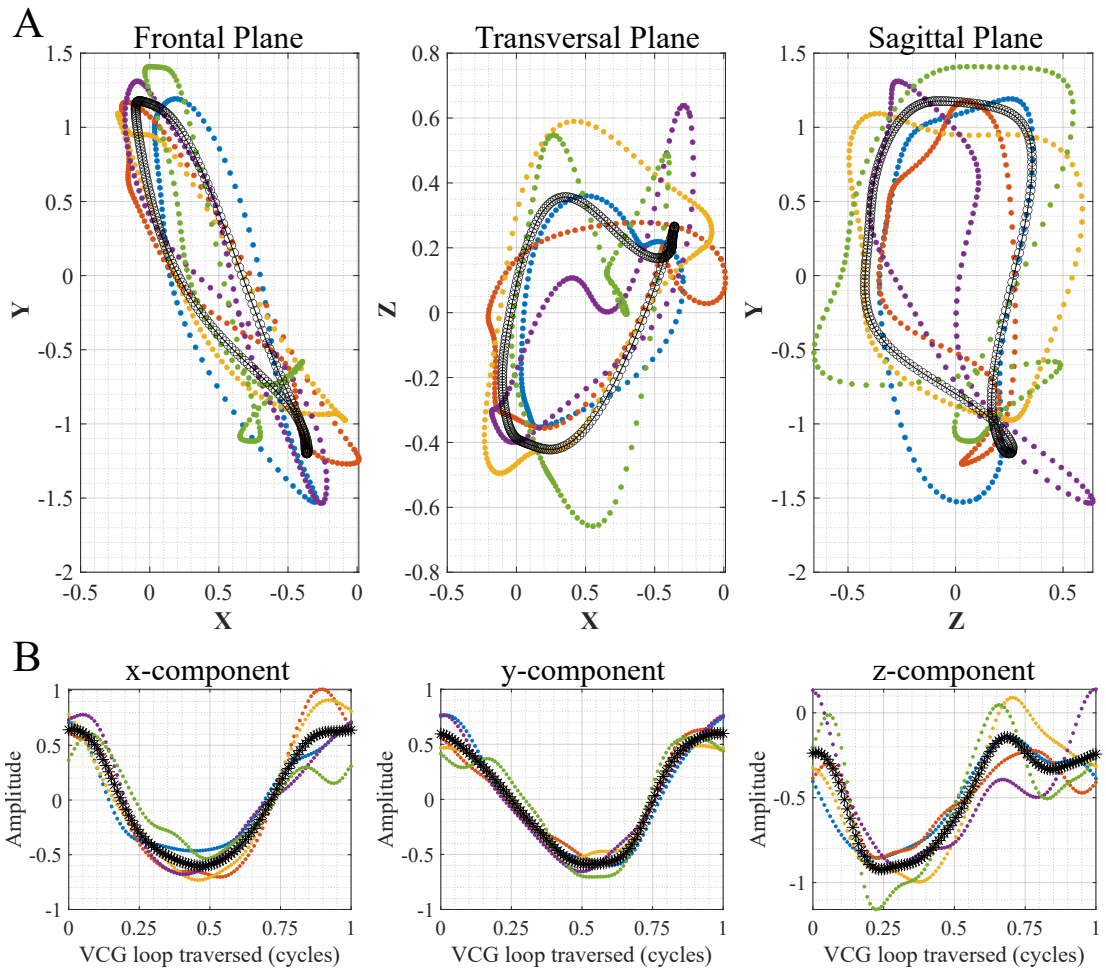

Figure 6.10. Depiction of the common CCW AFL VCGs and their archetype in 3D (frontal, transversal and sagittal planes) and their x,y,z components. VCG signals have been subsampled and normalised to have a better illustration. The archetypes are represented in a black pattern (circles for VCG projections (A) and asterisks for x,y,z components (B)). **A:** Representation of the three-standard projection of the VCG for all the common CCW AFL cases and their archetype. Slow regions are found to be in similar regions of the space for the three projections. **B:** Representation of the x, y and z components for the amplitude of the normalised VCG over the region traversed (i.e. the percentage of VCG loop that have been travelled, ending in 1 as the whole loop was traversed). A significantly high similarity is found for x and y components among all AFL cases.

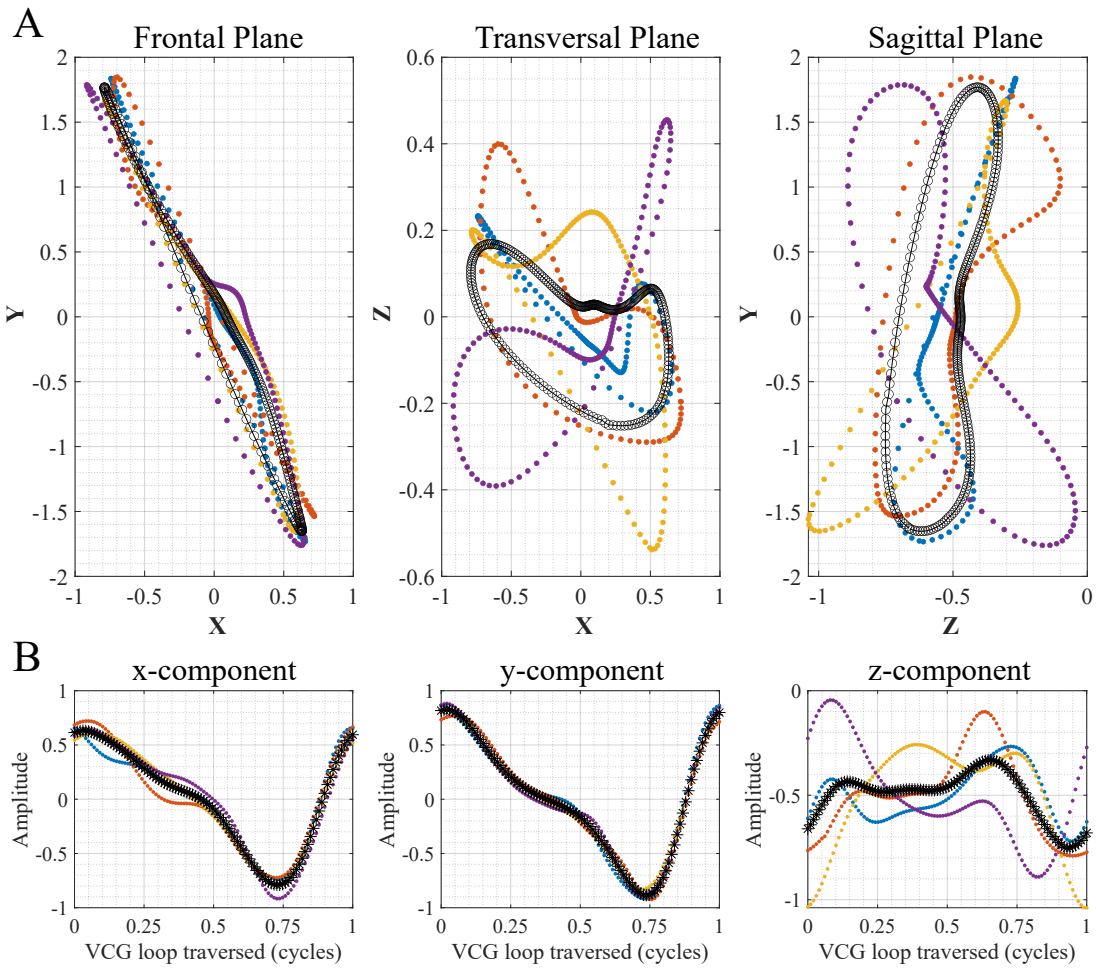

Figure 6.11. Depiction of the common CW AFL VCGs and their archetype in 3D (frontal, transversal and sagittal planes) and their x,y,z components. VCG signals have been subsampled and normalised to have a better illustration. The archetypes are represented in a black pattern (circles for VCG projections (A) and asterisks for x,y,z components (B)). **A:** Representation of the three-standard projection of the VCG for all the common CW AFL cases and their archetype. Slow regions are found to be in similar regions of the space for the three projections. **B:** Representation of the x, y and z components for the amplitude of the normalised VCG over the region traversed (i.e. the percentage of VCG loop that have been travelled, ending in 1 as the whole loop was traversed). A significantly high similarity is found for x and y components among all AFL cases.

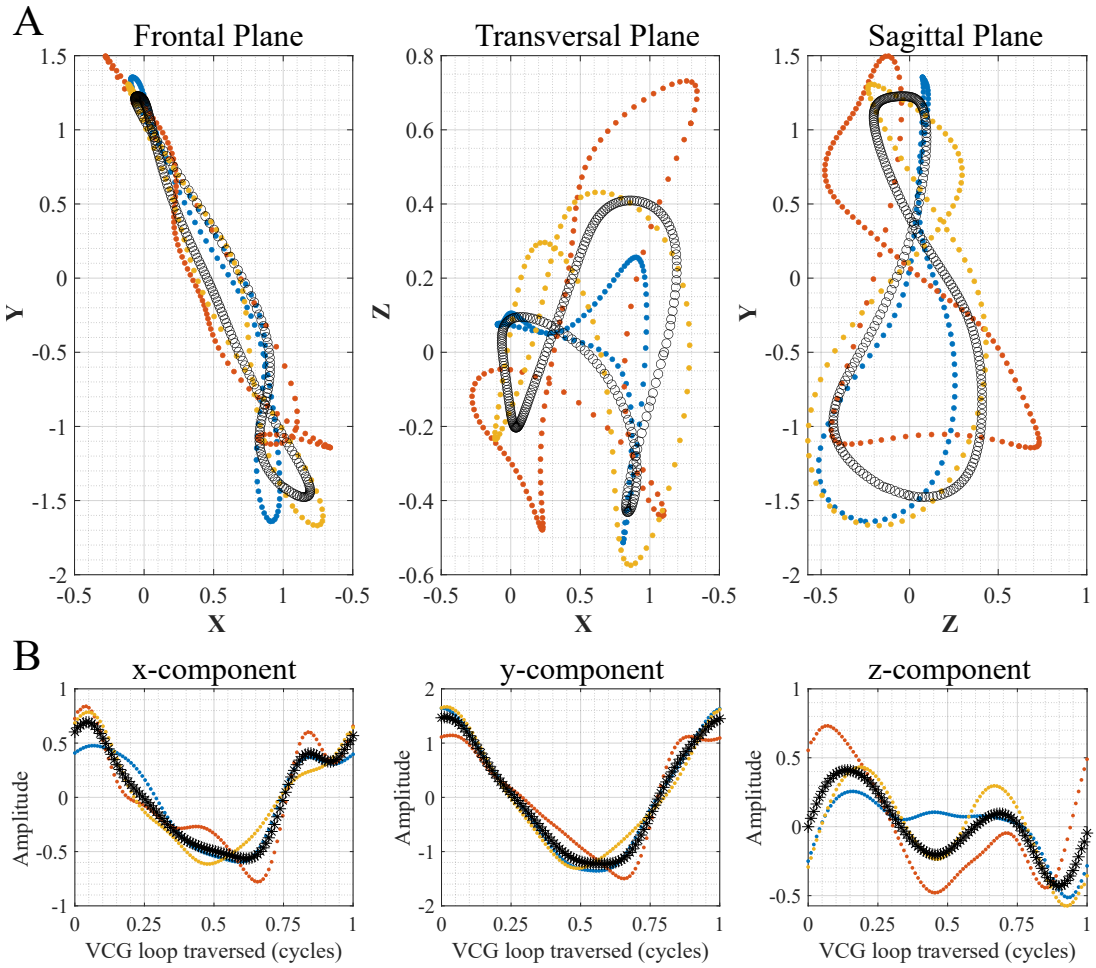

Figure 6.12. Depiction of the perimitral CCW AFL VCGs and their archetype in 3D (frontal, transversal and sagittal planes) and their x,y,z components. VCG signals have been subsampled and normalised to have a better illustration. The archetypes are represented in a black pattern (circles for VCG projections (A) and asterisks for x,y,z components (B)). **A:** Representation of the three-standard projection of the VCG for all the perimitral CCW AFL cases and their archetype. Slow regions are found to be in similar regions of the space for the three projections. **B:** Representation of the x, y and z components for the amplitude of the normalised VCG over the region traversed (i.e. the percentage of VCG loop that have been travelled, ending in 1 as the whole loop was traversed). A significantly high similarity is found for x and y components among all AFL cases.

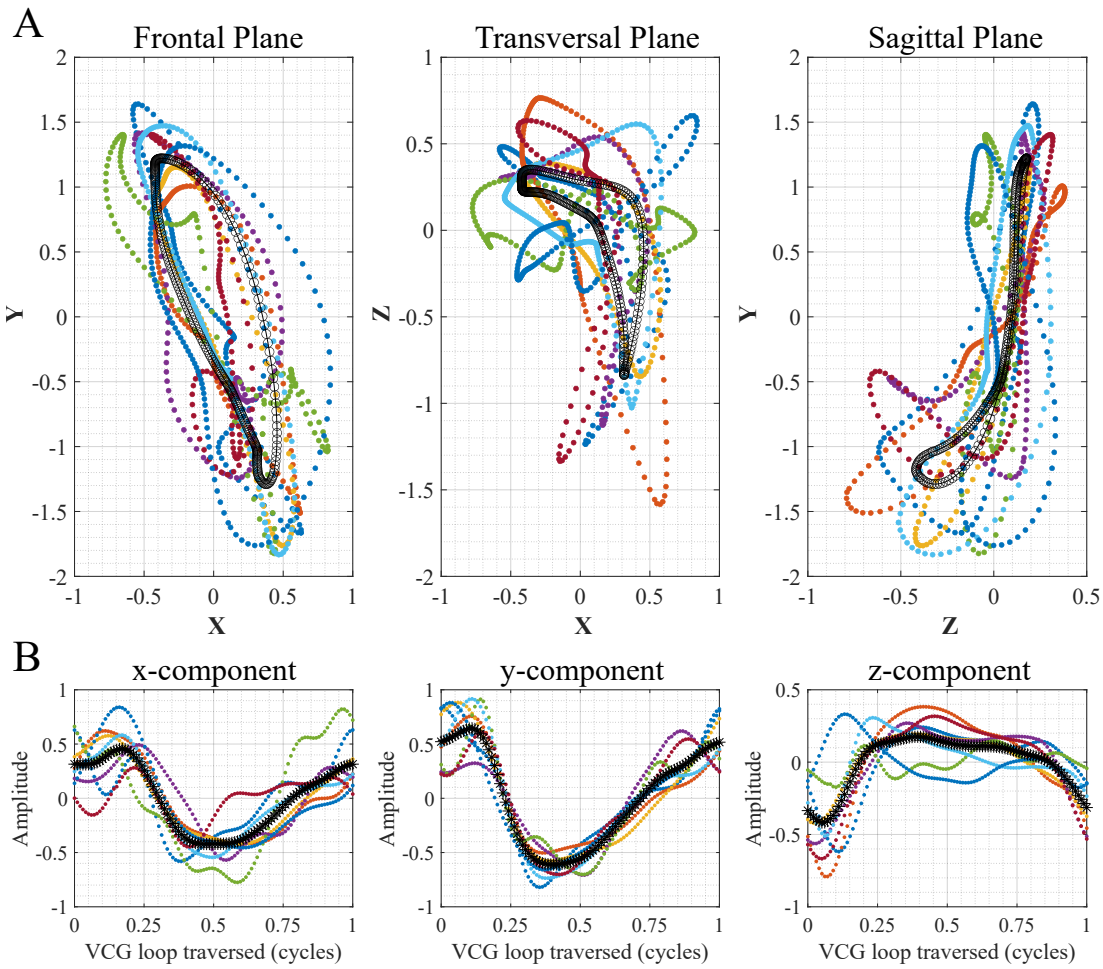

Figure 6.13. Depiction of the perimitral CW AFL VCGs and their archetype in 3D (frontal, transversal and sagittal planes) and their x,y,z components. VCG signals have been subsampled and normalised to have a better illustration. The archetypes are represented in a black pattern (circles for VCG projections (A) and asterisks for x,y,z components (B)). **A:** Representation of the three-standard projection of the VCG for all the perimitral CW AFL cases and their archetype. Slow regions are found to be in similar regions of the space for the three projections. **B:** Representation of the x, y and z components for the amplitude of the normalised VCG over the region traversed (i.e. the percentage of VCG loop that have been travelled, ending in 1 as the whole loop was traversed). A significantly high similarity is found for y and z components among all AFL cases.

7. FINAL CONCLUSIONS

The first conclusion that arises from this bachelor dissertation is the importance of the analysis of different perspectives when discussing about cardiac signals and human body indicators in a more general view. Although the vectorcardiographic representation of these physiological signals is not a high trend topic nowadays, it should not be forgotten since there is still a great amount of work to be done. Furthermore, as it has been hereby stated, there are plenty of different features that can be discovered when addressing cardiac problems with different methods. Hence, it has been shown how the analysis of signals after undergoing the IDT offers a whole range of possibilities and opportunities for new ways of characterisation towards a less invasive medicine in cardiology and surgery.

Another conclusion to emphasise is the importance of mathematical models based on geometry and parameters extracted from actual physiological features to recreate cardiac signals with the purpose of creating databases. These can be either based on previous models or, a tougher option, from the scratch. In this thesis, the latter has been approached, since a geometrical model has allowed the analysis and study of different variables with a full control over the others, although applying the IDT over already designed artificial ECG generators may have been easier. Moreover, it has been essential to give robustness to the results, something relevant to underline due to the main limitation of this project: a small number of patients available to support the initial hypothesis.

It is also significant to underscore the useful tool that has been developed in a form of an algorithm to characterise VCG types from a sheer computation based on features extracted from previous illness cases. Three essential elements are combined to support the success of the project: the certainty of the diagnosis of the patients from the cardiologists, our golden standard, whose signals are employed on the creation of archetypes; the conspicuous nature of the algorithm that analyses and characterises the signals based on pure unambiguous mathematics; and the translucent model used to generate a database of geometrical shapes painstakingly categorised to prove the efficiency and strengthens the analytic algorithm.

Thusly, the hypothesised bearing of the slow conduction regions when classifying atrial flutters has been demonstrated and a new vantage point has been established for future research and improvement in the specific area of endeavour of diagnosis through physiological signals analysis.

If I were to put the contributions of this project in a nutshell, I would emphasise the importance of orienting research to be done in this field to unmasking the relations among electrophysiological and anatomical features characterising AFL, and their biomedical-signal alter ego. The deep and clear knowledge on these relations are full of promise for science, biomedical engineering, and the non-invasive future of cardiac interventions in medicine. With the results of this dissertation, this foreseen future has been enlightened.

8. CONTRIBUTION, LIMITATIONS AND FUTURE APPROACHES

8.1. Scientific Contribution

The wish of a potential researcher at the stage of his bachelor thesis is to improve as a person and as a scientist. Not only this has been mine, but also to work in a discipline with such an impact in medicine and in society. The proposed hypothesis and analytic tools are aimed to reveal a new perspective in the way cardiac signal problems are addressed, offering innovative alternatives.

Besides, this research is being written by the author of this thesis in a scientific journal paper to be soon submitted for publication with the bio-ITACA research group – with the student as principal author. The proposed hypothesis, introduction, materials and methods, results and discussions will be included in such work in a scientific paper layout. Once this work is published, the contribution will be substantial, and the genuine motivation of the investigation will have been fully successful.

Furthermore, the contribution to this area of study has already been tangible since the advancing outcomes of the research were presented by the author of this bachelor dissertation in the international congress 'Atrial Signals: Physicians Meet Engineers', which took place in November 2019 in Bordeaux. The aftermaths obtained by that time were exposed in this congress organised by IHU LIRYC, worldwide known institute, model in the field of study of cardiac physiology. In addition, the student also participated as poster presenter in the congress of the National Association of General Medicine (SEMG), celebrated in Talavera de la Reina in November 2019. The results and future impact of the methods were explained. There, the student was awarded with the highest award in recognition of the innovative and positive impact on contemporary research into atrial fibrillation. Next September, the final results of the project will be presented by the author of this publication in the international congress Computing in Cardiology (CinC), celebrated in Rimini (Italy).

8.2. Current Limitations of this Research Project

The main limitation that has been faced during this research project is the low number of diagnosed patients whose data was available for the experiment. The ground of this restriction comes from the small network that the legal framework of the experiments allowed. Nonetheless, for the continuation of this line of research,

the contracts and bureaucracy would be implemented to have access to a larger network of patient data suffering from AFL.

Another shortcoming given by the nature of this condition is the unbalanced number of cases from different groups. In layman's terms, there was a considerable quantity of patients suffering from common AFL, especially from the CW subtype, but just a few patients suffering from the non-common version of this sickness. Furthermore, the fact that most of the latter were perimitral has allowed to discern among four archetypes of this cardiac illness. If a bigger quantity of cases had been provided from patients suffering from other non-common versions of AFL (such as right peri-veins, mural...), the algorithm could have been tested in a wider range of possibilities.

Some constraints about the VCG generator could also be mentioned, but because of having been developed from the scratch based on a mathematical model, it can be easily implemented and adapted to new variables, ranges of values, randomisation techniques or variability of shapes and groups. Thus, there are not insurmountable limitations in this area, and the toughness provided to the analytic tools has been the desired.

Lastly, it has been of great importance the abrupt and unprecedented situation generated by the CoVid-19, which has encompassed the lack of diagnosed cases and data coming from the cardiologists of the hospital. This shortage has been tried to be amended by the creation of this synthetic VCG generator, but, although it proves the efficiency of the analysis, an elevated number of cases would reinforce the outcome and results from the statistical analysis of real cases. Despite the fact that some features could have been implemented, the hypothesis and presumptions can be certainly said to have been demonstrated, apprising the objectives as doubtlessly successfully fulfilled.

8.3. Guides for Future Work

The presented work opens several lines of research in a methodological sense, regarding the analytic tools developed, and on the other hand, in terms of the application. Undoubtedly, the proposed techniques could be refined and more complex methods could be used based on the ones presented in the methodological sections of this dissertation. Nevertheless, the author suggests focusing not only on this implementation, but several other directions, more on the application of the developed methodology.

The principal proposed idea is to relate the results obtained through vectorcardiographic analysis characterisation with the pathophysiological basis of the arrhythmogenicity of atria harbouring fibrosis. Manifestation of varying degrees of fibrosis have been demonstrated to range from macroreentry to small reentry, entailing circle

reentry or rotors and even unexcitable atria [112, 113]. Thus, the relation between the anatomical and specific physiological condition of the heart could be considered in future research, unveiling relations among VCG features and specific conditions of AFL or other atrial tachyarrhythmias. Machine learning and deep learning algorithms would have to be implemented with a significant increase in the cases provided by physicians, as well as a wider diagnosis furnishing the algorithm with a variegated assortment of features to consider both in medical evaluation and VCG features.

The previously mentioned track could come together with the analysis of the main frequency in the atrial signal, which has been proved to be critical in clinical decision-making [114]. In some studies [115, 116], it has been employed for the monitoring of drug effects, and the evolution of this frequency with time could be studied, as wavelets and spectrograms have been shown to be essential in biomedical signals [117, 118]. Furthermore, it may help to reveal key factors in the initiation and termination of AFL. All this ideas, again related to the features extracted from VCG shapes and parameters, could be a noticeably advantageous tool in the course of implementing analysis and diagnostic procedures towards a less invasive cardiac medicine – especially when testing, diagnosing and characterising illnesses and patients.

Likewise, the relation between the vectorcardiographic representation of the projection of the electrophysiological path that the cardiac signals follows in cases of AFL, and the indexes addressed as ablation sites, is apparent. The possibility of rapidly and autonomously targeting the ablation regions for a given specific AF or AFL class would be an ambitions but feasible aim of study. Additionally, the techniques outlined in the text could be combined with such purposes with 3D atrial models and simulations of electroanatomical maps, already under study and development [119, 120].

The importance of improving this field of research is boundless, as discovering relations among physics, mathematics, and electronics with physiology and physiopathologies creates a combination that may lead to the non-invasive future of most diagnosis and treatments. The collaboration between scientists, engineers and physicians is necessary to improve in this field with such an important impact in society.

9. REGULATORY FRAMEWORK AND SOCIO-ECONOMICAL IMPACT

9.1. Regulatory Frames: Bioethics, Licensing and Law

It is worldwide accepted that health care systems need of data transmission [121] and that patients's history is necessary for both health systems and research of illnesses or methods to improve techniques, such as the main purpose of this bachelor dissertation. Nonetheless, privacy of these data is a reference point in both legal and ethical standpoints.

In ethical terms, the doctor-patient relationship is a sacred matter since ancient times, as clearly stated by the Hippocratic Oath. Hence, it is a good ethical practice to respect privacy matters [122]. In bioethics, there are four known principles that must be respected for the good practice of medicine when referring to private data of patients regarding health: the principles of autonomy, beneficence, non-maleficence and justice [123].

The Universal Declaration of Human Rights addresses this privacy matters in its twelfth article [124]:

"No one shall be subjected to arbitrary interference with his privacy, family, home or correspondence, nor to attacks upon his honour and reputation. Everyone has the right to the protection of the law against such interference or attacks."

The *Convention for the Protection of Human Rights and Fundamental Freedoms*, commonly addressed as the *European Convention on Human Rights*, needs to be highlighted. There, the eighth article refers to the protection of private information [125].

In terms of the regulatory frame, the legal framework defined by the European Commission by articles 46 and 47 of Treaty on the functioning of European Union (TFEU) and the directive 2011/24/EU on the application of patients' rights needs to be considered. Also, referring to informative issues, the directive 2000/31/EC on Electronic Commerce and the directive 98/34/EC also on Electronic Commerce are noticeable.

In terms of the protocol followed to record ECG signals from patients, they were recruited at the Robotic Cardiac Electrophysiology and Arrhythmia Unit, Hospital Universitario La Paz (Madrid, Spain) according to a protocol approved by the hospital's ethics committee. The recruitment protocol was compliant with the *Declaration of Helsinki* [126] and all patients involved signed informed consent.

Finally, about the software licensing, the main software used was Matlab whose license is covered by University Carlos III de Madrid. Thus, the student had access during the project to a variegated sort of toolboxes as well as to the interface creator

AppDesigner legally with the university license. Inkscape and overleaf, license free, were also used.

In relation to this bachelor's dissertation and the research project that has been carried, all legal issues have been taken into account with the appropriate documentation to treat patients' data in relation to their health condition addressed from their cardiac signals.

9.2. Socio-Economical Impact

9.2.1. Socio-Economical Environment

AFL is the second most common atrial tachyarrhythmia with an increasing prevalence nowadays. Furthermore, it is expected to find an increase of more than one hundred percent in the prevalence of AFL in the United States by 2050 according to MarketScan research databases from Thomson Reuters [127]. It is also expected to have a significant increase in the cases of AF and AFL by 2060 in the European Union [128]. Not only do AF and AFL constitute a relevant health issue, but it also constitutes a significant economic impact in the system of healthcare for our population [7].

Hence, the idea of diagnosing AFL in a non-invasive manner does positively affect the health conditions of patients and saves time, procedural costs and in the end supposes a positive impact in the economy of healthcare systems. Furthermore, this way to a non-invasive approach opens the possibility of finding non-invasive methods of ablation. Research has already taken this direction implementing non-invasive mapping techniques [129]. This would entail an enormous positive socio-economical impact, addressed from great savings in treatment costs in this field and a great improve in the health of patients suffering from this increasing-prevalence condition.

Nonetheless, this impact is not immediate. Not even the improvement that the non-invasive diagnosis would entail is instantaneous since further studies should be made to corroborate these techniques previous to clinical trials proving the efficiency of the methods. Hence, being critical, the ongoing impact is not positive in economical terms, but it means an inversion to a near future when benefits will be reaped. In social terms the impact is doubtlessly positive, as it encompasses a great contribution in scientific terms for the medical engineering and therapeutic field.

9.2.2. Project Resources and Costs

9.2.2.1. Human Resources

There is a selection of resources utilised to carry this project, although the multifariousness is not very noticeable since there is a great component consisting on data analysis, processing and computational work.

In terms of human resources, the principal investigator and another member of the laboratory, both full professors, were needed as advisors and supporters of

the work that the student performed – also required as a human resource. The PI is considered the project manager. Two cardiologists from 'La Paz' Hospital were in charge of acquiring the data from patients and performing the diagnosis, collaborating with their work. Technicians and other staff (such as cleaning, porters or specific installations workers) were also required for the proper functioning of the project. Finally, the supervisor at University Carlos III de Madrid, also full professor was needed in this bachelor's thesis. The approximate value and time spent by all these people is summarised in table 9.1, which illustrates the cost of the work performed to achieve the goals of the project.

Data has been calculated from different sources, subscripted in the first column: Cost (€) per Time (h). Those are: {1} Studies of Jose-Gines Mora, Centre for the Study of Higher Education Management (CEGES), Technical University of Valencia [130]; {2} Instituto Nacional de Estadística: INE (National Institute of Statistics [131]; {3} This quantity is illustrative, corresponding to the minimum salary perceived by a bachelor graduate working in a research project at University Carlos III de Madrid.

	Cost/Time (€/hour)	Working Time (hours)	Total Cost (€)
Principal Investigator	$27_{\{1,2\}}$	170	4.590
Laboratory Professor	$27_{\{1,2\}}$	170	4.590
Cardiologists (x2)	$35_{\{2\}}$ (x2)	80 (x2)	5.600
UC3M Professor (Advisor)	$27_{\{1,2\}}$	40	1.080
Technicians	$12_{\{2\}}$	15	180
Other Staff	$10_{\{2\}}$	30	300
Student	$10.5_{\{3\}}$	1020	10.710
		Total:	**27.050€**

Table 9.1. HUMAN RESOURCES

9.2.2.2. Material Resources and Equipment

In terms of material resources, due to the high computational component and design work of this project, there is not a high expenditure. The costs are estimated from real and approximated prices, although some are provided by the University (but their value is considered). Also, a proportion of the estimated lifespan and the time used is created to have more accurate values of the cost in this section. The estimation of the cost of the material resources is displayed in table 9.2.

9.2.2.3. Resources to Cover Congresses

In the process of development of this project, it was essential the participation of the student as congress poster presenter in the International Congress 'Atrial Signals: Physicians Meet Engineers', held in Bordeaux in October 2019. The cost of participation and accommodation or diaries for the two professors and the students were then necessary for the project. Also, the student participated in the congress of the National Association of General Medicine (SEMG), held in Talavera de la Reina in November 2019. He presented the project in a poster in representation of the whole research team, although the presented results were just to ones of his work and research. In the latter, the student received the first prize for poster

	Unit Cost (€)	Lifespan (years)	Time Used (years)	Total (€)
Personal Computer	1100	5	1	220
Office Computer	900	5	1	180
Additional Screen	200	8	1	25
Computer Accesories	85	5	1	17
Hard Drive (2TB)	80	8	1	10
MS Office 2016	140	1	1	140
Matlab Software R2019B	250	1	1	250
Electronic Components	20	-	**-**	**20**
Office Material	25	-	-	25
Hospital ECG Machine (x2)	1500 (x2)	10	1	300
			Total:	**1.197 €**

Table 9.2. MATERIAL RESOURCES

presentation, although this quantity is not included in the costs since it is not a direct expenditure of the research institution, but of an external association in favour of the student. The above information is summarised in table 9.3 with specifications about the costs.

Congress	Object	Party	Cost (€)/Person	Total (€)
Atrial Signals	Congress Presenter	Student	400	400
	Congress Presenter	Professors (x2)	450	900
	Accommodation (x3)	Student and Professors (x2)	250	750
	Travel Costs (x3)	Student and Professors	130	390
SEGM	Congress Presenter	Student	275	275
	Accommodation	Student	150	150
	Travel Costs	Student	40	40
			Total:	**2.905€**

Table 9.3. RESOURCES FOR CONGRESSES

9.2.2.4. Total Costs

The total estimation of costs for the project having into account human and material resources, equipment utilised and congresses in which the project was involved is summarised in table 9.4. Thus, the total cost of the project is estimated to be €31.152.

Type of Resource	Cost (€)
Human	27.050
Material and Equipment	1.197
Congresses	2.905
Total:	**31.152**

Table 9.4. TOTAL COSTS

BIBLIOGRAPHY

[1] E. Herzog, E. Argulian, S. B. Levy, and E. F. Aziz, "Pathway for the management of atrial fibrillation and atrial flutter", *Critical pathways in cardiology*, vol. 16, no. 2, pp. 47–52, 2017.

[2] W. Dresen and P. K. Mason, "Atrial flutter after surgical maze: Incidence, diagnosis, and management", *Current opinion in cardiology*, vol. 31, no. 1, pp. 57–63, 2016.

[3] S. M. Markowitz *et al.*, "Approach to catheter ablation of left atrial flutters", *Journal of Cardiovascular Electrophysiology*, vol. 30, no. 12, pp. 3057–3067, 2019.

[4] K. Adelborg *et al.*, "Levels of and changes in childhood body mass index in relation to risk of atrial fibrillation and atrial flutter in adulthood", *American journal of epidemiology*, vol. 188, no. 4, pp. 684–693, 2019.

[5] A. J. Foy, J. Mandrola, G. Liu, and G. V. Naccarelli, "Relation of obesity to new-onset atrial fibrillation and atrial flutter in adults", *The American journal of cardiology*, vol. 121, no. 9, pp. 1072–1075, 2018.

[6] K. Monahan *et al.*, "Relation of the severity of obstructive sleep apnea in response to anti-arrhythmic drugs in patients with atrial fibrillation or atrial flutter", *The American journal of cardiology*, vol. 110, no. 3, pp. 369–372, 2012.

[7] R. J. Till and M. R. Cowie, "Atrial fibrillation in heart failure: New directions in diagnosis, risk assessment and risk reduction", *Journal of atrial fibrillation*, vol. 6, no. 6, 2014.

[8] F. G. Cosıo, A. Pastor, A. Núñez, A. P. Magalhaes, and P. Awamleh, "Atrial flutter: An update", *Revista Española de Cardiologıa (English Edition)*, vol. 59, no. 8, pp. 816–831, 2006.

[9] N. Saoudi *et al.*, "A classification of atrial flutter and regular atrial tachycardia according to electrophysiological mechanisms and anatomical bases. a statement from a joint expert group from the working group of arrhythmias of the european society of cardiology and the north american society of pacing and electrophysiology", *European heart journal*, vol. 22, no. 14, pp. 1162–1182, 2001.

[10] J. E. Olgin, J. M. Kalman, A. P. Fitzpatrick, and M. D. Lesh, "Role of right atrial endocardial structures as barriers to conduction during human type i atrial flutter: Activation and entrainment mapping guided by intracardiac echocardiography", *Circulation*, vol. 92, no. 7, pp. 1839–1848, 1995.

[11] F. G. Cosio, F. Arribas, M. LÓPEZ-GIL, and J. Palacios, "Atrial flutter mapping and ablation i: Studying atrial flutter mechanisms by mapping and entrainment", *Pacing and clinical electrophysiology*, vol. 19, no. 5, pp. 841–853, 1996.

[12] C.-H. Lin *et al.*, "Novel electrophysiological characteristics of atrioventricular nodal continuous conduction curves in atrioventricular nodal re-entrant tachycardia with concomitant cavotricuspid isthmus-dependent atrial flutter", *Ep Europace*, vol. 18, no. 8, pp. 1259–1264, 2016.

[13] V. Y. See, "Organized atrial arrhythmias after cardiac transplantation: The overlooked value of the 12-lead electrocardiogram and cavotricuspid atrial flutter isthmus", *The Journal of Heart and Lung Transplantation*, vol. 37, no. 2, pp. 192–194, 2018.

[14] M. Yokokawa *et al.*, "The relationship between the p wave and local atrial electrogram in predicting conduction block during catheter ablation of cavo-tricuspid isthmus-dependent atrial flutter", *Journal of Interventional Cardiac Electrophysiology*, vol. 53, no. 2, pp. 187–193, 2018.

[15] K. W. Lee, Y. Yang, and M. M. Scheinman, "Atrial flutter: A review of its history, mechanisms, clinical features, and current therapy", *Current problems in cardiology*, vol. 30, no. 3, pp. 121–167, 2005.

[16] C. Pedrinazzi *et al.*, "Atrial flutter: From ecg to electroanatomical 3d mapping", *Heart international*, vol. 2, no. 3-4, pp. 1 826 186 806 002 003–405, 2006.

[17] M. S. Baccillieri *et al.*, "Anatomy of the cavotricuspid isthmus for radiofrequency ablation in typical atrial flutter", *Heart rhythm*, vol. 16, no. 11, pp. 1611–1618, 2019.

[18] A. Madaffari *et al.*, "Ablation of typical atrial flutter guided by the paced pr interval on the surface electrocardiogram: A proof of concept study", *EP Europace*, vol. 21, no. 11, pp. 1750–1754, 2019.

[19] J. L. Cox *et al.*, "The surgical treatment of atrial fibrillation: Ii. intraoperative electrophysiologic mapping and description of the electrophysiologic basis of atrial flutter and atrial fibrillation", *The Journal of thoracic and cardiovascular surgery*, vol. 101, no. 3, pp. 406–426, 1991.

[20] H. Poty, N. Saoudi, A. A. Aziz, M. Nair, and B. Letac, "Radiofrequency catheter ablation of type 1 atrial flutter: Prediction of late success by electrophysiological criteria", *Circulation*, vol. 92, no. 6, pp. 1389–1392, 1995.

[21] B. Cauchemez *et al.*, "Electrophysiological effects of catheter ablation of inferior vena cava–tricuspid annulus isthmus in common atrial flutter", *Circulation*, vol. 93, no. 2, pp. 284–294, 1996.

[22] H. Calkins *et al.*, "Catheter ablation of atrial flutter using radiofrequency energy", *American Journal of Cardiology*, vol. 73, no. 5, pp. 353–356, 1994.

[23] F. Garcıa-Cosıo, F. Arribas, and M. López Gil, "Ablación con catéter del flutter y la fibrilación auricular", *Rev Esp Cardiol*, vol. 49, no. Supl 2, pp. 55–63, 1996.

[24] G. K. Feld *et al.*, "Radiofrequency catheter ablation for the treatment of human type 1 atrial flutter. identification of a critical zone in the reentrant circuit by endocardial mapping techniques.", *Circulation*, vol. 86, no. 4, pp. 1233–1240, 1992.

[25] M. D. Lesh *et al.*, "Radiofrequency catheter ablation of atrial arrhythmias. results and mechanisms.", *Circulation*, vol. 89, no. 3, pp. 1074–1089, 1994.

[26] G. Peigh, J. Wasserlauf, P. Sattayaprasert, N. Verma, and B. P. Knight, "Use of the cryoballoon to ablate pulmonary vein-dependent left atrial flutter", *Pacing and Clinical Electrophysiology*, vol. 42, no. 12, pp. 1589–1593, 2019.

[27] F. Morady, "Radio-frequency ablation as treatment for cardiac arrhythmias", *New England Journal of Medicine*, vol. 340, no. 7, pp. 534–544, 1999.

[28] P. Jaïs *et al.*, "Mapping and ablation of left atrial flutters", *Circulation*, vol. 101, no. 25, pp. 2928–2934, 2000.

[29] E. Frank, "An accurate, clinically practical system for spatial vectorcardiography", *circulation*, vol. 13, no. 5, pp. 737–749, 1956.

[30] A. D. Waller, "A demonstration on man of electromotive changes accompanying the heart's beat", *The Journal of physiology*, vol. 8, no. 5, pp. 229–234, 1887.

[31] J. Iwaniec, M. Iwaniec, and A. Kalukiewicz, "Application of vectorcardiography and recurrence-based methods to analysis of ecg signals", in *MATEC Web of Conferences*, EDP Sciences, vol. 241, 2018, p. 01 015.

[32] S. I. Cohen, D. Koh, S. Lau, K. M. Rosen, and A. N. Damato, "P loops during common and uncommon atrial flutter in man.", *Heart*, vol. 39, no. 2, pp. 173–180, 1977.

[33] J. M. Kalman *et al.*, "Electrocardiographic and electrophysiologic characterization of atypical atrial flutter in man: Use of activation and entrainment mapping and implications for catheter ablation", *Journal of cardiovascular electrophysiology*, vol. 8, no. 2, pp. 121–144, 1997.

[34] N. Saoudi *et al.*, "Electrocardiographic patterns and results of radiofrequency catheter ablation of clockwise type i atrial flutter", *Journal of cardiovascular electrophysiology*, vol. 7, no. 10, pp. 931–942, 1996.

[35] P. Milliez *et al.*, "Variable electrocardiographic characteristics of isthmus-dependent atrial flutter", *Journal of the American College of Cardiology*, vol. 40, no. 6, pp. 1125–1132, 2002.

[36] S. Choudhuri, T. Ghosal, D. P. Goswami, and A. Sengupta, "Planarity of the spatial qrs loop of vectorcardiogram is a crucial diagnostic and prognostic parameter in acute myocardial infarction", *Medical hypotheses*, vol. 130, pp. 109–251, 2019.

[37] E. P. Widmaier, H. Raff, K. T. Strang, and A. J. Vander, *Vander's Human physiology: the mechanisms of body function.* New York: McGraw-Hill Higher Education, 2016, 360–436".

[38] J. Eckenhoff, J. Hafkenschiel, C. Landmesser, and M. Harmel, "Cardiac oxygen metabolism and control of the coronary circulation", *American Journal of Physiology-Legacy Content*, vol. 149, no. 3, pp. 634–649, 1947.

[39] C. D. O'Malley, *Andreas Vesalius of Brussels, 1514-1564*. Univ of California Press, 1964.

[40] M. M. Shoja *et al.*, "Leonardo da vinci's studies of the heart.", *International journal of cardiology*, vol. 167, no. 4, pp. 1126–1133, 2013.

[41] V. Fuster, R. Harrington, J. Narula, and Z. Eapen, *Hurst's the Heart*, 14th ed. New York: McGraw-Hill, 2017, vol. 1, ch. 4, pp. 69–75.

[42] B. R. Wilcox, A. C. Cook, and R. H. Anderson, *Surgical anatomy of the heart*. Cambridge University Press, 2005.

[43] M. Zimmermann, "General principles of regulation", in *Human physiology*, Springer, 1989, pp. 439–479.

[44] P. A. Iaizzo, *Handbook of cardiac anatomy, physiology, and devices*. Springer Science & Business Media, 2009.

[45] S. Standring *et al.*, "Gray's anatomy: The anatomical basis of clinical practice", *American Journal of Neuroradiology*, vol. 26, no. 10, p. 2703, 2005.

[46] S. Y. Ho, K. P. McCarthy, and F. F. Faletra, "Anatomy of the left atrium for interventional echocardiography", *European Journal of Echocardiography*, vol. 12, no. 10, pp. i11–i15, 2011.

[47] R. H. Anderson and M. Loukas, "The importance of attitudinally appropriate description of cardiac anatomy", *Clinical Anatomy: The Official Journal of the American Association of Clinical Anatomists and the British Association of Clinical Anatomists*, vol. 22, no. 1, pp. 47–51, 2009.

[48] S. Y. Ho, J. A. Cabrera, and D. Sanchez-Quintana, "Left atrial anatomy revisited", *Circulation: Arrhythmia and Electrophysiology*, vol. 5, no. 1, pp. 220–228, 2012.

[49] S. Whiteman *et al.*, "An anatomical review of the left atrium", *Translational Research in Anatomy*, p. 100 052, 2019.

[50] M. Haissaguerre *et al.*, "Spontaneous initiation of atrial fibrillation by ectopic beats originating in the pulmonary veins", *New England Journal of Medicine*, vol. 339, no. 10, pp. 659–666, 1998.

[51] a. garson JR *et al.*, "Supraventricular tachycardia due to multiple atrial ectopic foci: A relatively common problem", *Journal of Cardiovascular Electrophysiology*, vol. 1, no. 2, pp. 132–138, 1990.

[52] F. H Netter, *Atlas of human anatomy*. Elsevier, 2019.

[53] J. E. Hall, *Guyton and Hall textbook of medical physiology e-Book*. Elsevier Health Sciences, 2010.

[54] F. Triposkiadis *et al.*, "The sympathetic nervous system in heart failure: Physiology, pathophysiology, and clinical implications", *Journal of the American College of Cardiology*, vol. 54, no. 19, pp. 1747–1762, 2009.

[55] H. Woollard, "The innervation of the heart", *Journal of anatomy*, vol. 60, no. Pt 4, p. 345, 1926.

[56] W. Randall, M. Milosavljevic, R. Wurster, G. Geis, and J. Ardell, "Selective vagal innervation of the heart", *Annals of Clinical & Laboratory Science*, vol. 16, no. 3, pp. 198–208, 1986.

[57] A. Brateanu, "Heart rate variability after myocardial infarction: What we know and what we still need to find out", *Current medical research and opinion*, vol. 31, no. 10, pp. 1855–1860, 2015.

[58] T. Nakayama, Y. Kurachi, A. Noma, and H. Irisawa, "Action potential and membrane currents of single pacemaker cells of the rabbit heart", *Pflügers Archiv*, vol. 402, no. 3, pp. 248–257, 1984.

[59] D. U. Silverthorn, W. C. Ober, C. W. Garrison, A. C. Silverthorn, and B. R. Johnson, *Human physiology: an integrated approach*. Pearson/Benjamin Cummings San Francisco, 2010.

[60] G. M. Wahler, "Cardiac action potentials", in *Cell Physiology Source Book*, Elsevier, 2001, pp. 887–898.

[61] E. Carmeliet, "Intracellular ca2+ concentration and rate adaptation of the cardiac action potential", *Cell calcium*, vol. 35, no. 6, pp. 557–573, 2004.

[62] J. T. Koivumäki, T. Korhonen, and P. Tavi, "Impact of sarcoplasmic reticulum calcium release on calcium dynamics and action potential morphology in human atrial myocytes: A computational study", *PLoS computational biology*, vol. 7, no. 1, 2011.

[63] P. de Chazal, M. O'Dwyer, and R. B. Reilly, "Automatic classification of heartbeats using ecg morphology and heartbeat interval features", *IEEE Transactions on Biomedical Engineering*, vol. 51, no. 7, pp. 1196–1206, 2004.

[64] L. H. Opie, *Heart physiology: from cell to circulation*. Lippincott Williams & Wilkins, 2004.

[65] P. De Chazal and R. B. Reilly, "A patient-adapting heartbeat classifier using ecg morphology and heartbeat interval features", *IEEE transactions on biomedical engineering*, vol. 53, no. 12, pp. 2535–2543, 2006.

[66] A. Noma, M. Morad, and H. Irisawa, "Does the "pacemaker current" generate the diastolic depolarization in the rabbit sa node cells?", *Pflügers Archiv*, vol. 397, no. 3, pp. 190–194, 1983.

[67] J. Achten and A. E. Jeukendrup, "Heart rate monitoring", *Sports medicine*, vol. 33, no. 7, pp. 517–538, 2003.

[68] S. Mitra, M. Mitra, and B. B. Chaudhuri, "A rough-set-based inference engine for ecg classification", *IEEE Transactions on instrumentation and measurement*, vol. 55, no. 6, pp. 2198–2206, 2006.

[69] S. S. Barold, "Willem einthoven and the birth of clinical electrocardiography a hundred years ago", *Cardiac electrophysiology review*, vol. 7, no. 1, pp. 99–104, 2003.

[70] W. Einthoven, "Le télécardiogramme "the telecardiogram"(1906)", *Archives Internationales de Physiologie*, vol. 35, pp. 132–164,

[71] E. Goldberger, "A simple, indifferent, electrocardiographic electrode of zero potential and a technique of obtaining augmented, unipolar, extremity leads", *American Heart Journal*, vol. 23, no. 4, pp. 483–492, 1942.

[72] F. N. Wilson *et al.*, "The precordial electrocardiogram", *American Heart Journal*, vol. 27, no. 1, pp. 19–85, 1944.

[73] F. N. Wilson and F. D. Johnston, "The vectorcardiogram", *American Heart Journal*, vol. 16, no. 1, pp. 14–28, 1938.

[74] J. Lee, Y. Chee, and I. Kim, "Personal identification based on vectorcardiogram derived from limb leads electrocardiogram", *Journal of Applied Mathematics*, vol. 2012, 2012.

[75] R. A. Helm, "Theory of vectorcardiography: A review of fundamental concepts", *American heart journal*, vol. 49, no. 1, pp. 135–159, 1955.

[76] H. Yang, S. T. Bukkapatnam, and R. Komanduri, "Spatiotemporal representation of cardiac vectorcardiogram (vcg) signals", *Biomedical engineering online*, vol. 11, no. 1, p. 16, 2012.

[77] J. Holmes, "A method of vectorcardiogram: Loop portrayal", *Equine Veterinary Journal*, vol. 2, no. 1, pp. 27–34, 1970.

[78] E. Frank, "An accurate, clinically practical system for spatial vectorcardiography", *circulation*, vol. 13, no. 5, pp. 737–749, 1956.

[79] ——, "The image surface of a homogeneous torso", *American Heart Journal*, vol. 47, no. 5, pp. 757–768, 1954.

[80] G. Daniel, G. Lissa, D. M. Redondo, L. Vásquez, and D. Zapata, "Real-time 3d vectorcardiography: An application for didactic use", in *Journal of Physics: Conference Series*, IOP Publishing, vol. 90, 2007, p. 012 013.

[81] K.-P. Bethge, "Classification of arrhythmias.", *Journal of cardiovascular Pharmacology*, vol. 17, S13–9, 1991.

[82] B. Lown, "Electrical reversion of cardiac arrhythmias.", *British heart journal*, vol. 29, no. 4, p. 469, 1967.

[83] J. A. Kastor, "Multifocal atrial tachycardia", *New England Journal of Medicine*, vol. 322, no. 24, pp. 1713–1717, 1990.

[84] J. McCord and S. Borzak, "Multifocal atrial tachycardia", *Chest*, vol. 113, no. 1, pp. 203–209, 1998.

[85] W. H. Maisel, J. D. Rawn, and W. G. Stevenson, "Atrial fibrillation after cardiac surgery", *Annals of internal medicine*, vol. 135, no. 12, pp. 1061–1073, 2001.

[86] M. Duchini, M. Ruggeri-Jozefowski, M. Di Valentino, and A. Menafoglio, "Atrial fibrillation induced by low-voltage electrical injury", *Cardiovascular Medicine*, vol. 21, no. 02, pp. 53–56, 2018.

[87] N. Saoudi *et al.*, "A classification of atrial flutter and regular atrial tachycardia according to electrophysiological mechanisms and anatomical bases. a statement from a joint expert group from the working group of arrhythmias of the european society of cardiology and the north american society of pacing and electrophysiology", *European heart journal*, vol. 22, no. 14, pp. 1162–1182, 2001.

[88] F. G. Cosıo, A. Pastor, A. Núñez, A. P. Magalhaes, and P. Awamleh, "Atrial flutter: An update", *Revista Española de Cardiologıa (English Edition)*, vol. 59, no. 8, pp. 816–831, 2006.

[89] F. G. Cosio, F. Arribas, M. LÓPEZ-GIL, and J. Palacios, "Atrial flutter mapping and ablation i: Studying atrial flutter mechanisms by mapping and entrainment", *Pacing and clinical electrophysiology*, vol. 19, no. 5, pp. 841–853, 1996.

[90] M. S. Sorokivskyy and U. P. Chernyaha-Royko, "Interpretation of uncommon ecg findings in patients with atrial flutter", *Heart, Vessels and Transplantation*, vol. 1, no. 1, pp. 20–24, 2017.

[91] N. Morita *et al.*, "Pronounced effect of procainamide on clockwise right atrial isthmus conduction compared with counterclockwise conduction: Possible mechanism of the greater incidence of common atrial flutter during antiarrhythmic therapy", *Journal of cardiovascular electrophysiology*, vol. 13, no. 3, pp. 212–222, 2002.

[92] E. van Rooij *et al.*, "Mcip1 overexpression suppresses left ventricular remodeling and sustains cardiac function after myocardial infarction", *Circulation research*, vol. 94, no. 3, e18–e26, 2004.

[93] J. Rieta, V. Zarzoso, J. Millet-Roig, R. Garcıa-Civera, and R. Ruiz-Granell, "Atrial activity extraction based on blind source separation as an alternative to qrst cancellation for atrial fibrillation analysis", in *Computers in Cardiology 2000. Vol. 27 (Cat. 00CH37163)*, IEEE, 2000, pp. 69–72.

[94] F. Castells, J. J. Rieta, J. Millet, and V. Zarzoso, "Spatiotemporal blind source separation approach to atrial activity estimation in atrial tachyarrhythmias", *IEEE Transactions on Biomedical Engineering*, vol. 52, no. 2, pp. 258–267, 2005.

[95] J. J. Rieta, F. Castells, C. Sánchez, V. Zarzoso, and J. Millet, "Atrial activity extraction for atrial fibrillation analysis using blind source separation", *IEEE Transactions on Biomedical Engineering*, vol. 51, no. 7, pp. 1176–1186, 2004.

[96] A. Bollmann *et al.*, "Frequency analysis of human atrial fibrillation using the surface electrocardiogram and its response to ibutilide", *The American journal of cardiology*, vol. 81, no. 12, pp. 1439–1445, 1998.

[97] R. Jaros, R. Martinek, and L. Danys, "Comparison of different electrocardiography with vectorcardiography transformations", *Sensors*, vol. 19, no. 14, p. 3072, 2019.

[98] A. Aranda, P. Bonizzi, J. Karel, and R. Peeters, "Performance of dower's inverse transform and frank lead system for identification of myocardial infarction", in *2015 37th Annual International Conference of the IEEE Engineering in Medicine and Biology Society (EMBC)*, IEEE, 2015, pp. 4495–4498.

[99] S. Maheshwari, A. Acharyya, M. Schiariti, and P. E. Puddu, "Frank vectorcardiographic system from standard 12 lead ecg: An effort to enhance cardiovascular diagnosis", *Journal of electrocardiology*, vol. 49, no. 2, pp. 231–242, 2016.

[100] R. Jaros, R. Martinek, and L. Danys, "Comparison of different electrocardiography with vectorcardiography transformations", *Sensors*, vol. 19, no. 14, p. 3072, 2019.

[101] H. Yang and F. Leonelli, "Self-organizing visualization and pattern matching of vectorcardiographic qrs waveforms", *Computers in biology and medicine*, vol. 79, pp. 1–9, 2016.

[102] G. Daniel, G. Lissa, D. M. Redondo, L. Vásquez, and D. Zapata, "Real-time 3d vectorcardiography: An application for didactic use", in *Journal of Physics: Conference Series*, IOP Publishing, vol. 90, 2007, p. 012 013.

[103] J. Ng, A. V. Sahakian, W. Fisher, and S. Swiryn, "A vectorcardiograpbic approacb to understanding the 12-lead electrocardiogram of atrial flutter", in *Computers in Cardiology, 2004*, IEEE, 2004, pp. 629–632.

[104] F. Castells *et al.*, "Characterization of typical and atypical atrial flutter loops from the vectorcardiogram", in *2011 Annual International Conference of the IEEE Engineering in Medicine and Biology Society*, IEEE, 2011, pp. 4976–4979.

[105] J. Wells Jr, W. MacLean, T. N. James, and A. L. Waldo, "Characterization of atrial flutter. studies in man after open heart surgery using fixed atrial electrodes.", *Circulation*, vol. 60, no. 3, pp. 665–673, 1979.

[106] P. Milliez *et al.*, "Variable electrocardiographic characteristics of isthmus-dependent atrial flutter", *Journal of the American College of Cardiology*, vol. 40, no. 6, pp. 1125–1132, 2002.

[107] A. S. Manolis, "Contemporary diagnosis and management of atrial flutter", *Cardiology in review*, vol. 25, no. 6, pp. 289–297, 2017.

[108] T. R. Chandrupatla and T. J. Osler, "The perimeter of an ellipse.", *Mathematical Scientist*, vol. 35, no. 2, 2010.

[109] R. W. Barnard, K. Pearce, and L. Schovanec, "Inequalities for the perimeter of an ellipse", *Journal of mathematical analysis and applications*, vol. 260, no. 2, pp. 295–306, 2001.

[110] M. B. Villarino, "Ramanujan's perimeter of an ellipse", *arXiv preprint math/0506384*, 2005.

[111] P. Abbott, "On the perimeter of an ellipse", *Mathematica Journal*, vol. 11, no. 2, p. 172, 2008.

[112] A. Verma *et al.*, "Pre-existent left atrial scarring in patients undergoing pulmonary vein antrum isolation: An independent predictor of procedural failure", *Journal of the American College of Cardiology*, vol. 45, no. 2, pp. 285–292, 2005.

[113] M. J. Janse, "Electrophysiological changes in heart failure and their relationship to arrhythmogenesis", *Cardiovascular research*, vol. 61, no. 2, pp. 208–217, 2004.

[114] A. Bollmann *et al.*, "Frequency measures obtained from the surface electrocardiogram in atrial fibrillation research and clinical decision-making", *Journal of cardiovascular electrophysiology*, vol. 14, S154–S161, 2003.

[115] D. Husser *et al.*, "Analysis of the surface electrocardiogram for monitoring and predicting antiarrhythmic drug effects in atrial fibrillation", *Cardiovascular drugs and therapy*, vol. 18, no. 5, pp. 377–386, 2004.

[116] D. Husser *et al.*, "Pilot study: Noninvasive monitoring of oral flecainide's effects on atrial electrophysiology during persistent human atrial fibrillation using the surface electrocardiogram", *Annals of noninvasive electrocardiology*, vol. 10, no. 2, pp. 206–210, 2005.

[117] M. Stridh, L. Sornmo, C. J. Meurling, and S. B. Olsson, "Characterization of atrial fibrillation using the surface ecg: Time-dependent spectral properties", *IEEE transactions on Biomedical Engineering*, vol. 48, no. 1, pp. 19–27, 2001.

[118] M. Akay and C. Mello, "Wavelets for biomedical signal processing", in *Proceedings of the 19th Annual International Conference of the IEEE Engineering in Medicine and Biology Society.'Magnificent Milestones and Emerging Opportunities in Medical Engineering'(Cat. No. 97CH36136)*, IEEE, vol. 6, 1997, pp. 2688–2691.

[119] G. R. Rıos-Muñoz *et al.*, "Patient-tailored in silico 3d simulations and models from electroanatomical maps of the left atrium", in *2018 Computing in Cardiology Conference (CinC)*, IEEE, vol. 45, 2018, pp. 1–4.

[120] G. R. Rıos-Muñoz, A. Artés-Rodrıguez, and J. Mıguez, "Particle filter tracking of complex stochastic systems applied to in silico wavefront propagation", in *2018 Computing in Cardiology Conference (CinC)*, IEEE, vol. 45, 2018, pp. 1–4.

[121] K. McClanahan, "Balancing good intentions: Protecting the privacy of electronic health information", *Bulletin of Science, Technology & Society*, vol. 28, no. 1, pp. 69–79, 2008.

[122] L. Edelstein, "The hippocratic oath: Text, translation and interpretation", *Ancient medicine: selected papers of Ludwig Edelstein*, pp. 3–63, 1943.

[123] J. F. Childress and T. L. Beauchamp, *Principles of biomedical ethics*. Oxford University Press New York, 2001.

[124] *Universal declaration of human rights*, https://www.un.org/en/universal-declaration-human-rights/, Accessed: 2020-04-25.

[125] *European convention on human rights*, https://www.echr.coe.int/Documents/Convention_ENG.pdf, Accessed: 2020-04-25.

[126] *Wma declaration of helsinki - ethical principles for medical research involving human subjects*, https://www.wma.net/policies-post/wma-declaration-of-helsinki-ethical-principles-for-medical-research-involving-human-subjects/2/, Accessed: 2020-02-17.

[127] G. V. Naccarelli, H. Varker, J. Lin, and K. L. Schulman, "Increasing prevalence of atrial fibrillation and flutter in the united states", *The American journal of cardiology*, vol. 104, no. 11, pp. 1534–1539, 2009.

[128] B. P. Krijthe *et al.*, "Projections on the number of individuals with atrial fibrillation in the european union, from 2000 to 2060", *European heart journal*, vol. 34, no. 35, pp. 2746–2751, 2013.

[129] A. de la Nava *et al.*, "Non-invasive electrophysiological mapping entropy predicts atrial fibrillation ablation efficacy better than clinical characteristics", in *2019 Computing in Cardiology (CinC)*, IEEE, 2019, Page–1.

[130] J.-G. Mora, "The academic profession in spain: Between the civil service and the market", *Higher education*, vol. 41, no. 1-2, pp. 131–155, 2001.

[131] *Instituto nacional de estadística (spanish national institute of statistics)*, https://www.ine.es, Accessed: 2020-04-20.